Powder diffraction-based techniques

Matteo Leoni

Università di Trento – Facoltà di Ingegneria
Dipartimento di Ingegneria dei Materiali e Tecnologie Industriali
via Mesiano, 77 – 38050 Trento (Italy)

E-mail: Matteo.Leoni@ing.unitn.it

Powder diffraction and the real world

Real space (3D)

Reciprocal space (3D)

structure

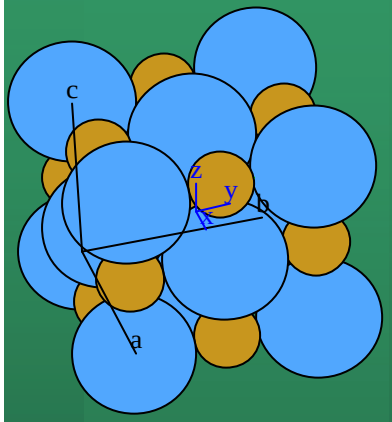

microstructure

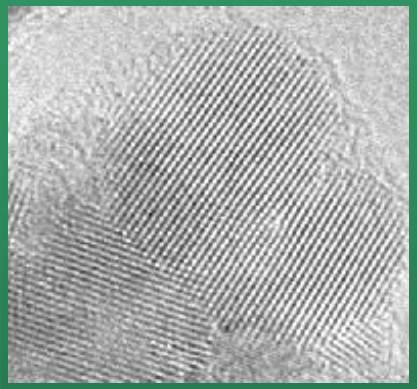

FT

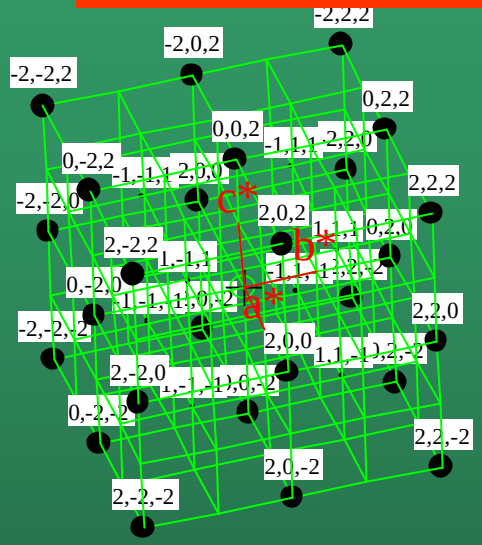

Diffraction pattern (1D)

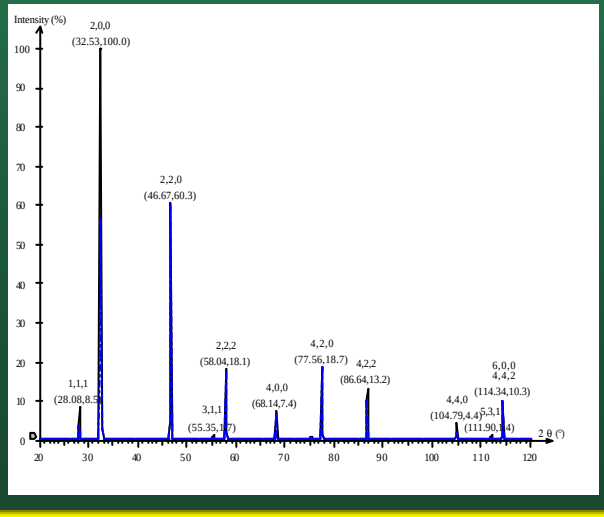

OUR PROBLEM!

Integration on spheres

Powder diffraction pattern

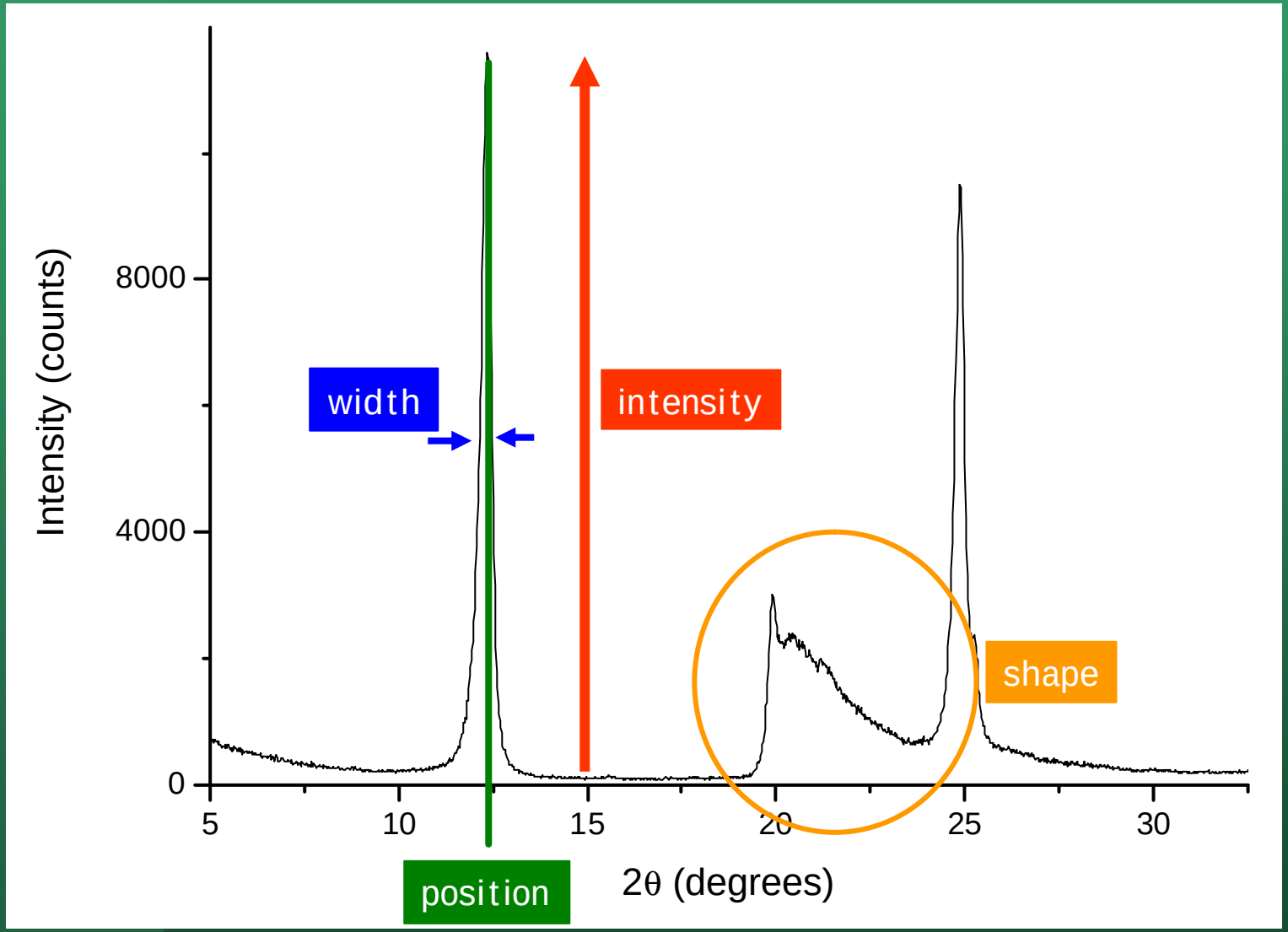

Information extracted from the pattern

- **Peak position**
  - Interplanar spacing (Bragg equation)
    - Crystalline cell
  - Phase identification
    - Qualitative analysis
  - Residual stress
- **Peak intensity**
  - Single phase material (structure factor)
    - Structural analysis/refinement (Rietveld method)
  - Multiphase material
    - Quantitative phase analysis (with/without standard)
  - Crystallographic texture
- **Peak width/shape**
  - Microstructural information
    - Size/distribution of domains
    - Linear/planar defects

Lattice and cell identification

Interplanar spacing

Experimental pattern

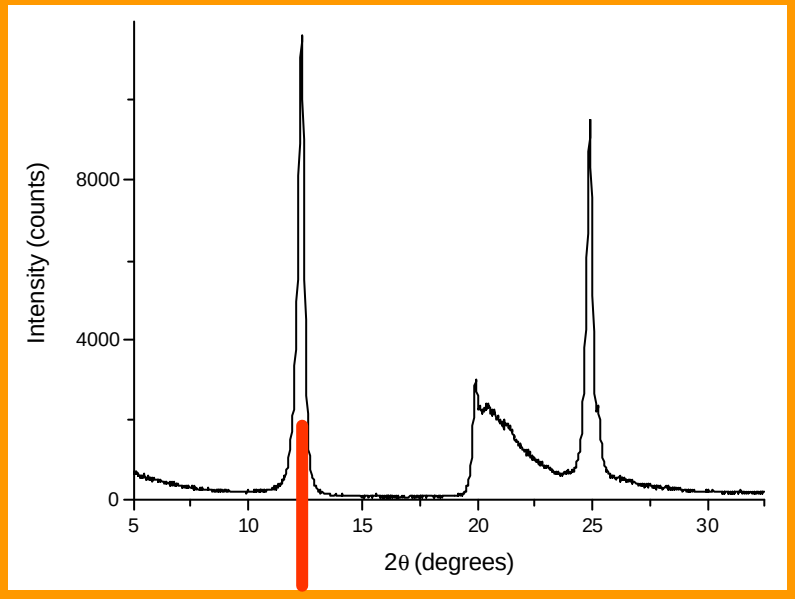

Bragg's law

$$l = 2d\sin q$$

$$d = \frac{l}{2\sin q}$$

Interplanar spacing corresponding to all reflections can be calculated

Fitting results

A table of profile parameters can be obtained e.g. through peak fitting

2Theta	d (Å)	Height	Area	FWHM
25.574	3.48029	5993.5	58566.4	0.1000
35.139	2.55179	18874.0	145082.7	0.0900
35.303	2.54026	374.2	3248.8	0.0900
37.767	2.38003	2469.4	20254.8	0.0900
41.666	2.16587	576.2	4915.4	0.0900
43.346	2.08573	8803.4	74545.1	0.0900
52.538	1.74040	3979.9	35662.6	0.0900
57.484	1.60186	13317.6	117690.5	0.0900
61.283	1.51134	2370.5	23440.4	0.1000
66.499	1.40489	2307.9	23039.4	0.1000
68.191	1.37410	2518.7	25172.9	0.1000
74.275	1.27587	237.7	2276.7	0.1000
76.846	1.23946	4965.6	42968.4	0.0900
77.209	1.23454	1549.5	15483.1	0.1000
80.676	1.18999	258.3	2231.7	0.0900
84.329	1.14751	229.7	2294.5	0.1000
86.470	1.12451	245.7	2211.5	0.0900
88.963	1.09933	1153.7	11452.0	0.1000
90.677	1.08296	596.0	6376.5	0.1100
91.155	1.07852	382.1	3784.7	0.1000
95.217	1.04296	880.7	8781.4	0.1000
101.039	0.99798	1374.2	13728.0	0.1000
110.951	0.93494	228.9	2514.3	0.1100
116.060	0.90800	392.1	4312.2	0.1100
116.560	0.90555	968.5	10037.9	0.1100

Indexing

Through indexing algorithms, lattice, cell and space group can be obtained

2Theta	d (Å)
25.574	3.48029
35.139	2.55179
35.303	2.54026
37.767	2.38003
41.666	2.16587
43.346	2.08573
52.538	1.74040
57.484	1.60186
61.283	1.51134
66.499	1.40489
68.191	1.37410
74.275	1.27587
76.846	1.23946
77.209	1.23454
80.676	1.18999
84.329	1.14751
86.470	1.12451
88.963	1.09933
90.677	1.08296
91.155	1.07852
95.217	1.04296
101.039	0.99798
110.951	0.93494
116.060	0.90800
116.560	0.90555

$$d = f\left(a,b,c,a,b,g,(h,k,l)\right)$$

$$d = \frac{a_0}{\sqrt{h^2 + k^2 + l^2}}$$ for cubics

Bravais lattice

cell parameters

Space group
via check of systematic absences

Area
58566.4
145082.7
3248.8
20254.8
4915.4
74545.1
35662.6
117690.5
23440.4
23039.4
25172.9
2276.7
42968.4
15483.1
2231.7
2294.5
2211.5
11452.0
6376.5
3784.7
8781.4
13728.0
2514.3
4312.2
10037.9

Qualitative phase analysis

Principle of operation

Phase identification is one of the first and most diffuse applications of powder diffraction (especially in industry), for research, production, quality control and diagnostics.

Each crystalline phase has its own pattern that can be used as a fingerprint.

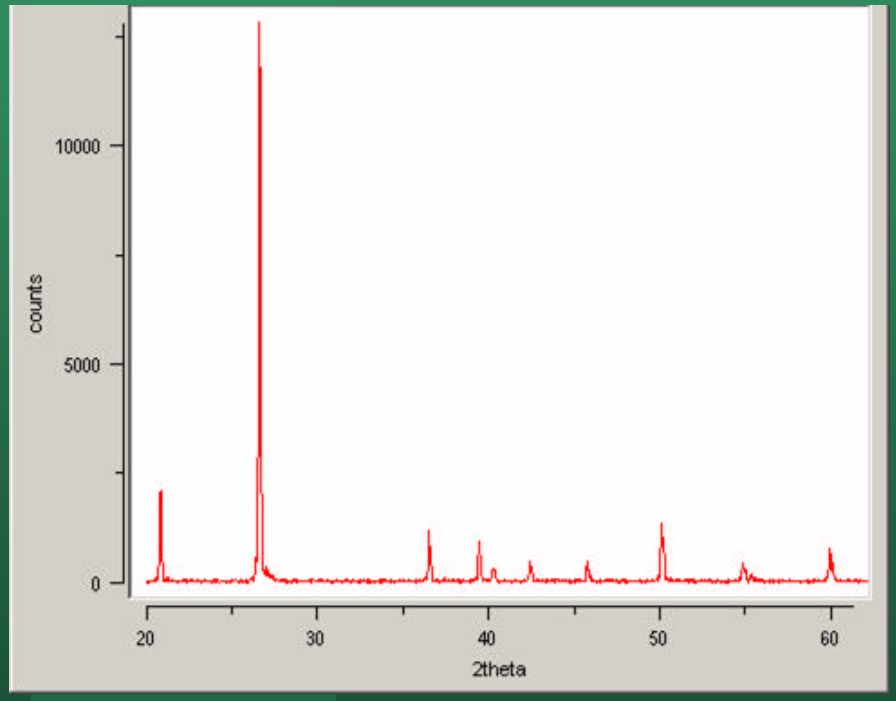

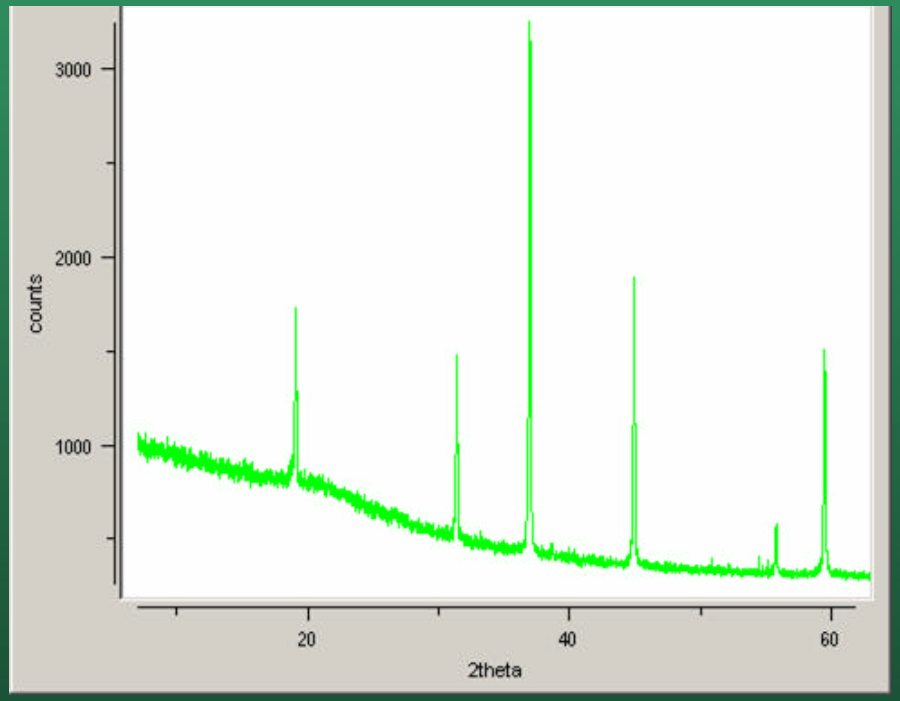

We just need to find the fingerprint of known substances in the pattern to be analysed

Fitting results

A table of profile parameters can be obtained e.g. through peak fitting

2Theta	d (Å)	Height	Area	FWHM
25.574	3.48029	5993.5	58566.4	0.1000
35.139	2.55179	18874.0	145082.7	0.0900
35.303	2.54026	374.2	3248.8	0.0900
37.767	2.38003	2469.4	20254.8	0.0900
41.666	2.16587	576.2	4915.4	0.0900
43.346	2.08573	8803.4	74545.1	0.0900
52.538	1.74040	3979.9	35662.6	0.0900
57.484	1.60186	13317.6	117690.5	0.0900
61.283	1.51134	2370.5	23440.4	0.1000
66.499	1.40489	2307.9	23039.4	0.1000
68.191	1.37410	2518.7	25172.9	0.1000
74.275	1.27587	237.7	2276.7	0.1000
76.846	1.23946	4965.6	42968.4	0.0900
77.209	1.23454	1549.5	15483.1	0.1000
80.676	1.18999	258.3	2231.7	0.0900
84.329	1.14751	229.7	2294.5	0.1000
86.470	1.12451	245.7	2211.5	0.0900
88.963	1.09933	1153.7	11452.0	0.1000
90.677	1.08296	596.0	6376.5	0.1100
91.155	1.07852	382.1	3784.7	0.1000
95.217	1.04296	880.7	8781.4	0.1000
101.039	0.99798	1374.2	13728.0	0.1000
110.951	0.93494	228.9	2514.3	0.1100
116.060	0.90800	392.1	4312.2	0.1100
116.560	0.90555	968.5	10037.9	0.1100

Manual search

Manual matching of most intense lines

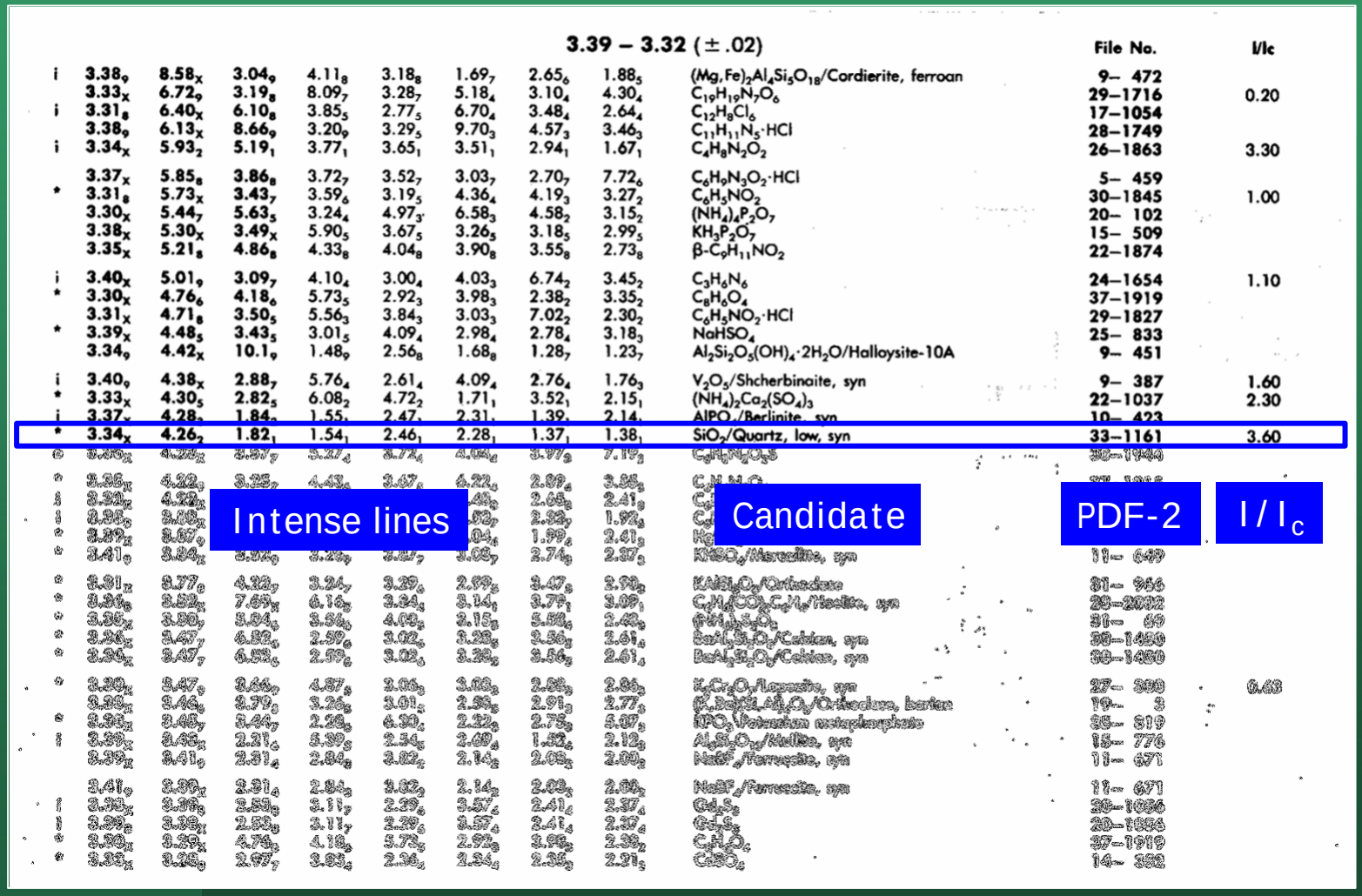

3.39 – 3.32 (±.02)

										File No.	I/Ic
i	3.38_9	8.58_X	3.04_9	4.11_8	3.18_8	1.69_7	2.65_6	1.88_5	$(Mg,Fe)_2Al_4Si_5O_{18}$/Cordierite, ferroan	9– 472	
	3.33_X	6.72_9	3.19_8	8.09_7	3.28_7	5.18_4	3.10_4	4.30_4	$C_{19}H_{19}N_7O_6$	29–1716	0.20
i	3.31_8	6.40_X	6.10_8	3.85_5	2.77_5	6.70_4	3.48_4	2.64_4	$C_{12}H_8Cl_6$	17–1054	
	3.38_9	6.13_X	8.66_9	3.20_9	3.29_5	9.70_3	4.57_3	3.46_3	$C_{11}H_{11}N_5 \cdot HCl$	28–1749	
i	3.34_X	5.93_2	5.19_1	3.77_1	3.65_1	3.51_1	2.94_1	1.67_1	$C_4H_8N_2O_2$	26–1863	3.30
	3.37_X	5.85_8	3.86_8	3.72_7	3.52_7	3.03_7	2.70_7	7.72_6	$C_6H_9N_3O_2 \cdot HCl$	5– 459	
*	3.31_8	5.73_X	3.43_7	3.59_6	3.19_5	4.36_4	4.19_3	3.27_2	$C_6H_5NO_2$	30–1845	1.00
	3.30_X	5.44_7	5.63_5	3.24_4	4.97_3	6.58_3	4.58_2	3.15_2	$(NH_4)_4P_2O_7$	20– 102	
	3.38_X	5.30_X	3.49_X	5.90_5	3.67_5	3.26_5	3.18_5	2.99_5	$KH_3P_2O_7$	15– 509	
	3.35_X	5.21_8	4.86_8	4.33_8	4.04_8	3.90_8	3.55_8	2.73_8	β-$C_9H_{11}NO_2$	22–1874	
i	3.40_X	5.01_9	3.09_7	4.10_4	3.00_4	4.03_3	6.74_2	3.45_2	$C_3H_6N_6$	24–1654	1.10
*	3.30_X	4.76_6	4.18_6	5.73_5	2.92_3	3.98_3	2.38_2	3.35_2	$C_8H_6O_4$	37–1919	
	3.31_X	4.71_8	3.50_5	5.56_3	3.84_3	3.03_3	7.02_2	2.30_2	$C_6H_5NO_2 \cdot HCl$	29–1827	
*	3.39_X	4.48_5	3.43_5	3.01_5	4.09_4	2.98_4	2.78_4	3.18_3	$NaHSO_4$	25– 833	
	3.34_9	4.42_X	10.1_9	1.48_9	2.56_8	1.68_8	1.28_7	1.23_7	$Al_2Si_2O_5(OH)_4 \cdot 2H_2O$/Halloysite-10A	9– 451	
i	3.40_9	4.38_X	2.88_7	5.76_4	2.61_4	4.09_4	2.76_4	1.76_3	V_2O_5/Shcherbinaite, syn	9– 387	1.60
*	3.33_X	4.30_5	2.82_5	6.08_2	4.72_2	1.71_1	3.52_1	2.15_1	$(NH_4)_2Ca_2(SO_4)_3$	22–1037	2.30
i	3.37_X	4.28_X	1.84_9	1.55_8	2.47_7	2.31_7	1.39_7	2.14_6	$AlPO_4$/Berlinite, syn	10– 423	
*	3.34_X	4.26_2	1.82_1	1.54_1	2.46_1	2.28_1	1.37_1	1.38_1	SiO_2/Quartz, low, syn	33–1161	3.60
*	3.36_X	4.22_X	3.25_X	4.43_X	3.67_X	4.22_X	2.89_4	3.35_3	$C_9H_8N_2O_3$	38–1944	
*	3.35_X	4.22_9	3.25_X	4.43_X	3.67_X	4.22_X	2.89_4	3.35_3	$C_9H_8N_2O_3$	37–1008	
i	3.32_X	4.22_X	3.25_X	4.43_X	3.67_X	4.22_X	2.89_4	3.35_3	$C_9H_8N_2O_3$	37–1008	
i	3.35_9	3.48_X	3.25_X	4.43_X	3.67_X	4.22_X	2.89_4	2.41_3	$C_9H_8N_2O_3$	37–1008	
*	3.39_X	3.47_9	3.25_X	4.43_X	3.67_X	4.22_X	2.89_4	3.35_3	$C_9H_8N_2O_3$	37–1008	
*	3.39_X	3.47_9	3.25_X	4.43_X	3.67_X	4.22_X	2.89_4	3.35_3	$C_9H_8N_2O_3$	37–1008	
*	3.41_9	3.34_X	3.25_X	4.43_X	3.67_X	4.22_X	2.89_4	3.35_3	$C_9H_8N_2O_3$	37–1008	
*	3.31_X	3.77_9	4.22_9	3.24_7	3.29_6	2.59_5	3.47_5	3.30_5	$KAlSi_3O_8$/Orthoclase	31– 966	
*	3.26_9	3.52_X	7.65_X	6.16_9	3.24_4	3.14_1	3.75_1	3.09_1	$C_4H_4CO_3C_4H_4$/Hoelite, syn	29–2092	
*	3.35_X	3.50_9	5.04_X	3.56_9	4.09_5	2.15_3	5.58_4	2.48_3	$PbH_4P_2O_8$	31– 69	
*	3.26_X	3.47_7	6.52_X	2.59_6	3.02_6	3.28_5	3.56_3	2.61_4	$BaAl_2Si_2O_8$/Celsian, syn	38–1450	
*	3.26_X	3.47_7	6.52_X	2.59_6	3.02_6	3.28_5	3.56_3	2.61_4	$BaAl_2Si_2O_8$/Celsian, syn	38–1450	
*	3.30_X	3.47_9	3.44_9	4.87_8	2.06_3	3.08_3	2.28_3	2.86_3	$K_2Cr_2O_7$/Lopezite, syn	27– 369	6.48
	3.28_X	3.46_X	2.79_X	3.26_X	3.01_5	2.55_3	2.91_3	2.77_3	$(K,Ba)Al_2Si_2O_8$/Orthoclase, barian	19– 3	
*	3.32_X	3.45_9	3.44_9	2.26_8	4.30_4	2.32_3	2.75_3	5.67_3	KPO_3/Potassium metaphosphate	35– 819	
i	3.39_X	3.43_X	2.21_4	5.39_5	2.54_5	2.69_4	1.82_4	2.12_3	$Al_2Si_2O_5$/Mullite, syn	15– 776	
	3.39_X	3.41_9	2.21_4	2.84_8	3.02_7	2.14_5	2.03_5	2.09_5	$NaBF_4$/Ferroxite, syn	11– 671	
	3.41_9	3.39_X	2.21_4	2.84_8	3.02_7	2.14_5	2.03_5	2.09_5	$NaBF_4$/Ferroxite, syn	11– 671	
i	3.36_X	3.36_X	2.55_9	3.11_7	2.39_6	3.57_4	2.41_4	2.37_4	CdS	36–1056	
i	3.39_9	3.39_X	2.55_9	3.11_7	2.39_6	3.57_4	2.41_4	2.37_4	CdS	20–1338	
*	3.30_X	3.39_X	4.76_6	4.18_6	5.73_5	2.92_3	3.98_3	2.38_2	$C_8H_6O_4$	37–1919	
*	3.33_X	3.29_9	2.97_7	3.83_4	2.34_4	2.34_4	2.35_3	2.21_3	$CaSO_4$	14– 352	

Intense lines

Candidate

PDF-2

I / I_c

The Powder Diffraction File (PDF)

Information on known substances are collected into the PDF

PDF-2

lattice info

PDF-4

lattice info
atomic positions
relational database

PDF-4 organics

PDF-4 minerals

database browser

The Powder Diffraction File (PDF)

Information on known substances are collected into the PDF

(14/100)

6- 2 JCPDS-ICDD Copyright (c) 2000 Radiation: Quality: i

Ca Mg (Si,Al) O (OH) !6H O
0.3 3 4 10 2 2

Magnesium Aluminum Silicate Hydroxide Hydrate

Saponite-18A, glycerol

Rad: CuKa Lambda: 1.5418 Filter: Ni d-sp:
Cutoff: Int: Visual I/Icor:
Ref: Midgley, Mineral. Mag., 29 526 (1951)

Sys: Hexagonal S.G.: P
a: 5.291(7) b: c: 18.05(5) A: C: 3.4115
A: B: C: Z: 1 mp:
Ref: Bayliss, P., Howie, R., Zussman, J., Powder Diffraction, 4 19 (1989)

Dx: 2.10 Dm: 2.24 SS/FOM: F(13)=1.5(0.113,76)

ea: nwB: 1.555 ey: Sign: - 2V: 0 deg.
Ref: Deer, W., Howie, R., Zussman, J., Rock Forming Minerals, 3 226 (1962)

Color: White, reddish white
Specimen from Lizard, Cornwall, England, UK. CAS no.: 12173-47-6. Glycerol treated. Smectite group, trioctahedral subgroup. PSC: hP39.30. Volume[CD]: 437.61.

d A	Int.	h k l
18.8	100	0 0 1
9.1	50	0 0 2
6.06	10	0 0 3
4.55	50	1 0 0
3.61	50	0 0 5
3.01	40	0 0 6
2.61	60	1 1 1
2.48	30	
2.26	20	0 0 8
2.00	10	0 0 9
1.736	40	2 1 0
1.536	70	3 0 0
1.321	40	2 2 0
1.271	20	3 1 0

Boolean search

Line position matched against database entries of known substances

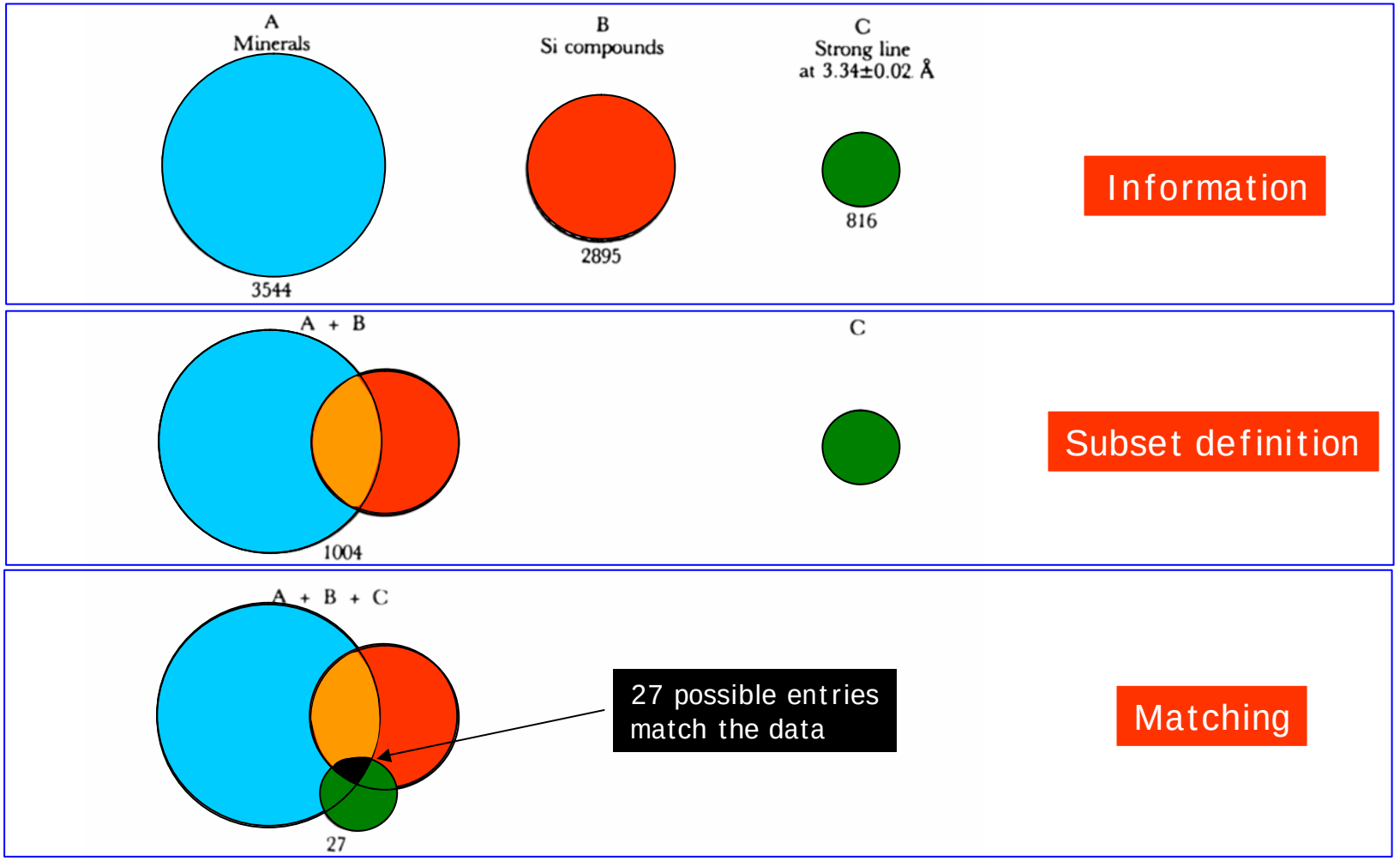

Automatic search match

Modern software does boolean search automatically on multiple peaks.

Example of search match done by using the MDI Jade 5.0 software on an unknown specimen (mixture of Al_2O_3, CaF_2 and ZnO)

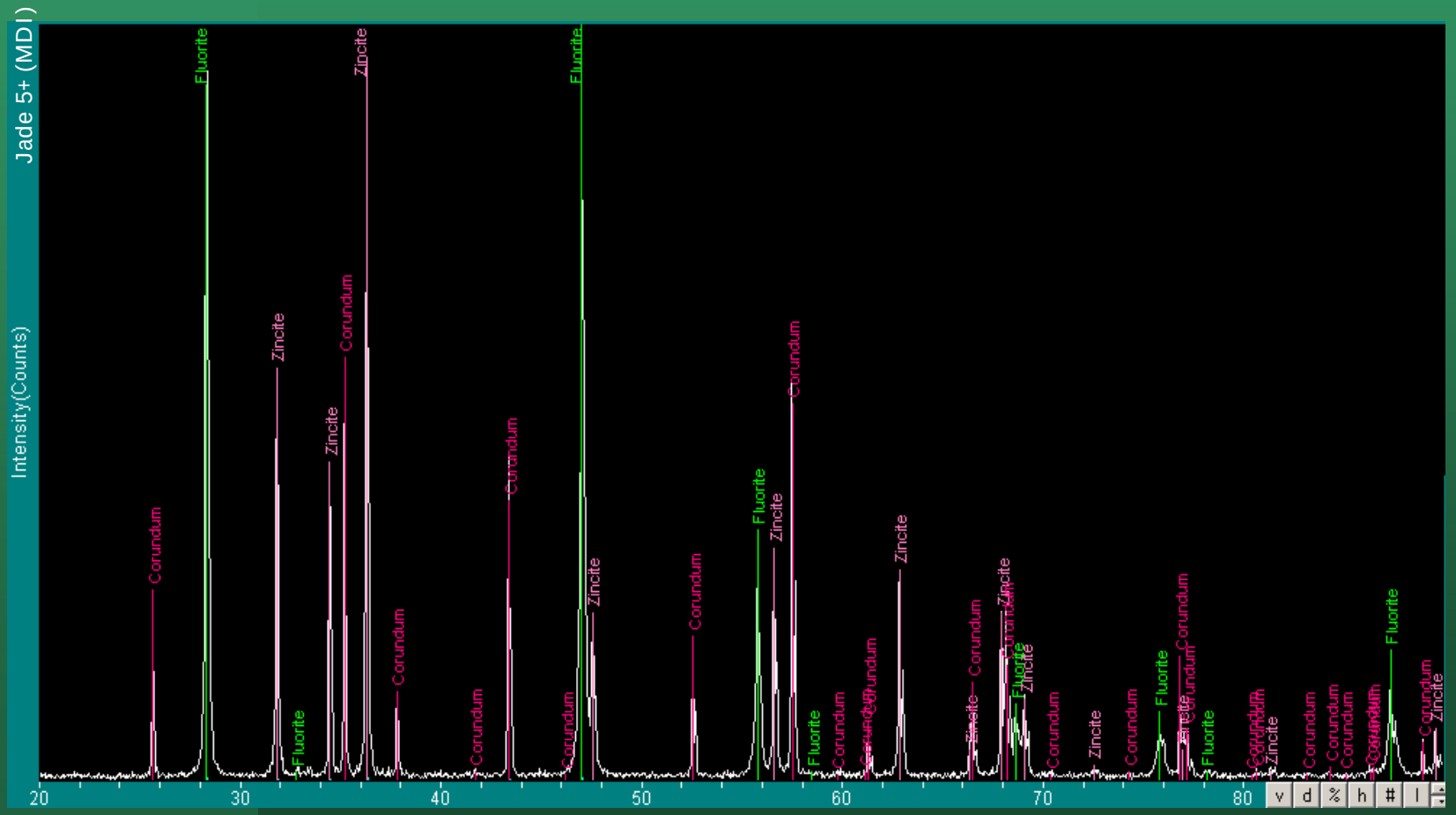

Quantitative Phase Analysis (QPA)

Quantitative Phase Analysis (QPA)

The pattern of a mixture is the WEIGHTED sum of the patterns corresponding to the constituent phases.

Qualitative analysis via **SEARCH-MATCH**

Must we stick to qualitative results only???

NOT ALWAYS! Several techniques based on XRD exists for a quantitative determination of the phase content:

- QPA with **internal standard**
- QPA "**standardless**" (RIRs, Reference Intensity Ratios)
- QPA via **Rietveld method**

Quantitative Phase Analysis (QPA)

Mass absorption coefficient for a mixture if *n* phases:

$$(m/r)_m = w_1(m/r)_1 + w_2(m/r)_2 + \ldots + w_n(m/r)_n = \sum_{i=1}^{n} w_i(m/r)_i$$

Intensity for the *i*-th reflection in a single-phase pattern

$$I_i = k_i \frac{|F_i|^2}{m_i} LP = \frac{k_i'}{m_i}$$

Intensity for the *i*-th reflection and *j*-th phase in a multi-phase pattern

$$I_{i,j} = \frac{k_{i,j}' v_j}{(m/r)_m r_m} = \frac{k_{i,j}' v_j}{m_m}$$

volume fraction j-th phase

linear absorption mixture

Quantitative Phase Analysis (QPA)

We can conveniently introduce the weight fractions

$$r_j = \frac{w_j}{v_j} r_m \qquad I_{i,j} = \frac{k'_{i,j} v_j}{m_m} = \frac{k'_{i,j} w_j}{r_j (m/r)_m} = \frac{k''_{i,j} w_j}{(m/r)_m}$$

mass absorption coefficient for the mixture

For two phases, the formula for the i-th reflection reduces to:

$$I_{i,1} = \frac{k''_{i,1} w_1}{(m/r)_m} = \frac{k''_{i,1} w_1}{\left[(m/r)_1 - (m/r)_2\right] w_1 + (m/r)_2} \qquad w_1 = 1 - w_2,\ v_1 = 1 - v_2$$

The mass absorption coefficient is however unknown!

What is therefore all of this useful for?

Internal standard

We can solve the problem by adding a known amount of a standard material.

Assuming that the amount of phase to be determined is w_j , we can add a known amount of an extra phase (spiking) w_s

By effect of the extra phase, we have:

$$w'_j = (1 - w_s) w_j$$

and, therefore the ratio of the intensities of two peaks for the *j* and *s* phases read:

$$\frac{I'_{i,j}}{I_{l,s}} = \frac{k_{i,j} w'_j}{k_{l,s} w_s} = f_{j,s} \frac{w'_j}{w_s} = f_{j,s} \frac{w_j (1 - w_s)}{w_s}$$

from which, if we know the structure of the phases and therefore $f_{j,s}$:

$$w_j = \frac{I_{i,j}}{I_{r,s}} \cdot \frac{w_s}{f_{j,s} (1 - w_s)}$$

RIR formula

There is a possible elegant alternative.
For a 1:1 mixture of our phase and a corundum standard the *f* reads:

$$f_{j,s} = \frac{I_{i,j}}{I_{l,c}} \cdot \frac{w_c}{w_j (1 - w_c)} = 2 \frac{I_{i,j}}{I_{l,c}}$$

The ratio between the most intense peaks of our phase and of corundum is defined as Reference Intensity Ratio (RIR) with corundum:

$$RIR_{j,corundum} = I_j / I_c = \frac{I_{i,j}}{I_{l,c}} \frac{I_{l,c}^{rel}}{I_{i,j}^{rel}} \frac{w_c}{w_j}$$

For a peak *i* and phase *j* with relative intensity $I_{i,j}^{rel}$ we have:

$$w_j = \frac{I_{i,j} / I_{i,j}^{rel}}{I_j / I_c} \left[\sum_{k=1}^{n} \frac{I_{l,k} / I_{l,k}^{rel}}{I_k / I_c} \right]^{-1}$$

The Rietveld method

Rietveld method

Definition: page 2 R.A. Young 1993:

In the Rietveld method the least-squares refinements are carried out until the best fit is obtained between the entire observed powder diffraction pattern taken as a whole and the entire calculated pattern based on the simultaneously refined models for the crystal structure(s), diffraction optics effects, intrumental factors, and other specimen characteristics

It is a minimization procedure (Nonlinear Least Squares refinement) of the residual:

$$S_y = \sum_i w_i \left(y_i - y_{ci} \right)^2$$

weight

observed

calculated

Rietveld method: basic equation

Intensity of the i-th point in the pattern

$$y_{ci} = S \sum_k L_k \left|F_k\right|^2 f\left(2q_i - 2q_k\right) P_k A + y_{bi}$$

scale factor

Structure factor

Profile function

Background term

Using the normalization condition: $\sum_k x_k = 1$

it is possible to calculate the weight fraction x_α of the phase a in a polyphasic mixture:

$$x_j = \frac{S_j r_j v_j}{\sum_l S_l r_l v_l}$$

Is the fit good?

Statistical indices

$$R_F = \frac{\sum |(I_K(\text{'obs'}))^{1/2} - (I_K(\text{calc})^{1/2})|}{\sum (I_K(\text{'obs'}))^{1/2}} \qquad (\text{'}R\text{-structure factor'})$$

$$R_B = \frac{\sum |I_K(\text{'obs'}) - I_K(\text{calc})|}{\sum I_K(\text{'obs'})} \qquad (\text{'}R\text{-Bragg factor'})$$

$$R_p = \frac{\sum |y_i(\text{obs}) - y_i(\text{calc})|}{\sum y_i(\text{obs})} \qquad (\text{'}R\text{-pattern'})$$

$$R_{wp} = \left\{ \frac{\sum w_i (y_i(\text{obs}) - y_i(\text{calc}))^2}{\sum w_i (y_i(\text{obs}))^2} \right\}^{1/2} \qquad (\text{'}R\text{-weighted pattern'})$$

Here I_K is the intensity assigned to the Kth Bragg reflection at the end of the refinement cycles. In the expressions for R_F and R_B the 'obs' (for observed) is put in quotation marks because the Bragg intensity, I_K, is rarely observed directly; instead the I_K values are obtained from programmatic allocation of the total observed intensity in a 'scramble' of overlapped reflections to the individual reflections, according to the ratios of those reflection intensities in the calculated pattern.

The '*Goodness-of-fit*' indicator, S, is

$$S = [S_y/(N - P)]^{1/2} = R_{wp}/R_e$$

where

$$R_e = \text{'}R\text{-expected'} = [(N - P)/\sum w_i y_{oi}^2]^{1/2}.$$

The *Durbin–Watson statistic*, 'd', is

$$\text{'}d\text{'} = \sum_{i=2}^{N} (\Delta y_i - \Delta y_{i-1})^2 \Big/ \sum_{i=1}^{N} \Delta y_i^2$$

where

$$\Delta y_i = y_{oi} - y_{ci}.$$

Example of Rietveld-based QPA

QPA of zirconia polymorphs in Partially-Stabilised Zirconia TBCs (Thermal Barrier Coatings)

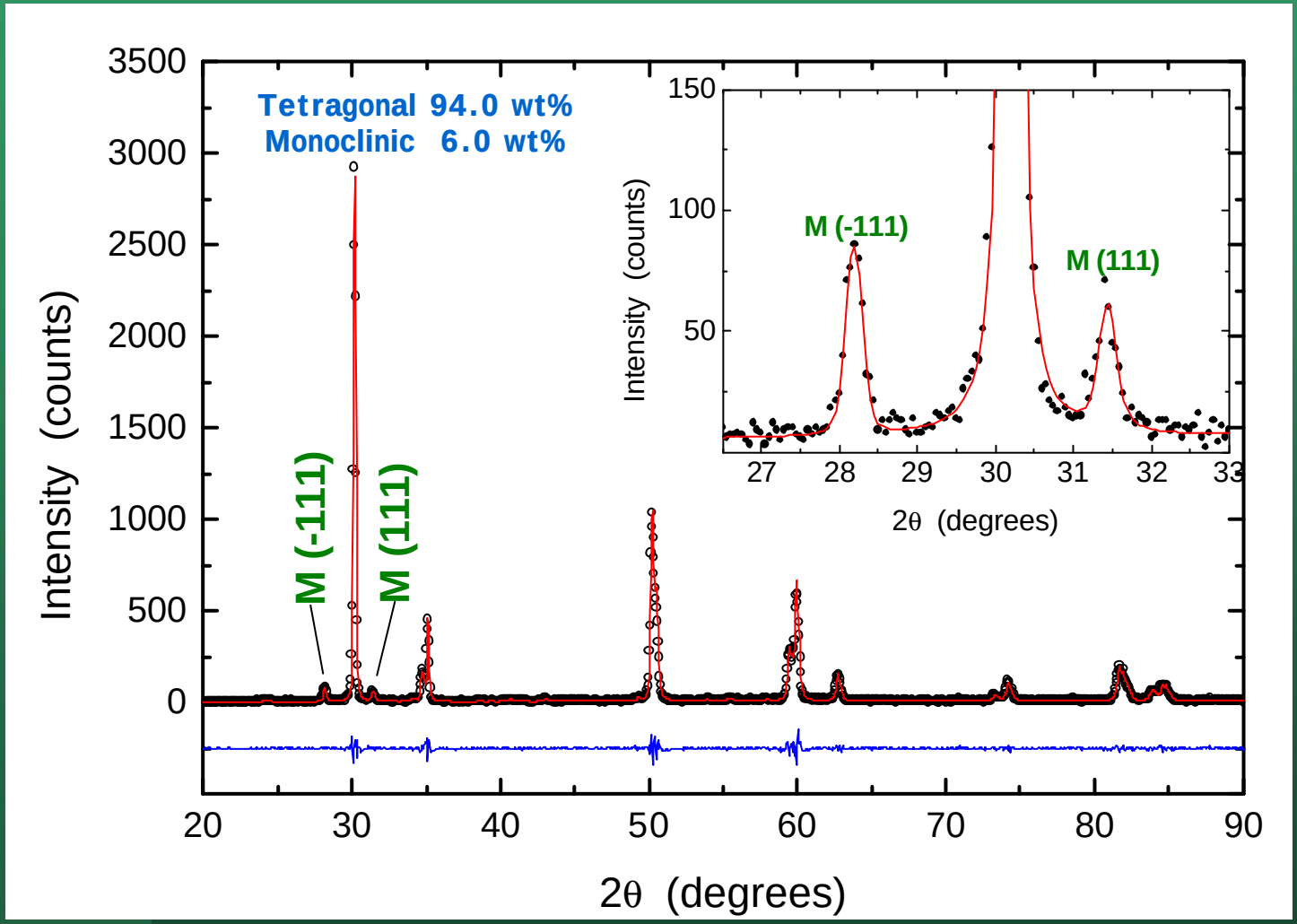

Example: GSAS

The same elements are always present to allow visual feeling for the fit quality

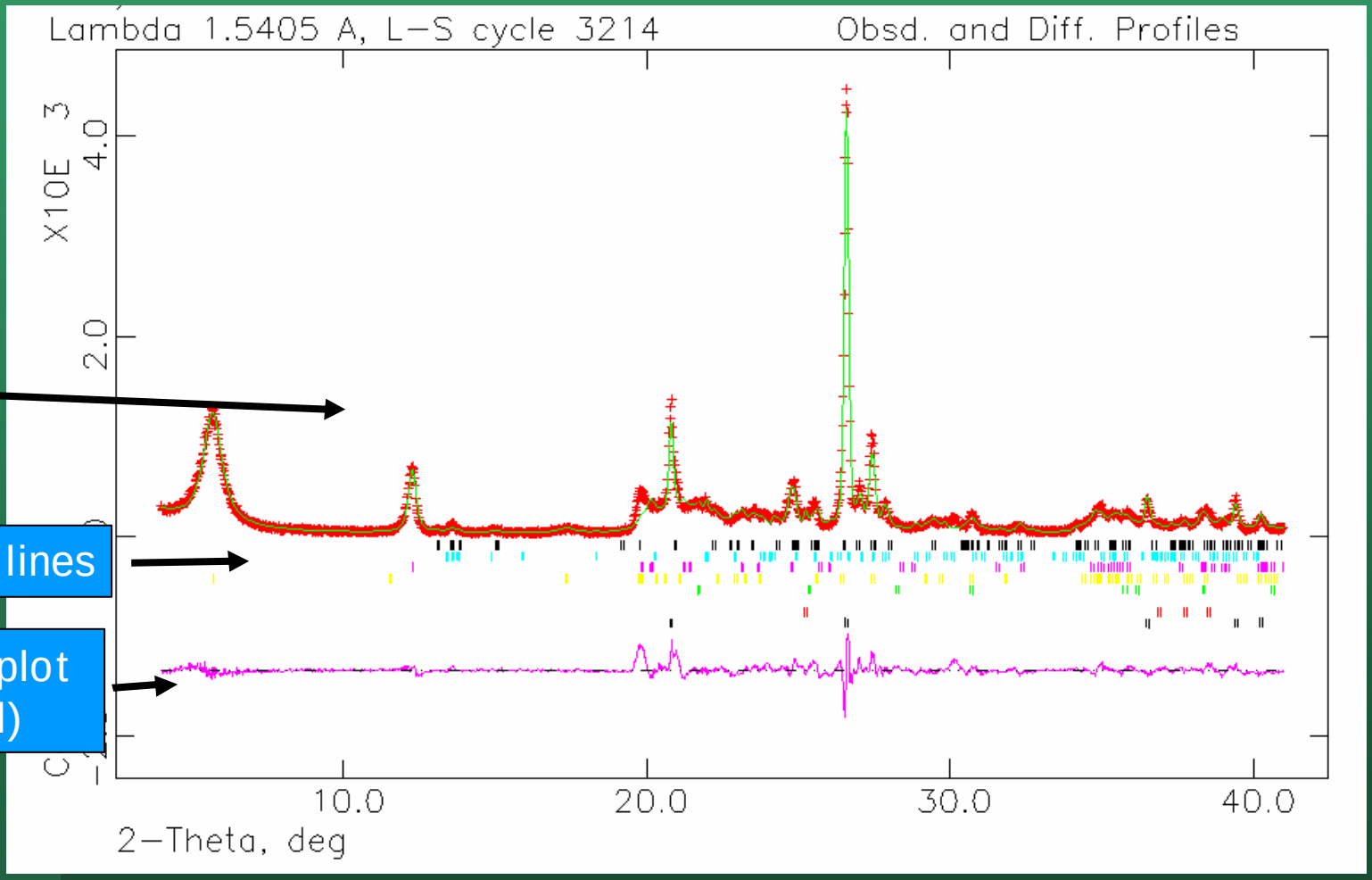

Structure solution/refinement

Structure solution/refinement

Structure solution of heptamethylene-1,7-bis(diphenylphosphane oxide)

Structural formula

$Ph_2P(O)(CH_2)_7P(O)Ph_2$

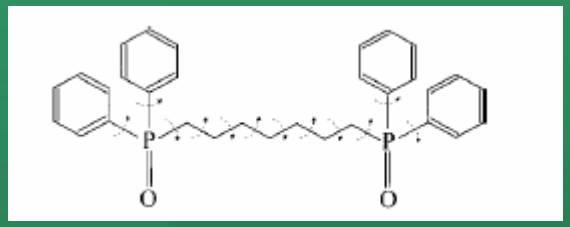

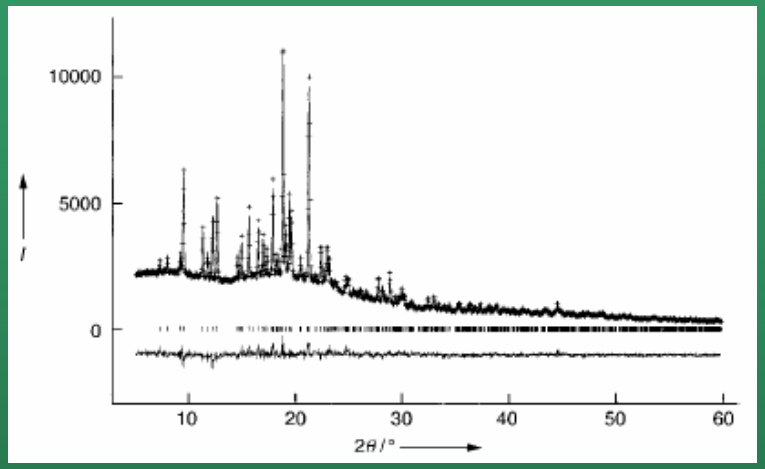

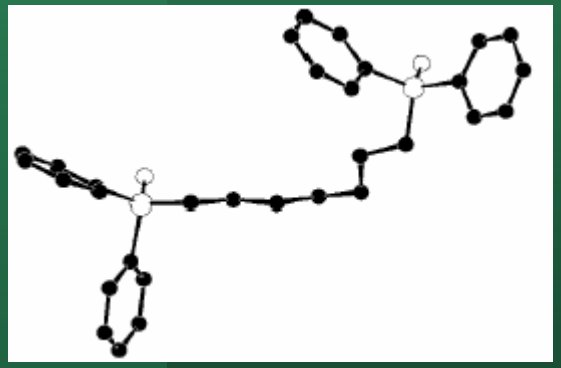

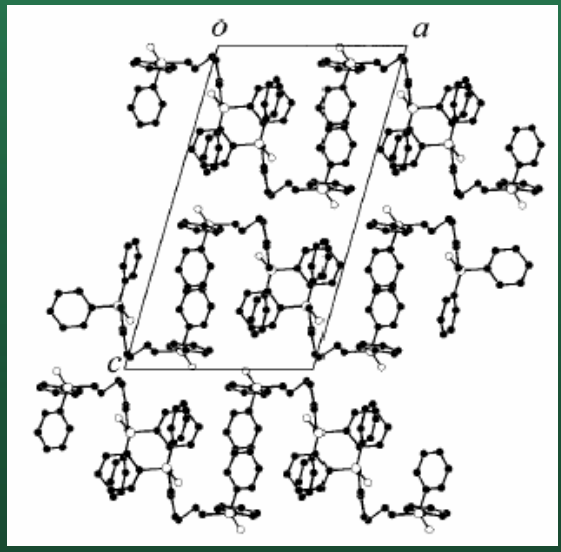

Table 1. Fractional coordinates for the non-hydrogen atoms in the final refined crystal structure of $Ph_2P(O)(CH_2)_7P(O)Ph_2$ ($P2_1/n$; $a = 12.560(1)$, $b = 10.203(1)$, $c = 22.889(2)$ Å, $\beta = 105.53(1)°$).

Atom	x/a	y/b	z/c
C(1)	0.224(2)	0.940(2)	0.6306(5)
C(2)	0.299(3)	0.989(4)	0.6830(6)
C(3)	0.290(3)	0.953(4)	0.7404(5)
C(4)	0.209(3)	0.862(4)	0.7457(7)
C(5)	0.137(3)	0.809(4)	0.694(1)
C(6)	0.146(3)	0.845(3)	0.6361(7)
C(7)	0.205(1)	1.173(1)	0.558(1)
C(8)	0.097(1)	1.223(1)	0.549(2)
C(9)	0.080(2)	1.356(2)	0.557(2)
C(10)	0.171(2)	1.442(1)	0.573(3)
C(11)	0.277(2)	1.394(1)	0.577(2)
C(12)	0.294(1)	1.261(1)	0.570(2)
P(1)	0.227(1)	0.998(1)	0.5565(6)
O(1)	0.144(2)	0.932(2)	0.5067(6)
C(13)	0.366(2)	0.977(1)	0.553(1)
C(14)	0.413(2)	0.844(2)	0.573(1)
C(15)	0.486(2)	0.790(2)	0.536(1)
C(16)	0.509(3)	0.645(2)	0.5459(7)
C(17)	0.562(5)	0.610(2)	0.611(1)
C(18)	0.568(5)	0.464(2)	0.623(1)
C(19)	0.612(3)	0.418(1)	0.687(1)
P(2)	0.628(1)	0.245(1)	0.6950(5)
O(2)	0.542(1)	0.170(2)	0.6507(7)
C(20)	0.766(1)	0.209(3)	0.6889(7)
C(21)	0.782(2)	0.164(4)	0.634(1)
C(22)	0.889(2)	0.147(5)	0.628(1)
C(23)	0.980(1)	0.168(5)	0.677(1)
C(24)	0.965(1)	0.208(5)	0.733(1)
C(25)	0.858(1)	0.226(5)	0.739(1)
C(26)	0.631(2)	0.207(1)	0.7726(6)
C(27)	0.663(4)	0.303(2)	0.8179(6)
C(28)	0.668(4)	0.273(2)	0.8782(6)
C(29)	0.635(4)	0.149(2)	0.8929(7)
C(30)	0.597(4)	0.055(2)	0.847(1)
C(31)	0.596(5)	0.084(2)	0.787(1)

B.M. Kariuki, P. Calcagno, K. D. M. Harris, D. Philp and R.L. Johnston, Angew. Chem. Int. Ed. 1999, 38, No. 6, 831-835.

Structural solution

- Direct methods
  - Pattern decomposition and extraction of integrated intensities
  - Trying to reconstruct the missing information (phase) directly from the pattern
- "Two steps" method:
  - Pattern decomposition and extraction of integrated intensities
  - Determination of the structure by matching measured and calculated intensities
- Rietveld method:
  - Matching between the whole experimental pattern and the pattern built on the basis of a trial structure. Refinement of the structure by least square fitting

Structure solution/refinement

Commercial and free (shareware) software for structure solution and refinement

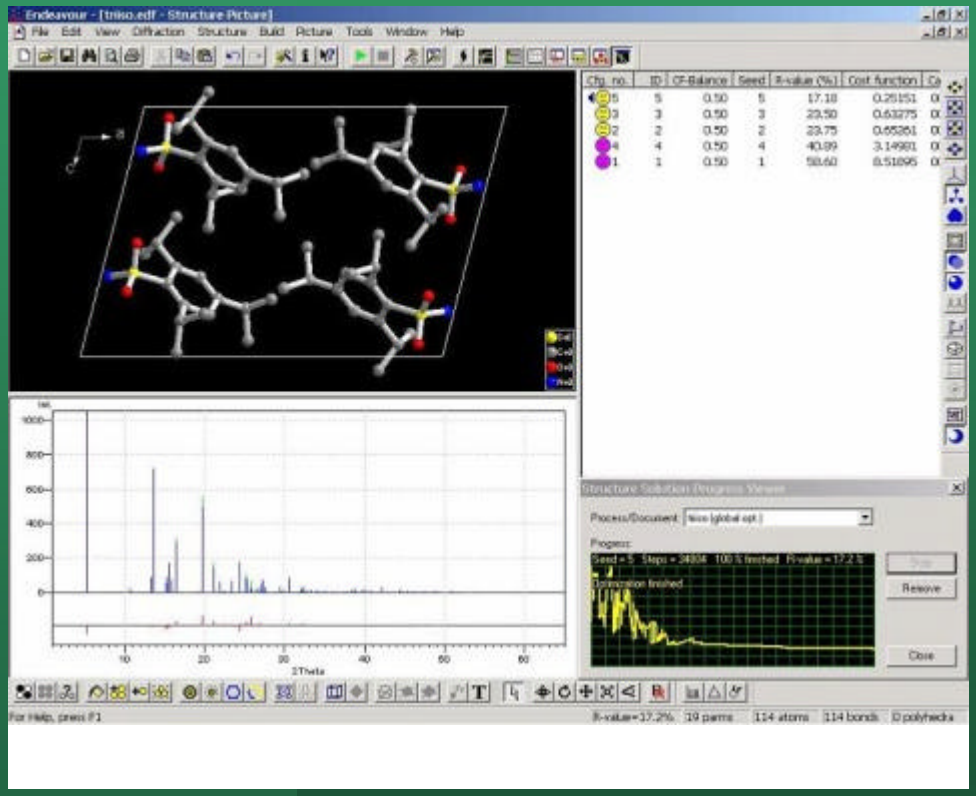

Structural parameters

- Cell symmetry (S.G.)
- Lattice parameters
- Atomic coordinates
- Bond angles and distances
- Site occupancy
- Thermal factors

Rietveld method can be used:
parameters of a synthetic pattern are refined against measured data

Amorphous materials

Radial distribution function

The long-range order typical of crystalline structures is absent in amorphous materials. However, a certain degree of short-range order is always present.

Diffraction can be used to measure the ***radial distribution function***, i.e., the probability distribution to find an atom at a distance between r and $r+dr$ taken from a reference atom.

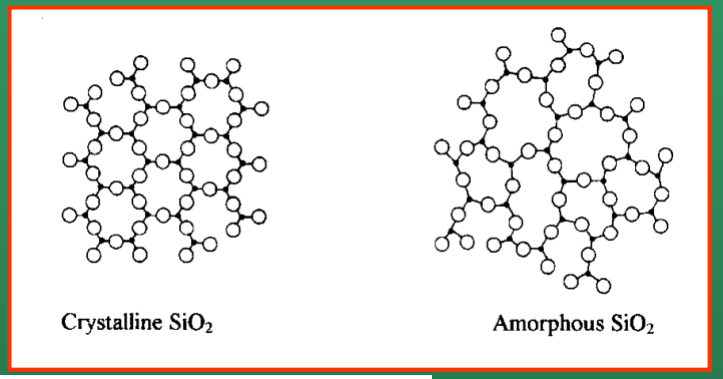

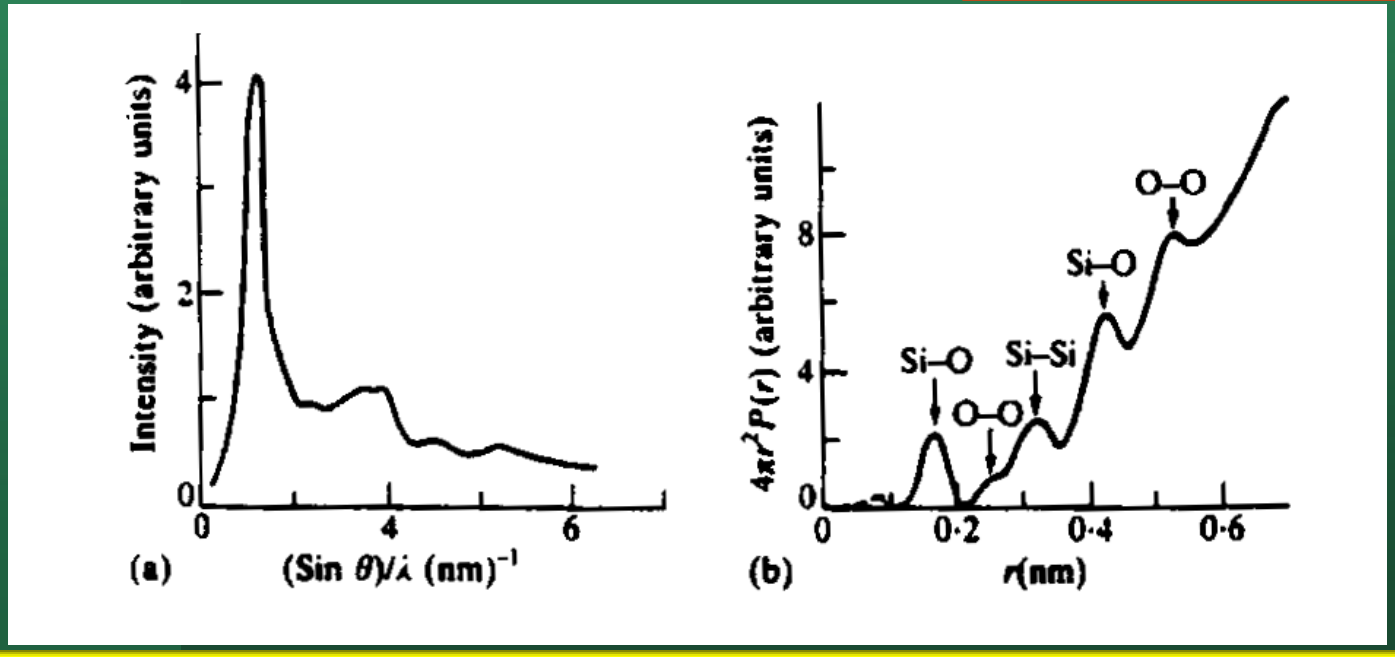

Amorphous content

Amorphous content

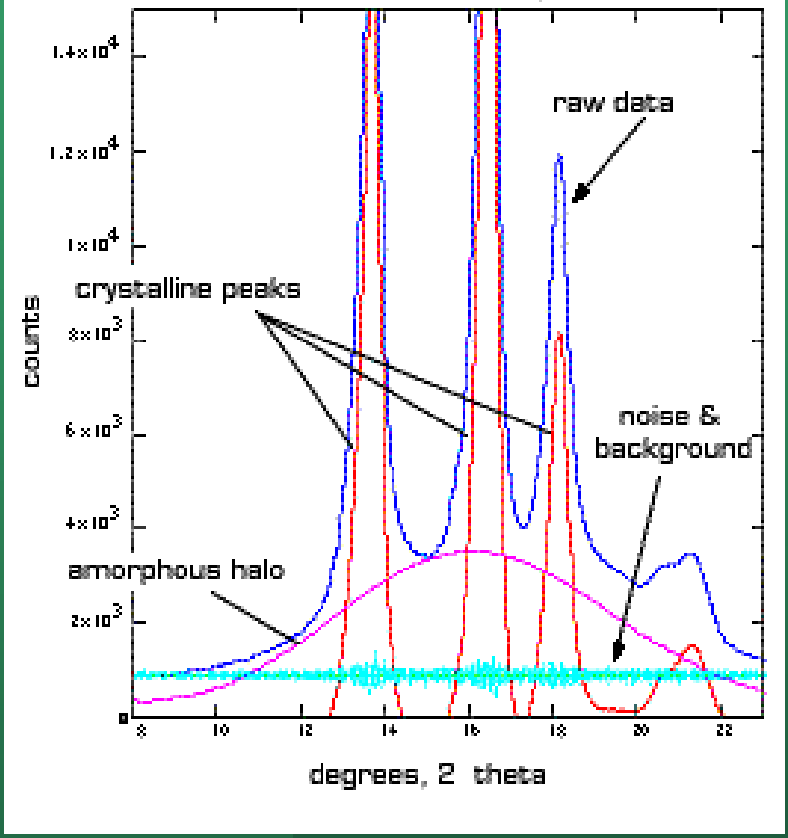

In a diffraction pattern both the amorphous halo and the crystalline peaks can be simultaneously present above the background (50% crystalline polymeric material).

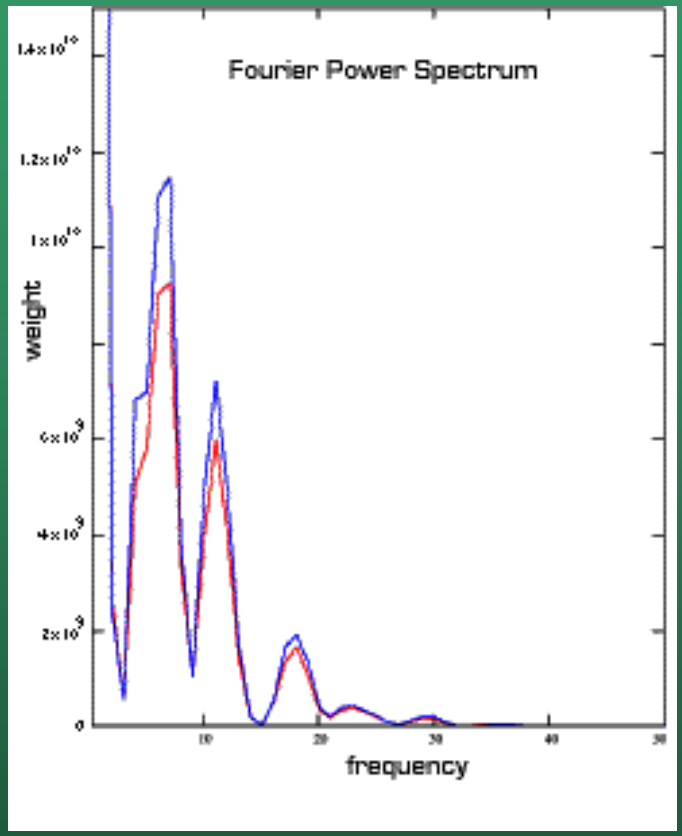

Fourier Power Spectrum of two samples with different percentage crystallinity showing the amorphous and crystalline frequency bands.

Corundum + amorphous silica

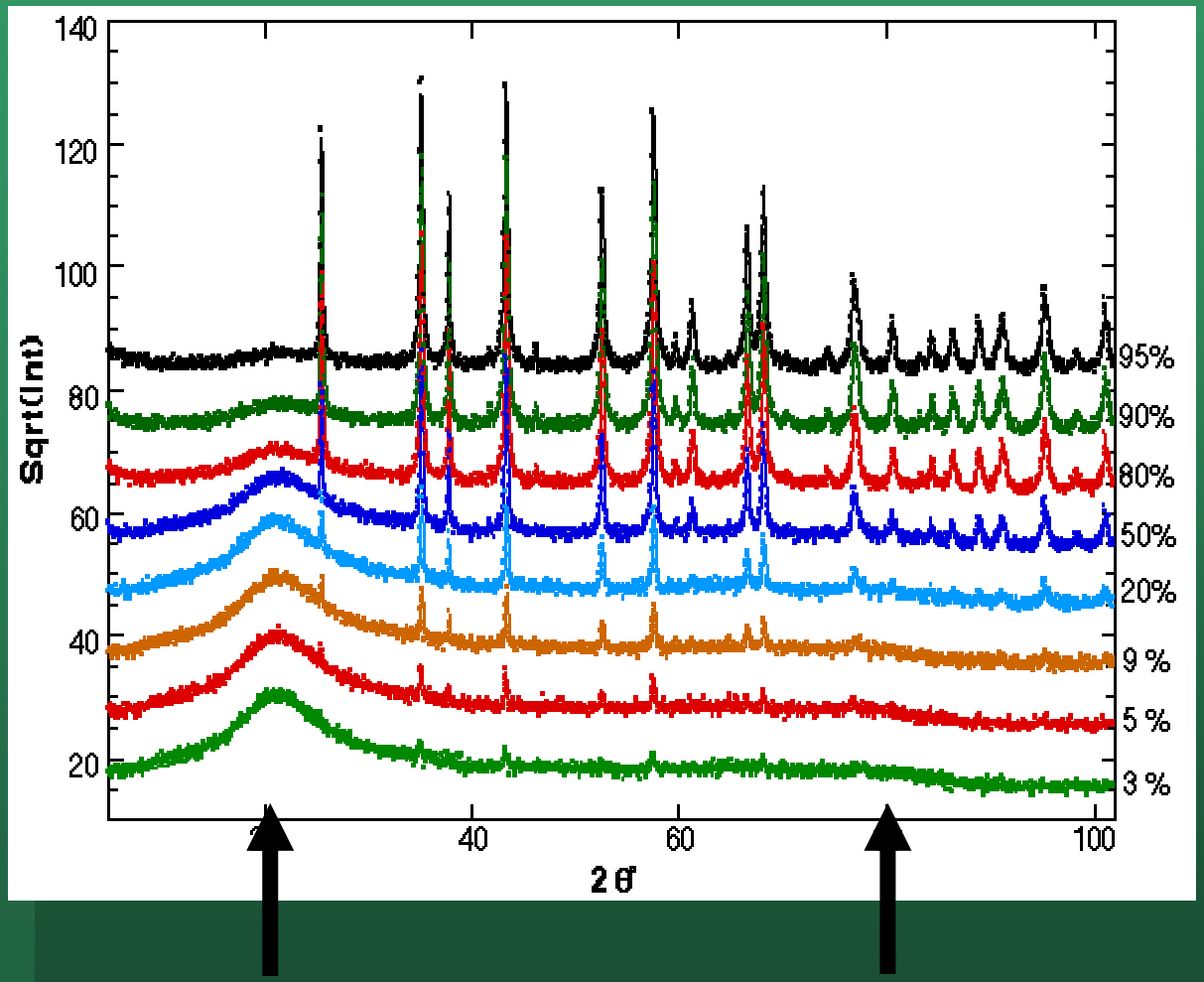

amorphous bands typical of a glassy phase

Amorphous phases: QPA and crystallinity

Modeling of amorphous and crystalline peaks allows obtaining the **fraction of amorphous phase** in mixtures.

Diffraction can also measure the **degree of crystallinity** in partly-crystalline materials, like polymers or glass-ceramics.

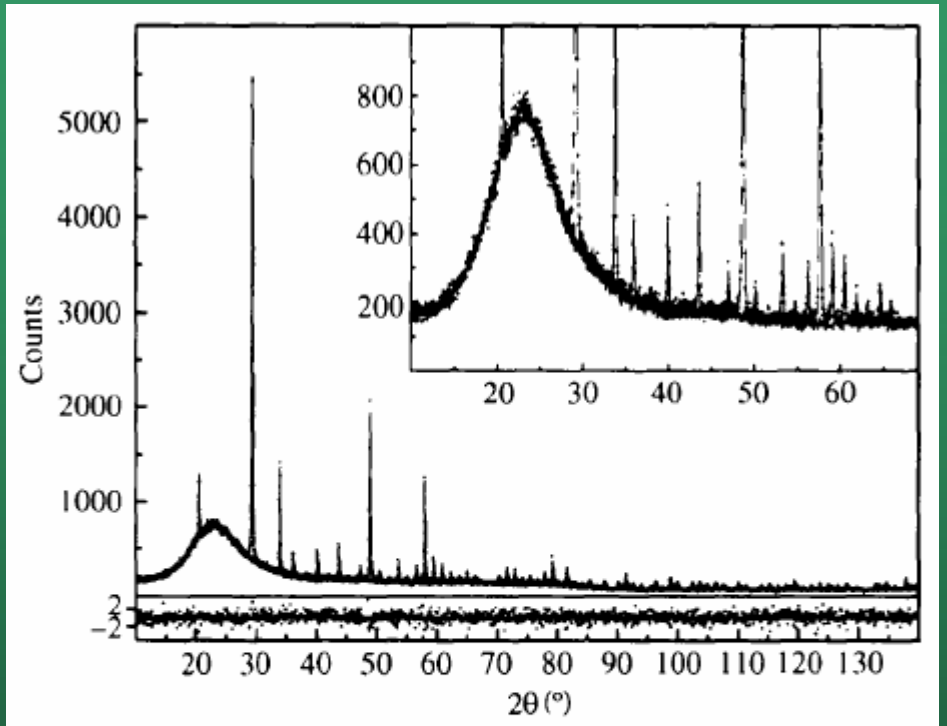

Fig. 1. Rietveld analysis of sample C (Y_2O_3/amorphous silica with weight ratio 10:90) with air scattering subtracted. In the inset, which shows an enlargement, the experimental noise of the amorphous scattering used in the fitting is evident. At the bottom, the weighted residuals are reported. Because of the noise in the amorphous pattern, the normalized residuals are defined as $\Delta Y_i(\text{weighted}) = (Y_{oi} - Y_{ci})/[Y_{oi} + (K^{am})^2 Y^{am}]^{1/2}$ and consequently the goodness of fit is $S^2 = \{\sum[\Delta Y_i(\text{weighted})]^2\}/(N - P) = 1.3$.

P. Riello, P. Canton, G. Fagherazzi, J. Appl. Cryst. 1998, 31, 78-82.

Microstructural analysis

Line profile analysis

Profile information extracted as FWHM or Integral Breadth (β)

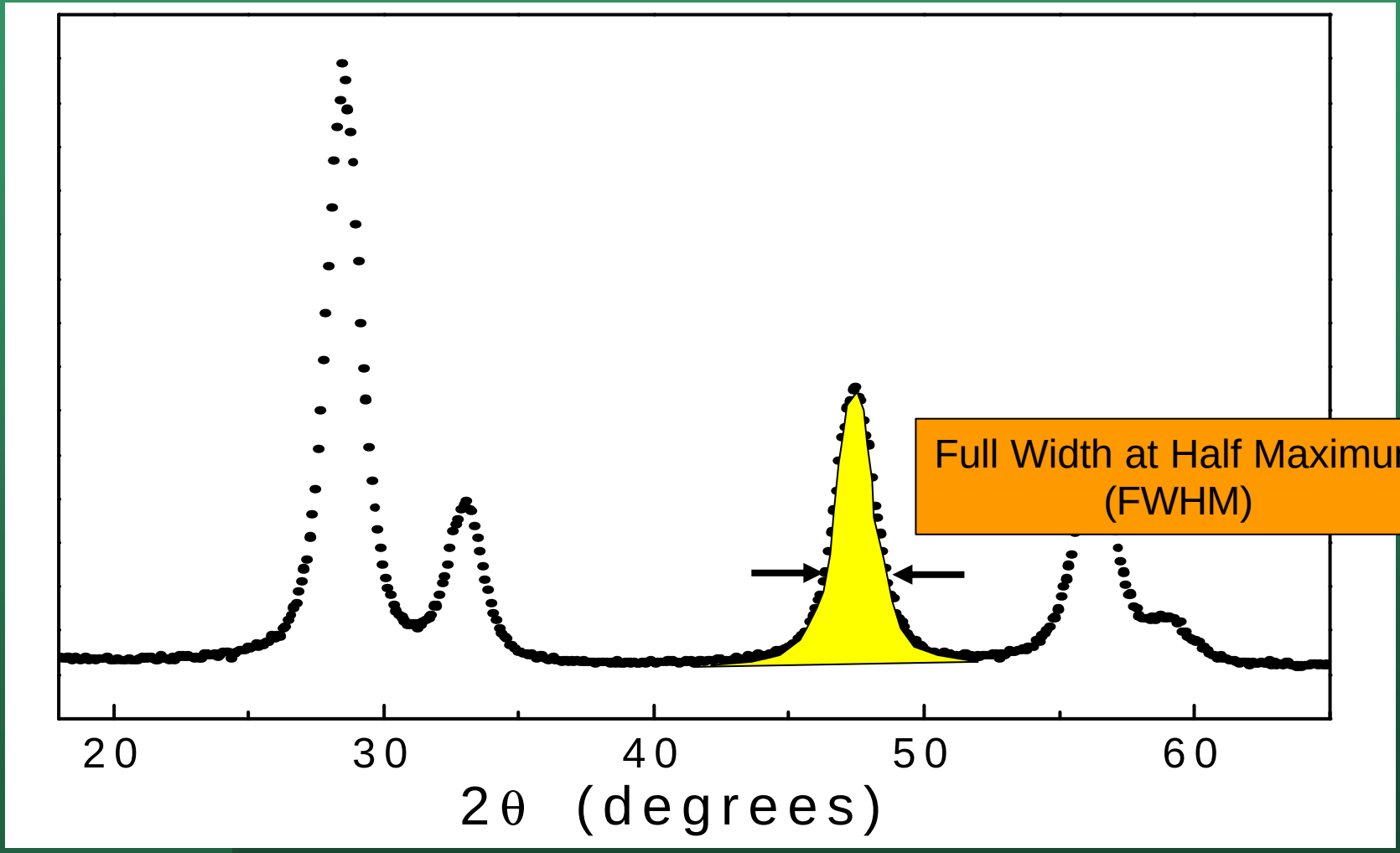

Line profile analysis

Traditional methods are based on the study of the integral breadth of X-ray peaks:

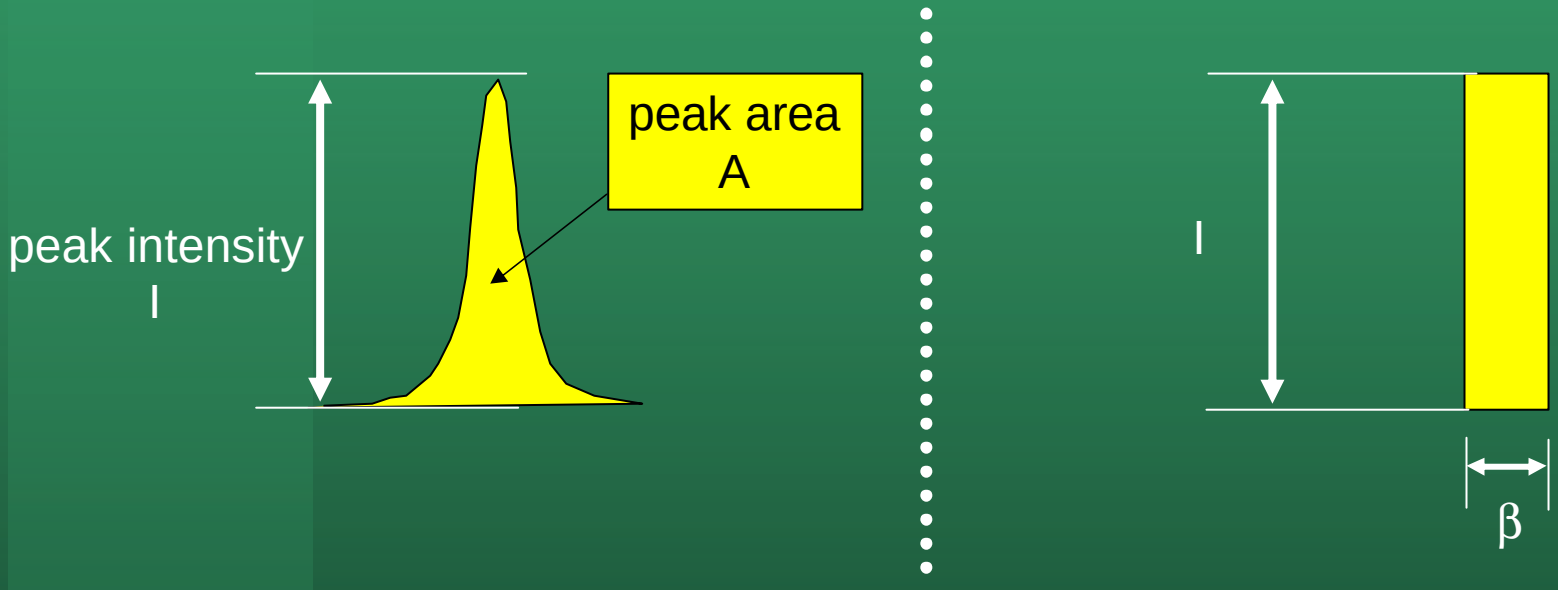

integral breadth (width of equivalent rectangle)

$$b = \frac{A}{I}$$

Line profile analysis

It is possible to correlate the integral breadth with the size L of the coherently diffracting domains (Scherrer formula):

reciprocal space

$$b\left(d^*\right)=\frac{K_b}{L}$$

2q space

$$b\left(2q\right)=\frac{K_b\, l}{\cos q\cdot L}$$

$$\frac{l}{d^*}=2\sin q \quad \Rightarrow \quad dd^*=\frac{\cos q}{l}d2q \quad \Rightarrow \quad d2q=\frac{l}{\cos q}dd^*$$

The constant K_β is related to the shape of the domains and is of the order of magnitude of 1

Line profile analysis: traditional methods

Considering multiple peaks, a trend can be found

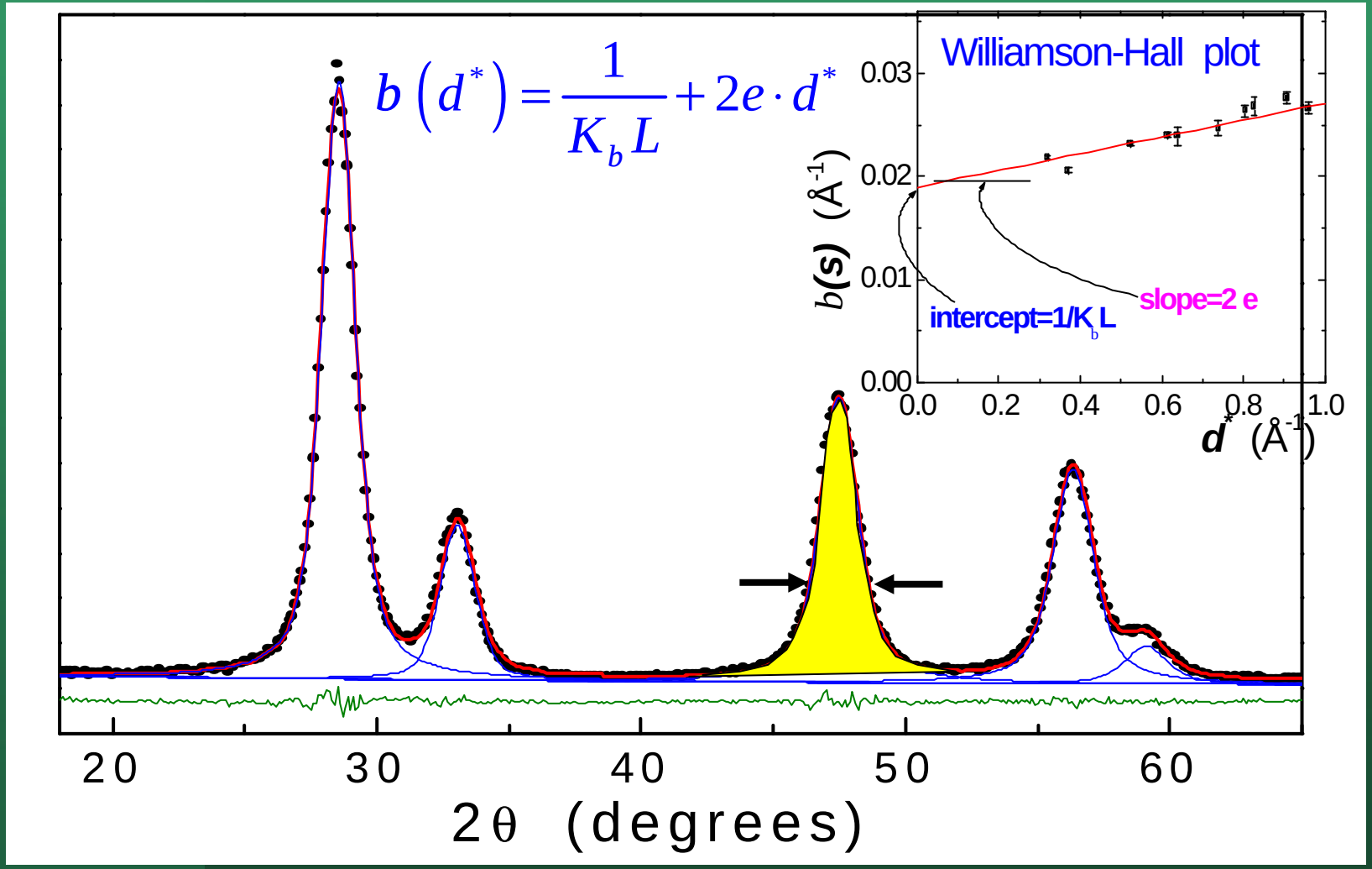

Alternative advanced methods: WPPM

Alternative exists where the whole X-ray diffraction pattern is analysed in terms of physical models of the microstructure

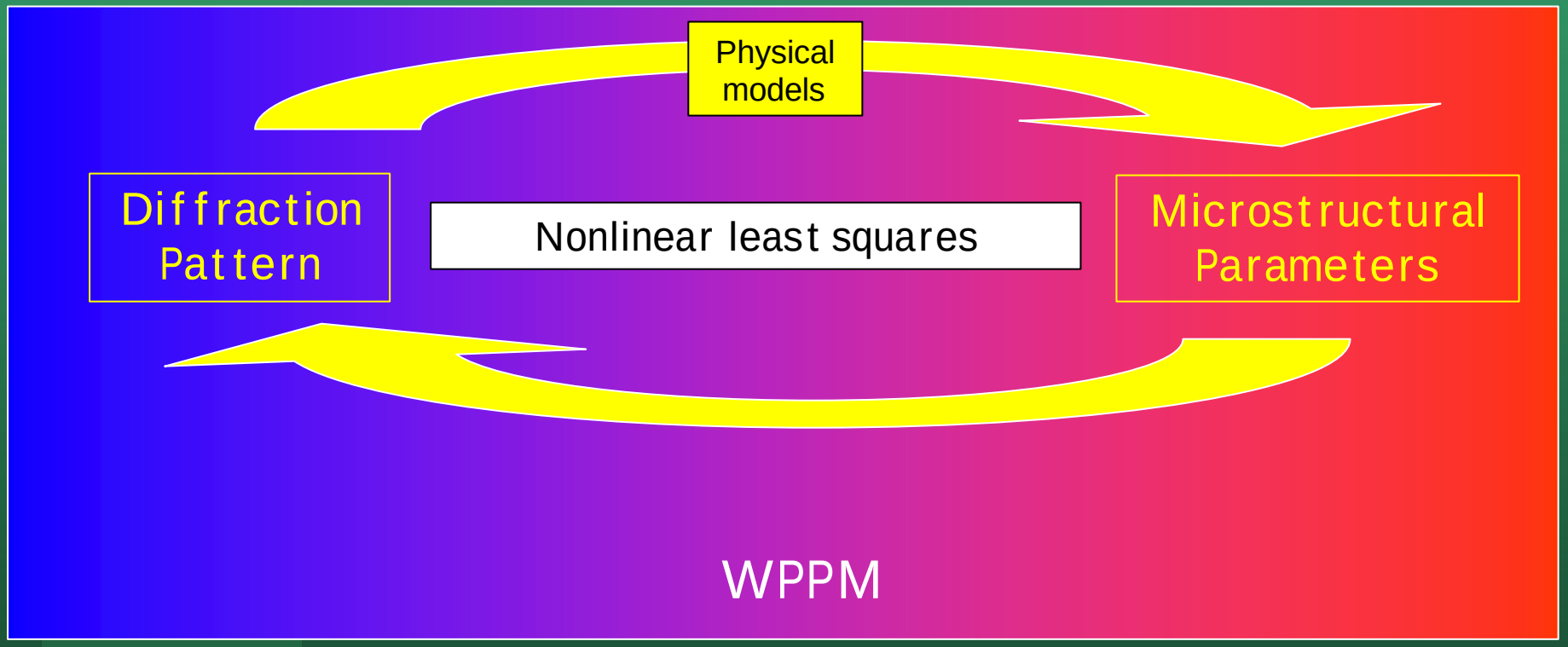

It is a self-consistent one-step procedure: fine details in the pattern can be unveiled

Alternative advanced methods: WPPM

$$I_{\{hkl\}}\left(d^*, d^*_{\{hkl\}}\right) = k\left(d^*\right)\cdot\sum_{hkl} w_{hkl}\int_{-\infty}^{\infty}\mathbb{C}_{hkl}(L)\exp\left(2p\,iL\cdot s_{hkl}\right)dL$$

Diffraction profiles result from a convolution of effects.

Therefore, Fourier Transforms of the various effects are multiplied:

$$T_{pV}^{IP}\cdot A_{\{hkl\}}^{S}\cdot A_{\{hkl\}}^{D}\cdot\left(A_{hkl}^{F}+iB_{hkl}^{F}\right)\cdot A_{\{hkl\}}^{APB}\cdot\left(A_{hkl}^{GSR}+iB_{hkl}^{GSR}\right)\cdot\left(A_{hkl}^{CF}+iB_{hkl}^{CF}\right)\cdot\ldots$$

Instrumental Profile

Domain size

Dislocations

Faulting

APB

Grain surface relaxation

Stoichiometry fluctuations

Instrumental Profile, Domain Size, Dislocations, Anti-Phase Domain terms are real functions of *L* (Fourier length), whereas Faulting, Grain Surface Relaxation and fluctuations in the composition give complex (A+iB) contributions

Additional line broadening sources can be included by adding (multiplying) corresponding FTs

WPPM application: nanocrystalline ceria

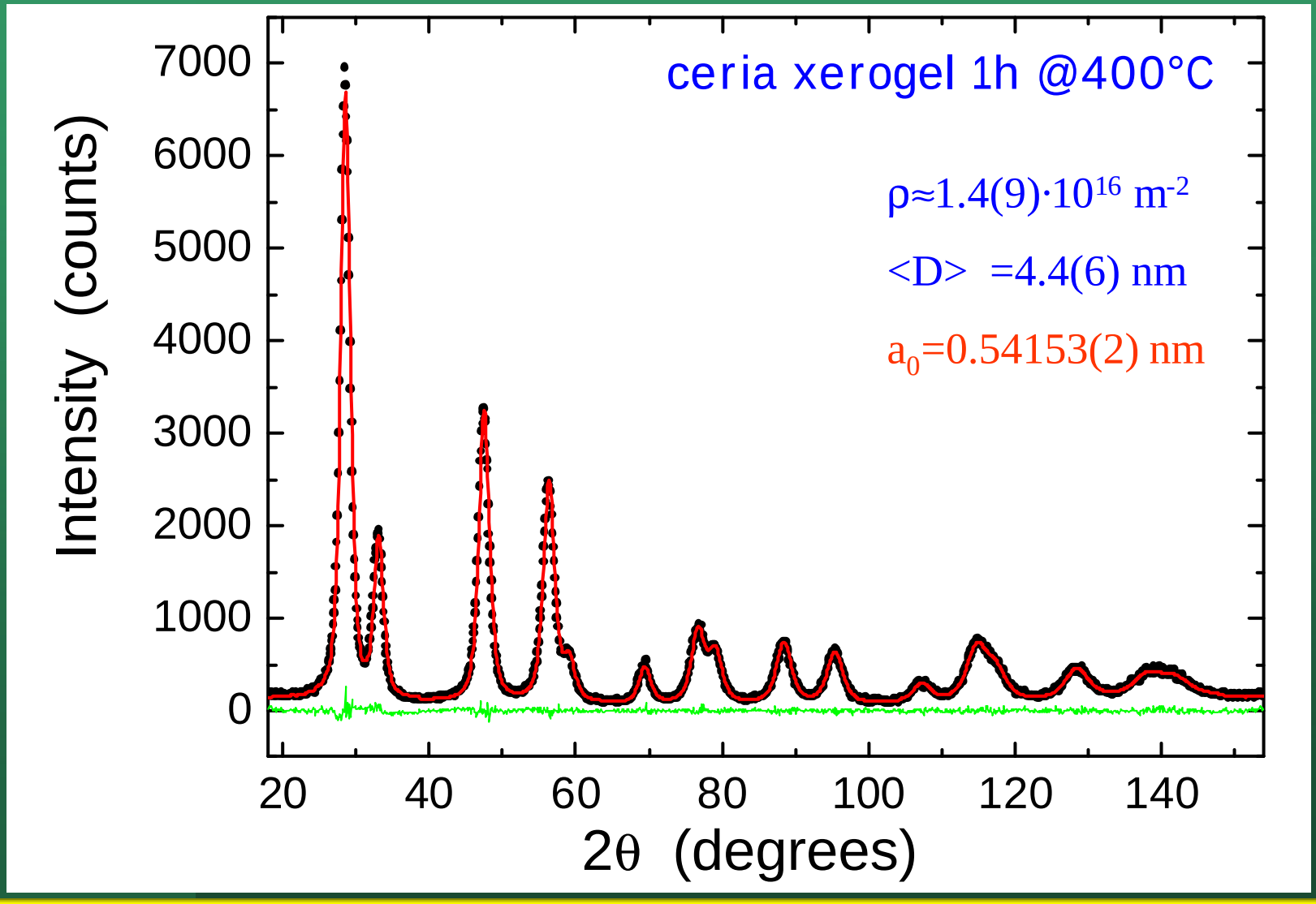

WPPM application: nanocrystalline ceria

Nanocrystalline cerium oxide from sol-gel route

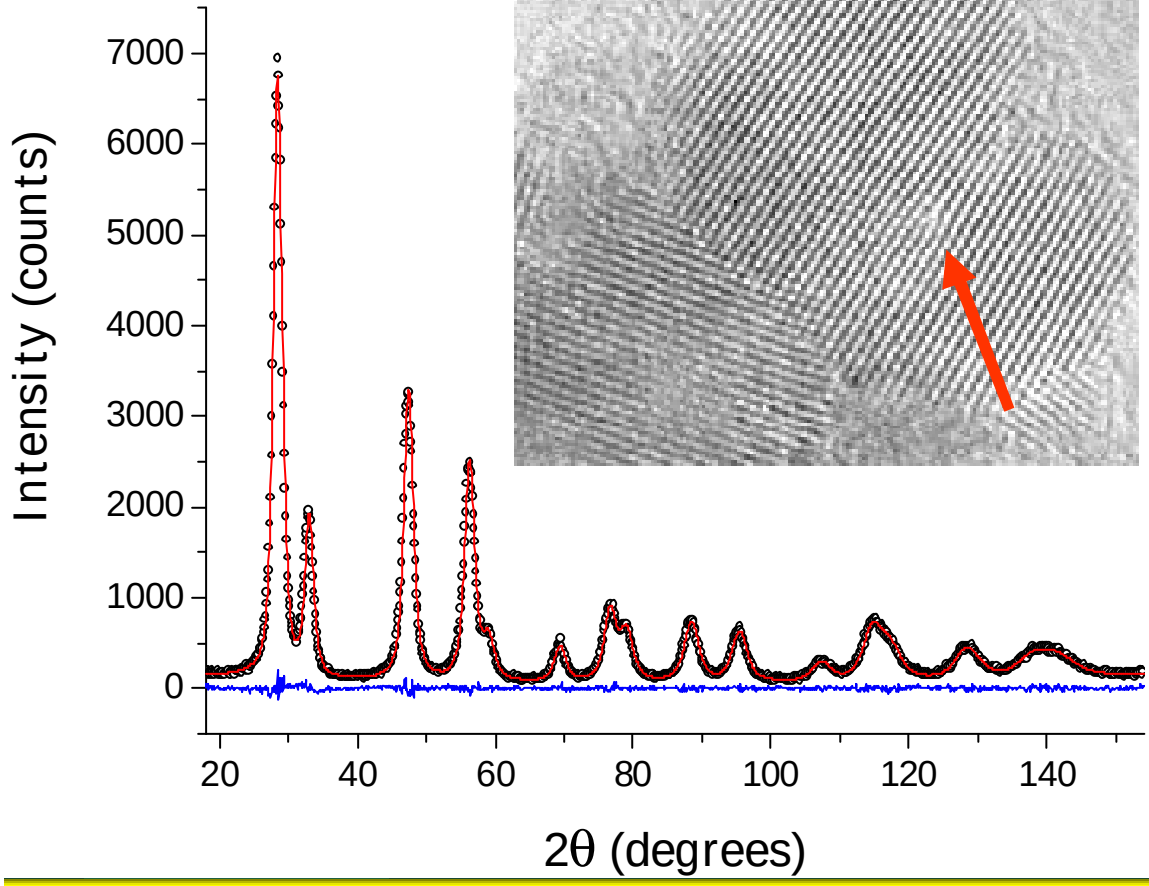

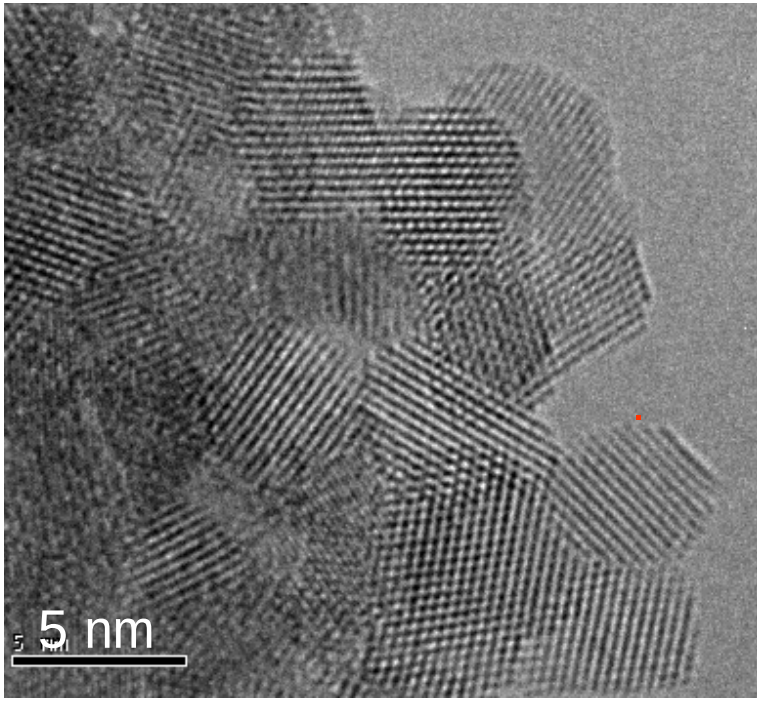

WPPM application: nanocrystalline ceria

Nanocrystalline cerium oxide from sol-gel route

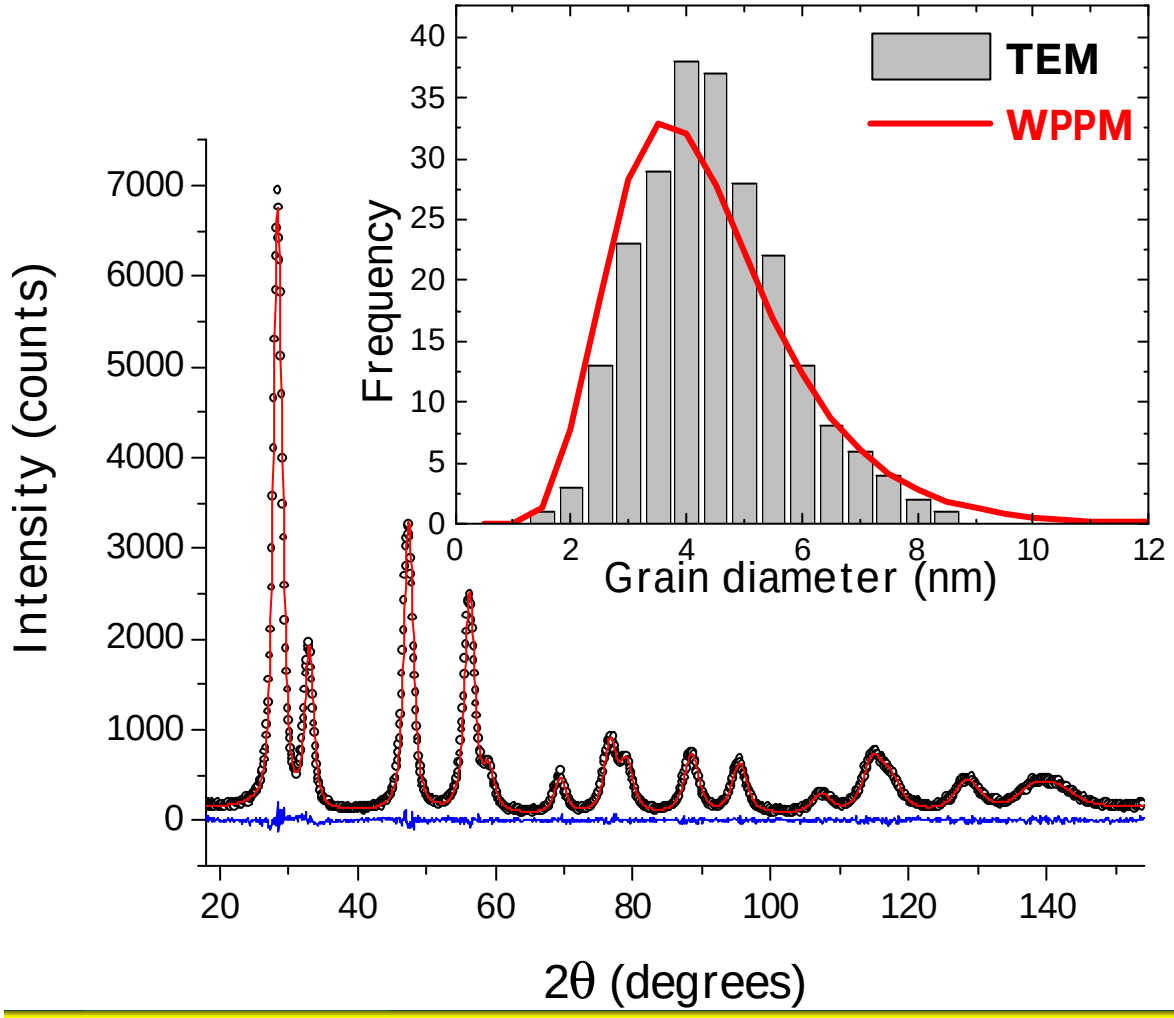

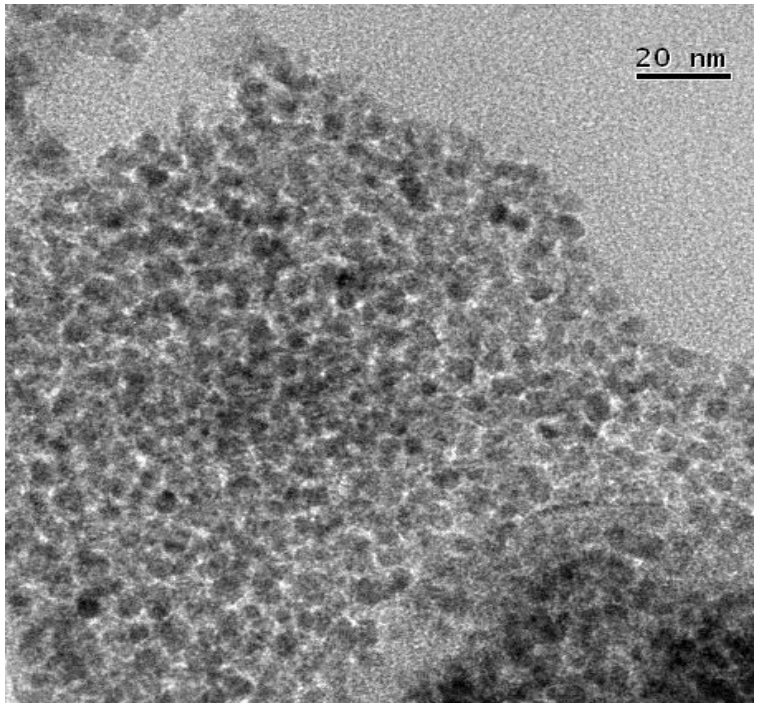

Residual stress analysis

Residual stresses

Why residual stresses?

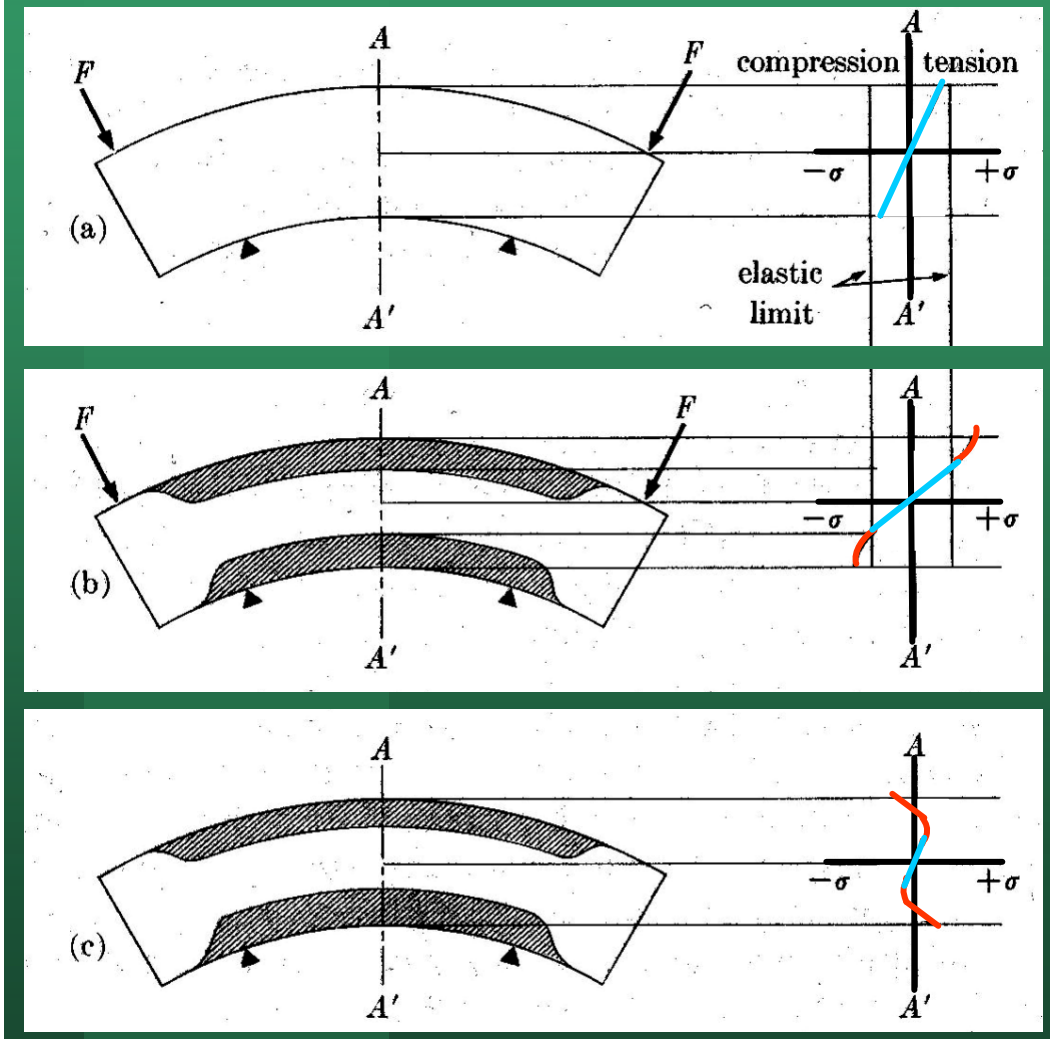

Residual stress by plastic flow in bending:

(a) loaded **below** elastic limit

(b) loaded **above** elastic limit

(c) unloaded

Shaded regions have been plastically deformed

Source: B.D. Cullity "Elements of X-ray diffraction" II Edition. Addison-Wesley. Reading (1978)

Residual stress

Tempered glass

glass sheet

rapid cooling

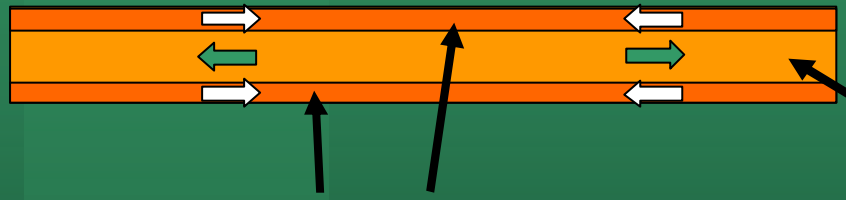

Surface under compression

Core under tension

The cold surface is drawn into compression by the core ("trapped" and slowly cooling)

Stress is present without external load

Residual stresses induced by tempering contributes to enhance the resistance of glass to cracking

Load – stress - strain

In most cases we cannot measure stress directly (unless we are in simple cases where a known force is applied to a known surface area). How we can solve the problem?

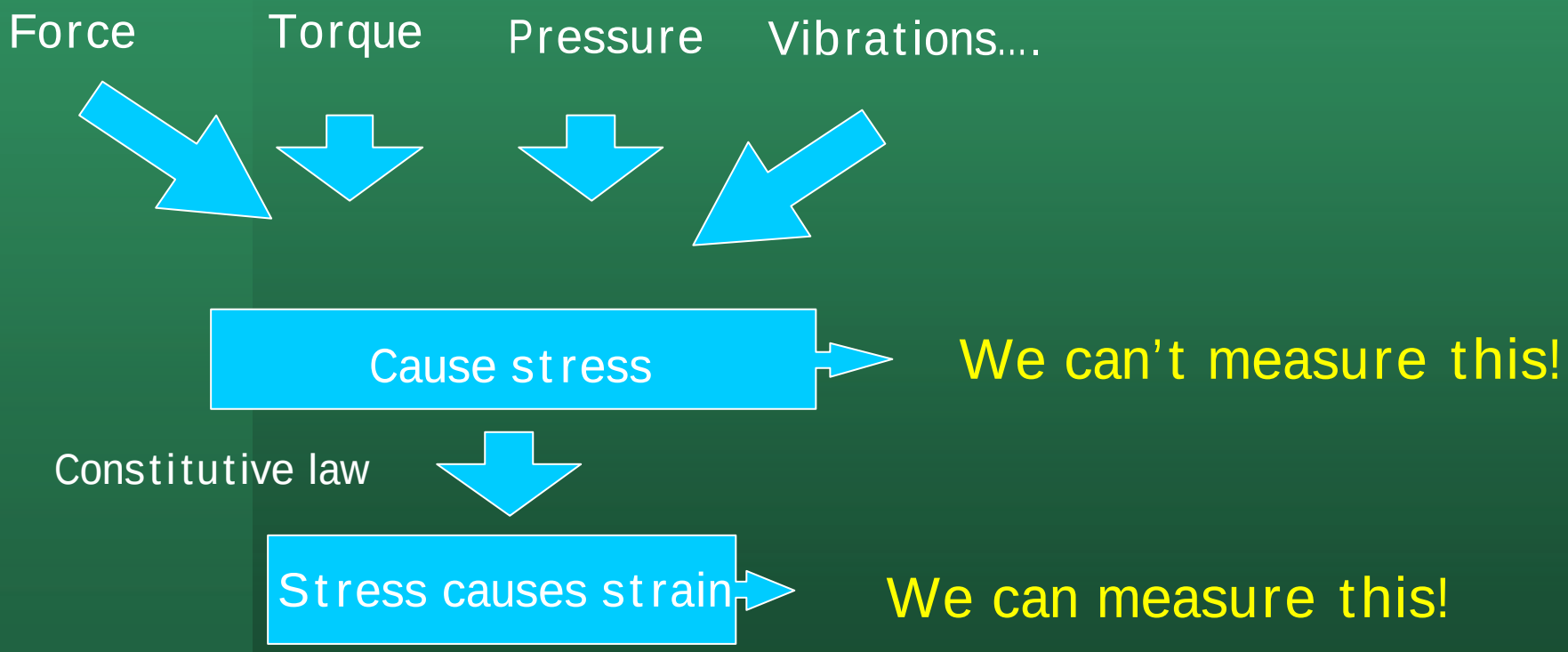

Residual stress analysis

Crystalline domains can be used as strain gauges

grain deformation

$$e = \frac{\Delta l}{l}$$

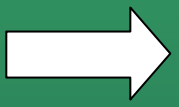

lattice deformation

$$e = \frac{\Delta d}{d}$$

The deformation is measured along different directions, by tilting the sample.
The in-plane strain is obtained by measuring *d* along off-plane directions.

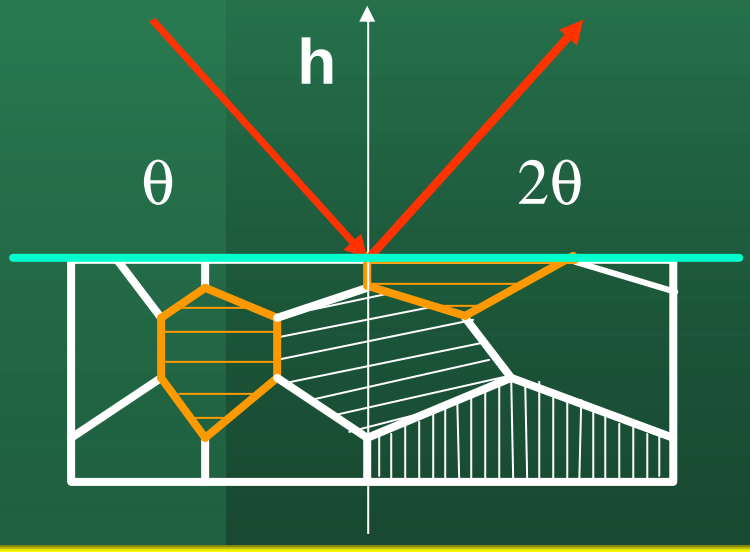

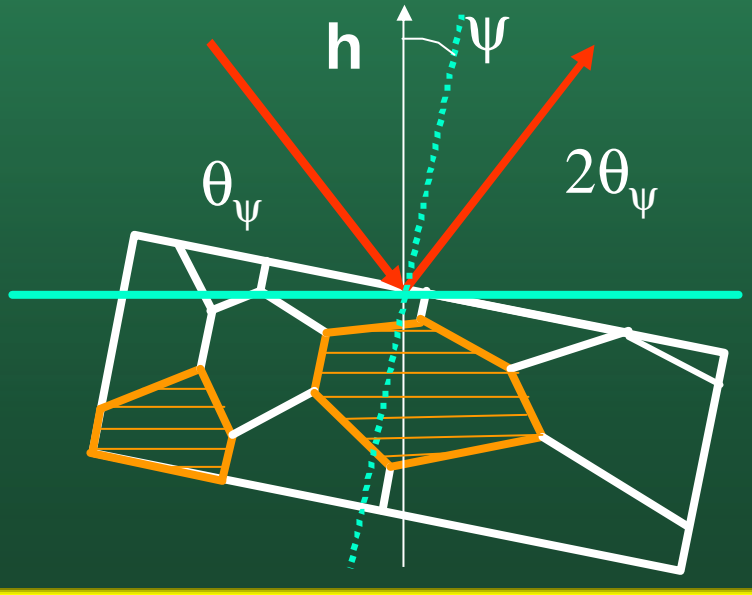

Measurement principle

We need therefore additional movements for the specimen, with respect to the traditional Bragg-Brentano setup

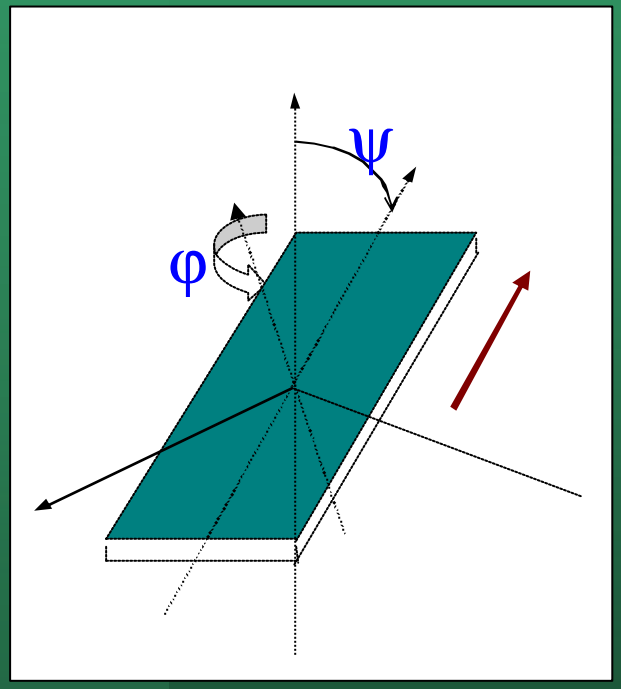

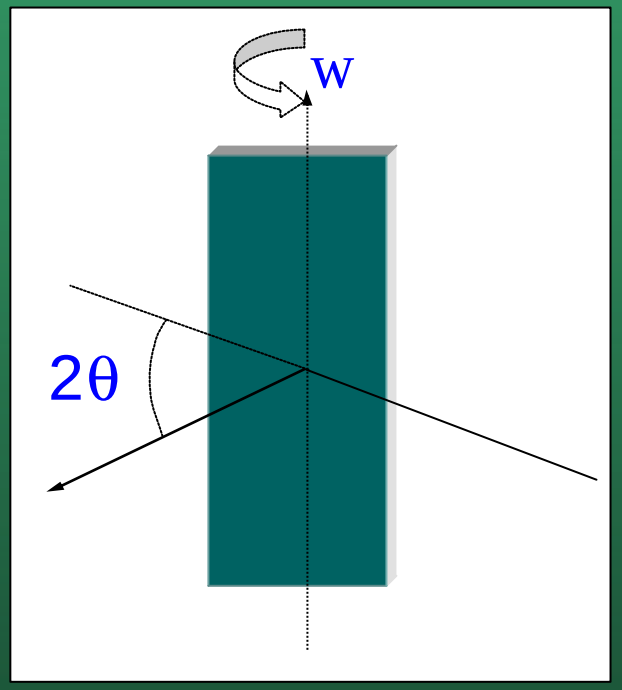

The sample should be tilted/rotated along its three axes.

XRSA diffractometer

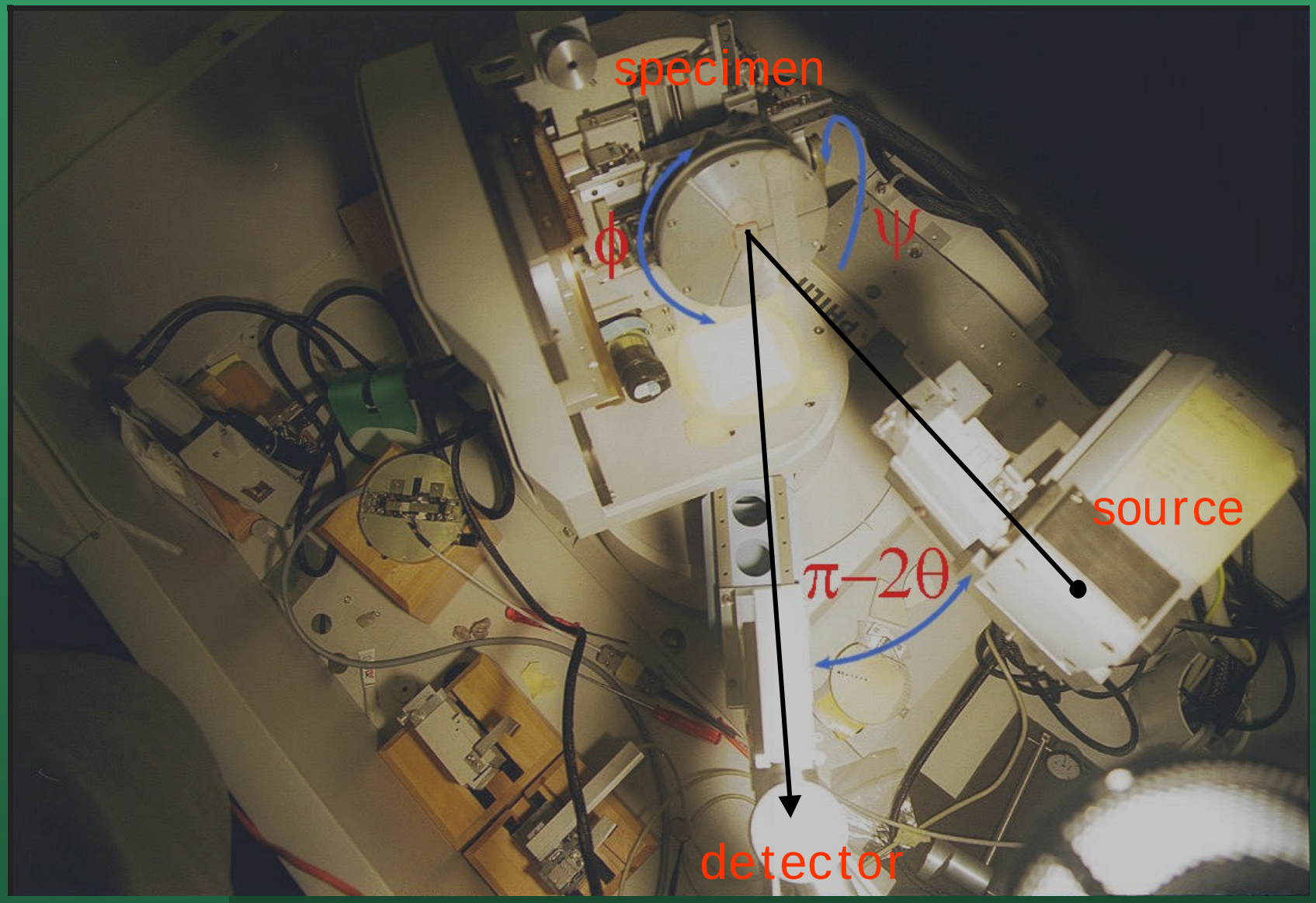

Residual stress analysis

If the stress field is plane and rotationally symmetric:

$\sigma_{11}=\sigma_{22}=\sigma_{||}$, $\sigma_{12}=\sigma_{13}=\sigma_{23}=\sigma_{33}=0$

and if no gradient and no texture are present, then:

$$< e_y^{hkl} >= \left(2S_1^{hkl} + \tfrac{1}{2} S_2^{hkl} \sin^2 y \right) s_{||}^{S}$$

"sin²ψ formula"

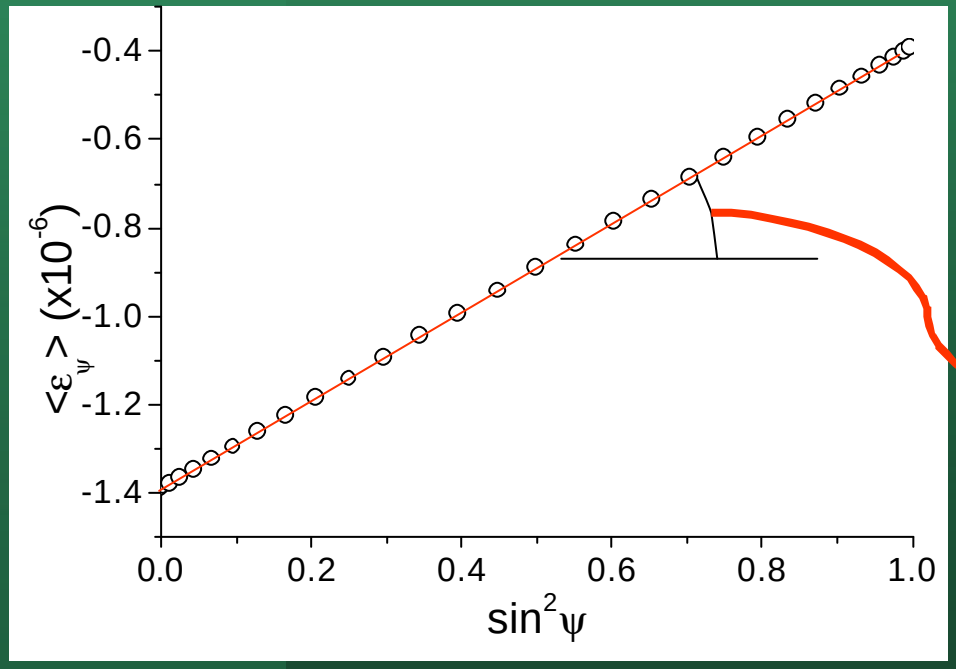

S_1^{hkl}, $\tfrac{1}{2} S_2^{hkl}$

X-ray elastic constants (XECs)

slope related to the average *in-plane* stress

Coated piston head

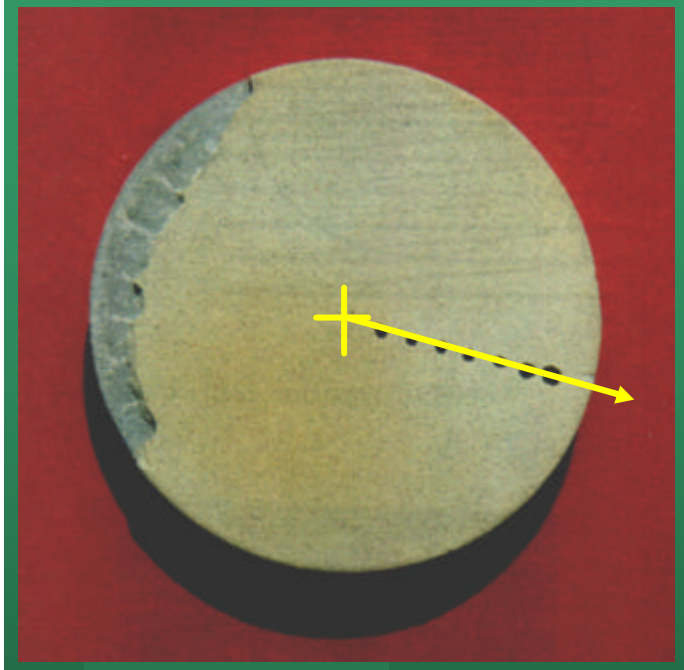

After the burner rig test the component failed starting from the rim.

How does failure occur?

measurement conducted along the yellow line on a laboratory diffractometer

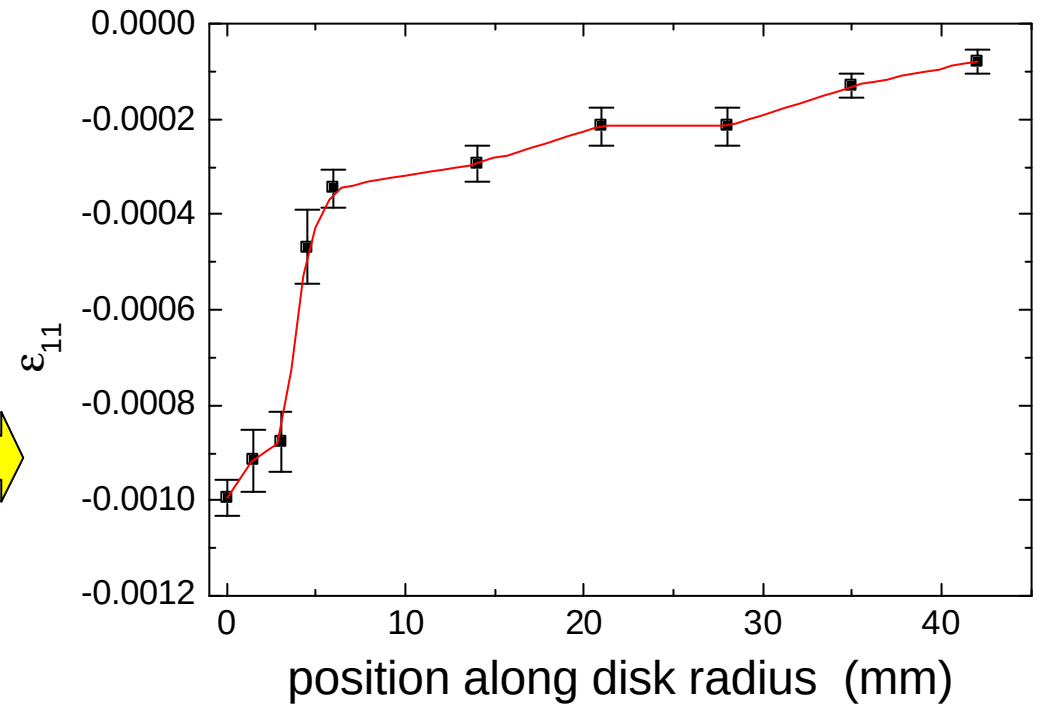

Texture analysis

Crystallographic texture

A ‘true’ powder has randomly oriented crystalline domains.
The diffracted intensity does not depend on the probing direction.

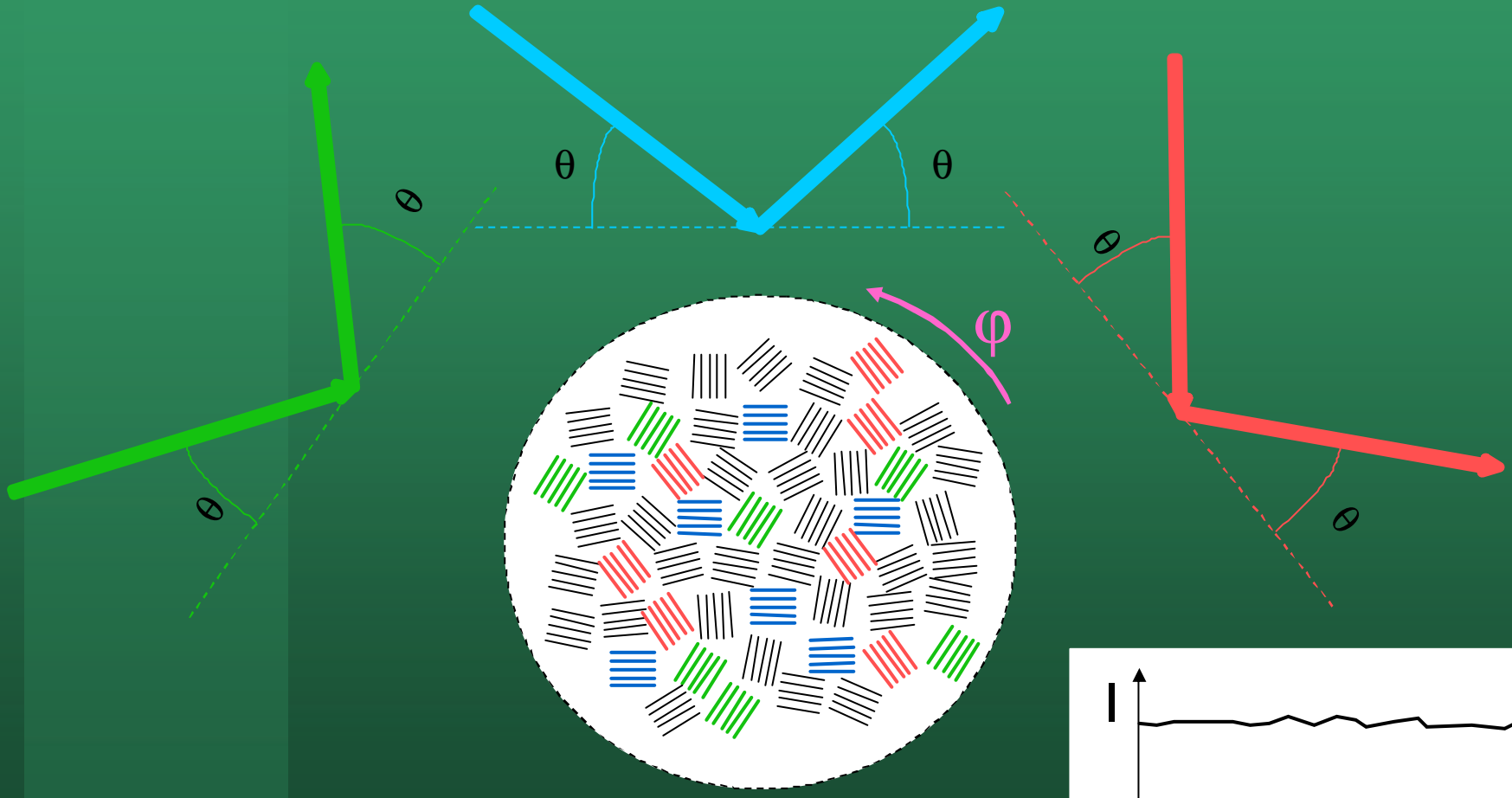

for any *hkl*

random orientation

Crystallographic texture

If crystalline orientation is not random, the diffracted signal depends on the incident angle.

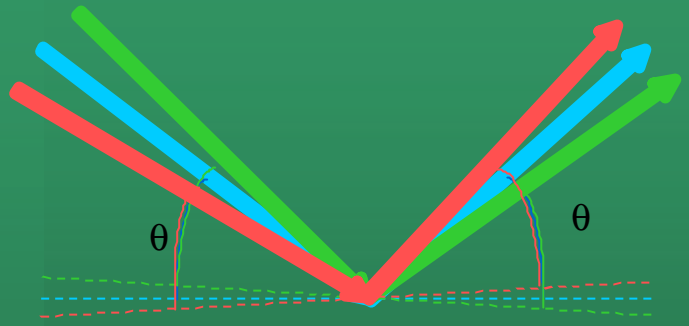

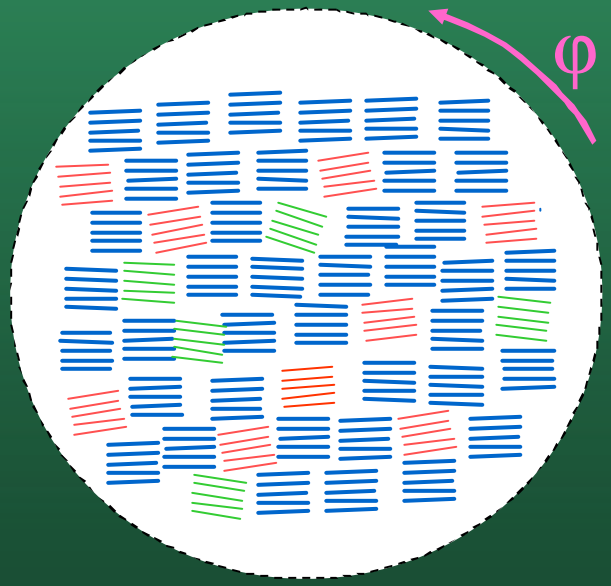

preferred orientation

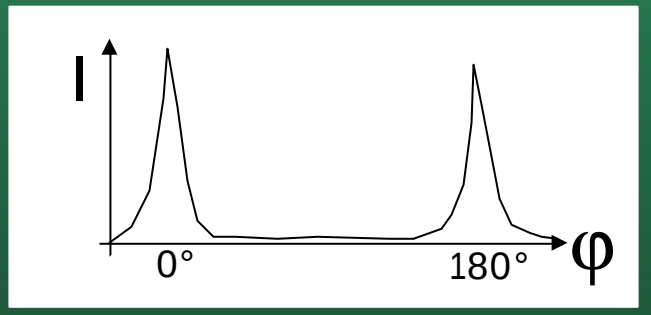

Stereographic projection: old cartography

The information can be reported on suitable maps: pole figures. The stereographic projection is adopted

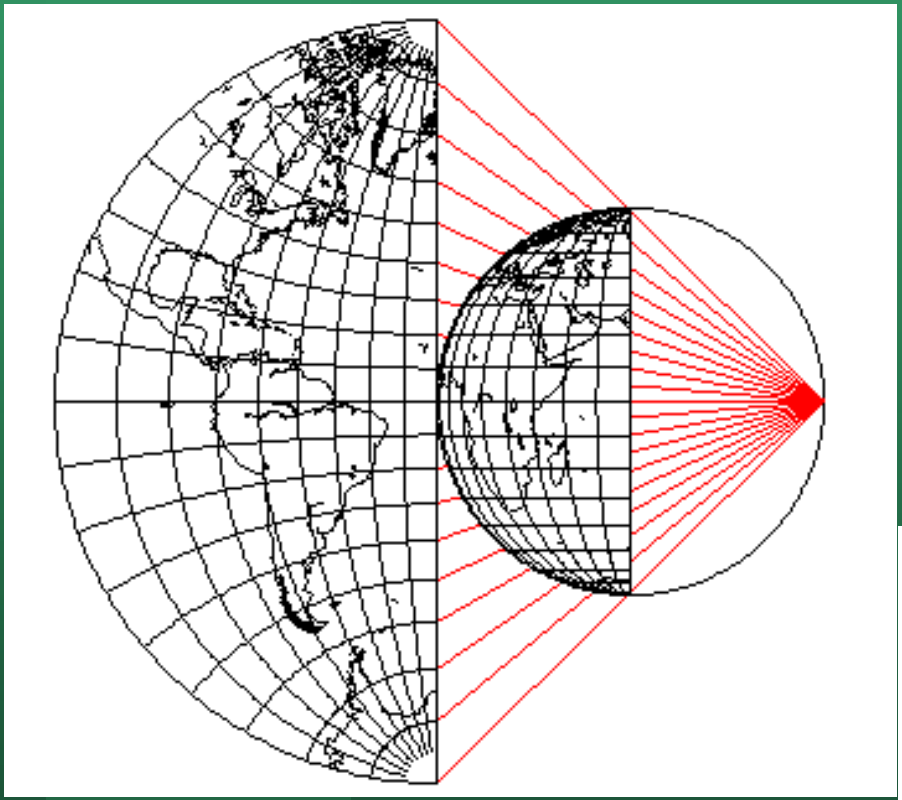

Two angles are used in the projection

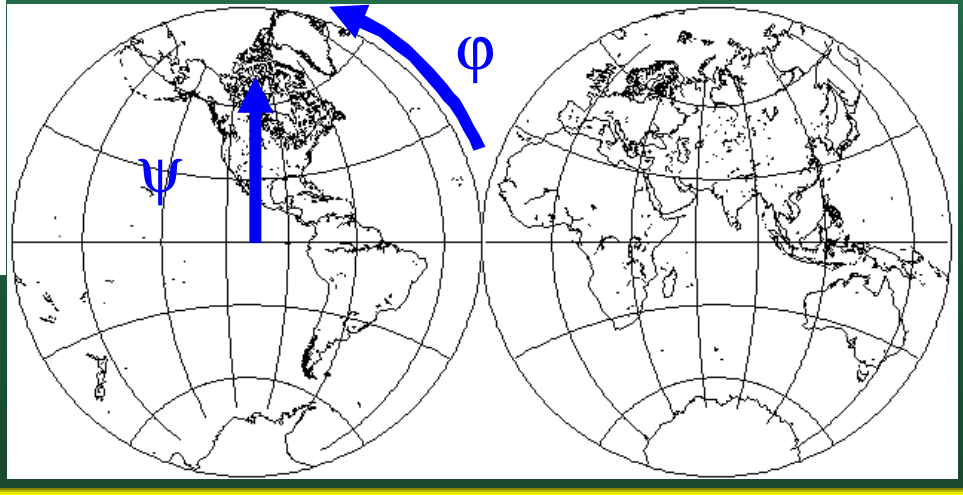

Laboratory instrument: PANalytical X'Pert MRD

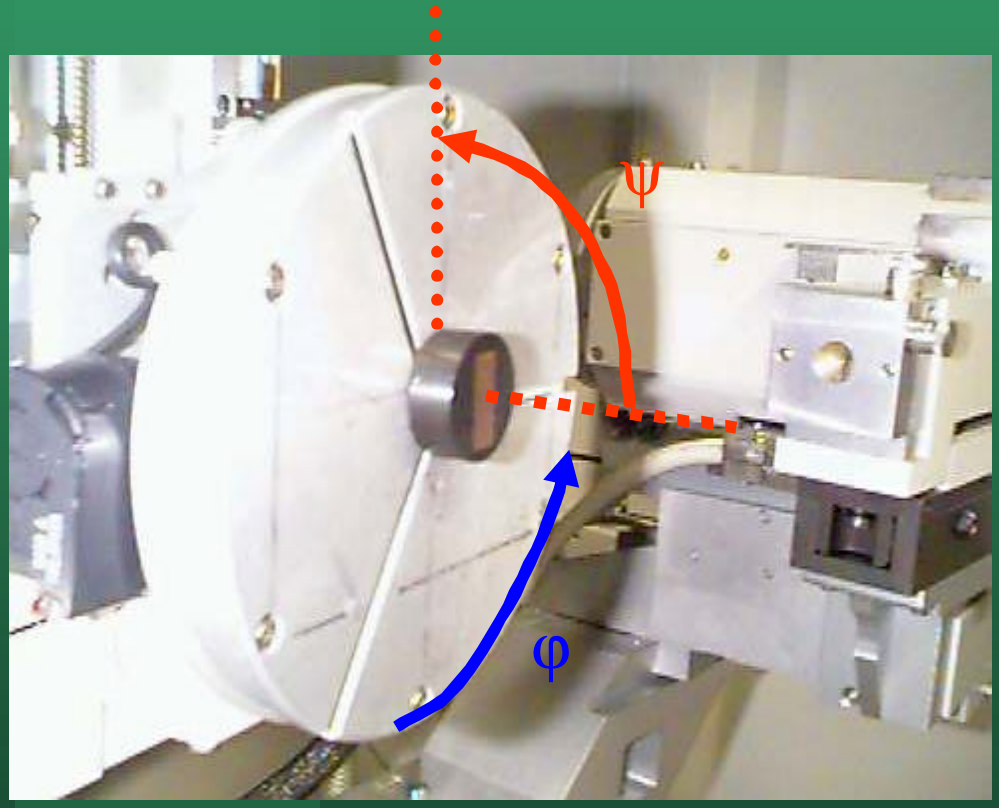

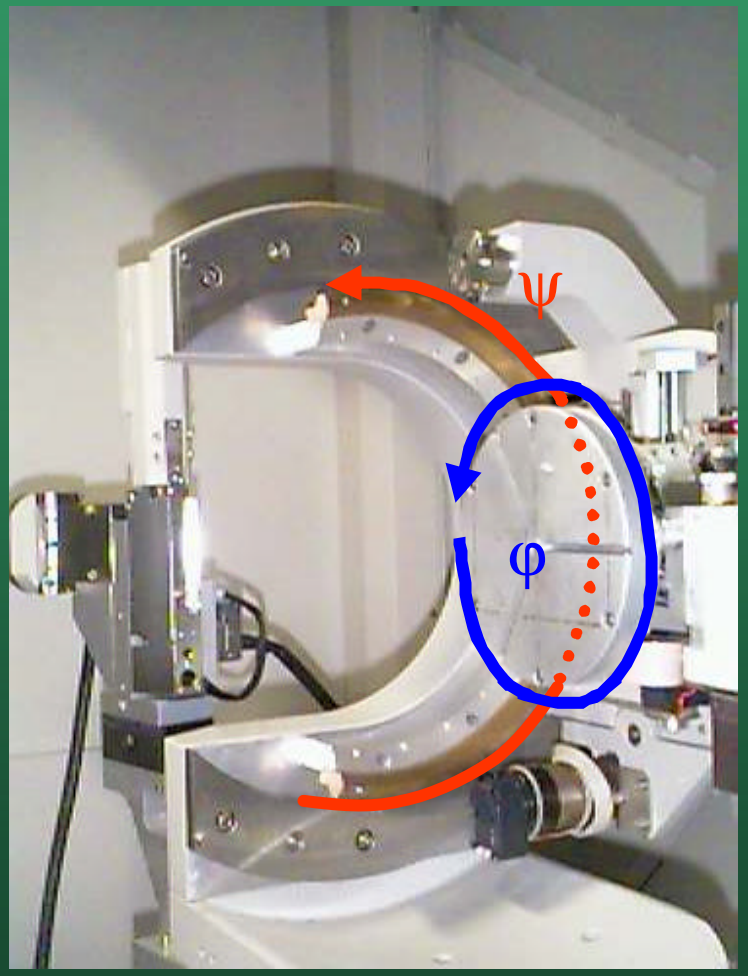

Synchrotron instrument: SRS station 2.3

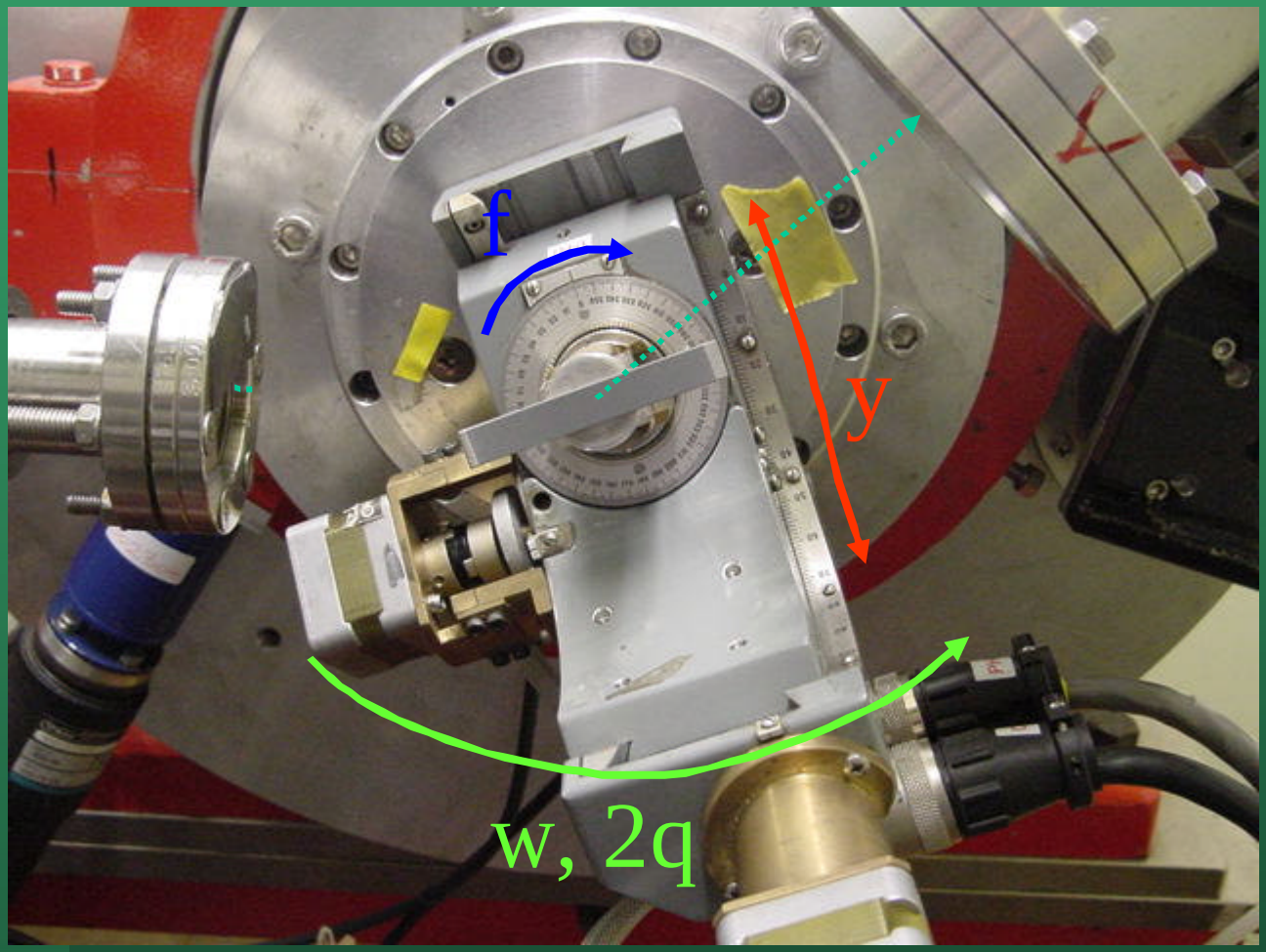

Eulerian cradle for stress/texture measurement

Crystallographic texture: pole figures

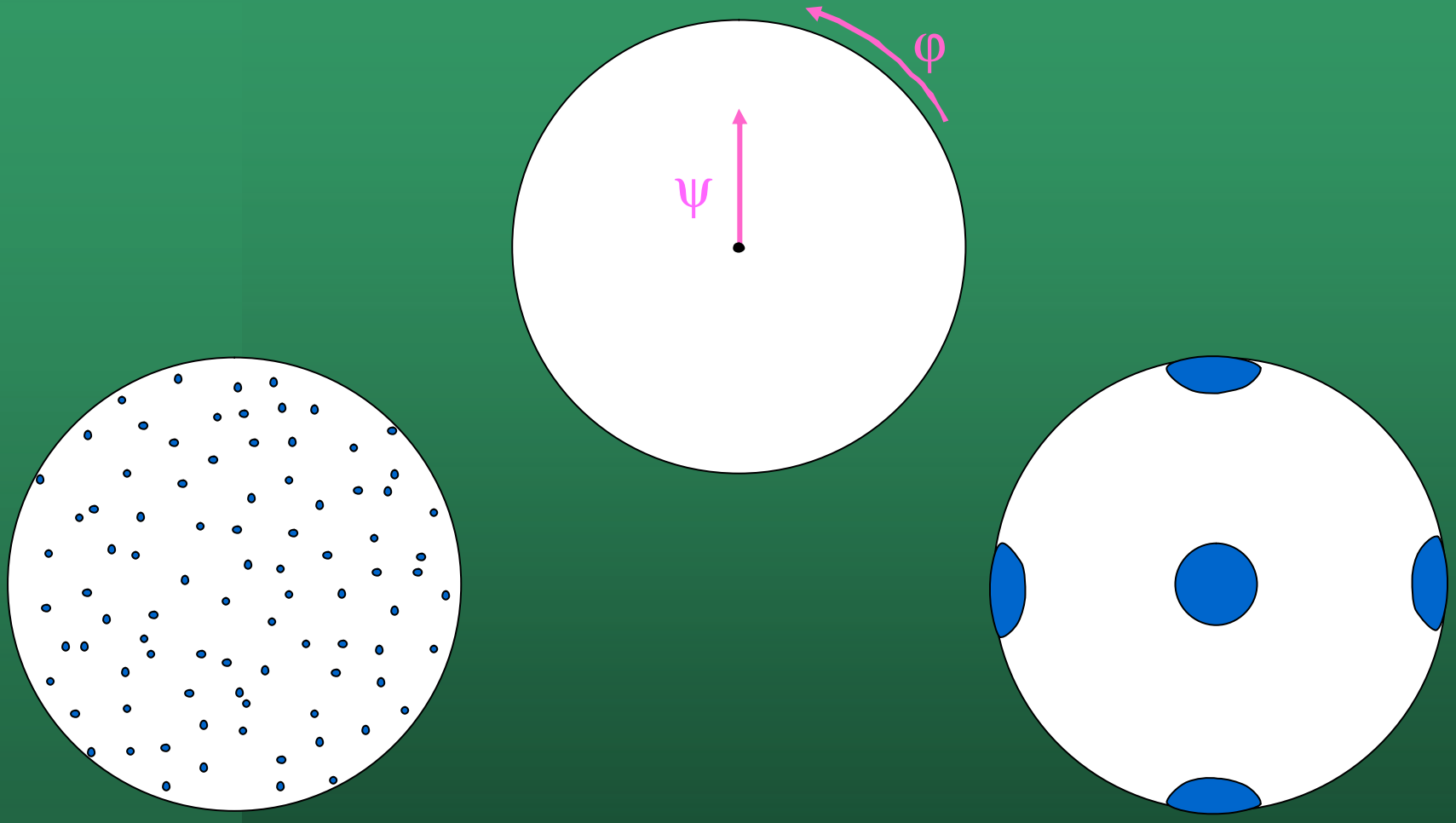

Crystallographic texture: pole figures

In general, texture can be quite complex. Several pole figures, for different (hkl), may be required to understand the orientation

(111) (200) (220)

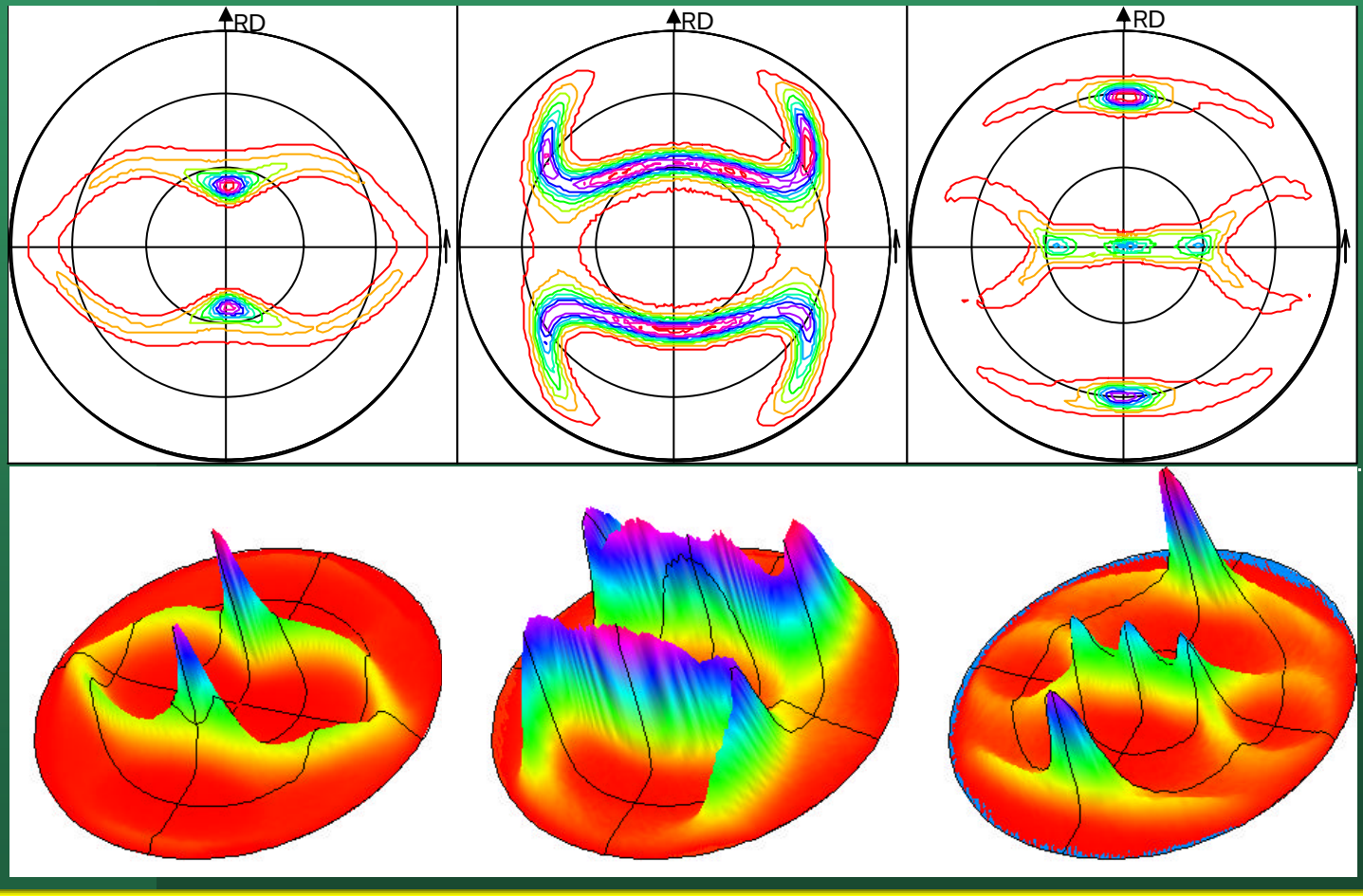

High temperature studies

Laboratory equipment

(a)

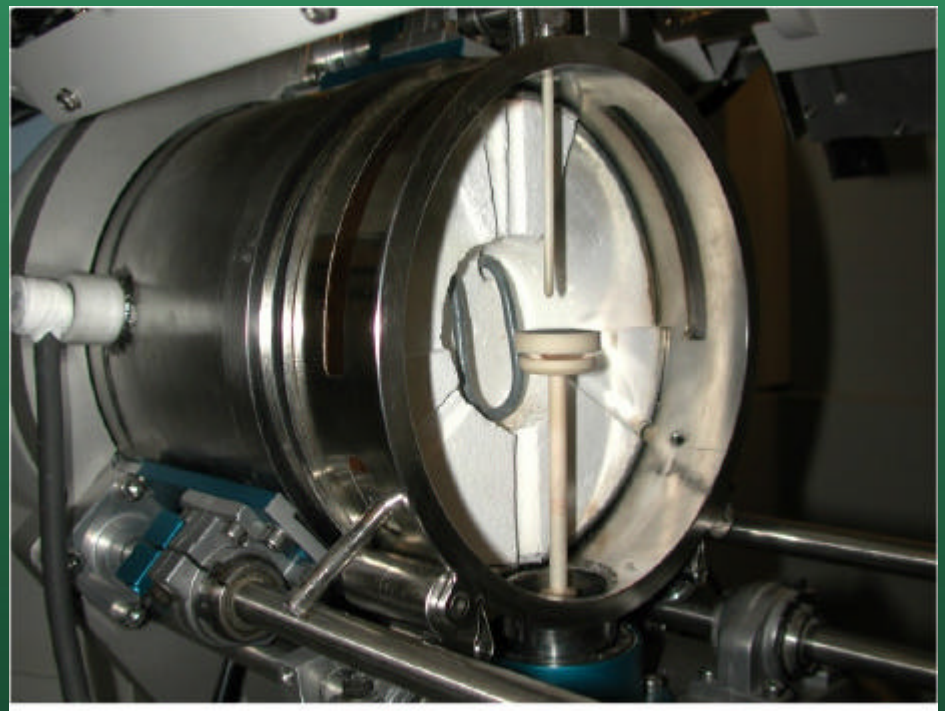

(b)

High temperature diffractometer setup

Laboratory instrument with strip heater

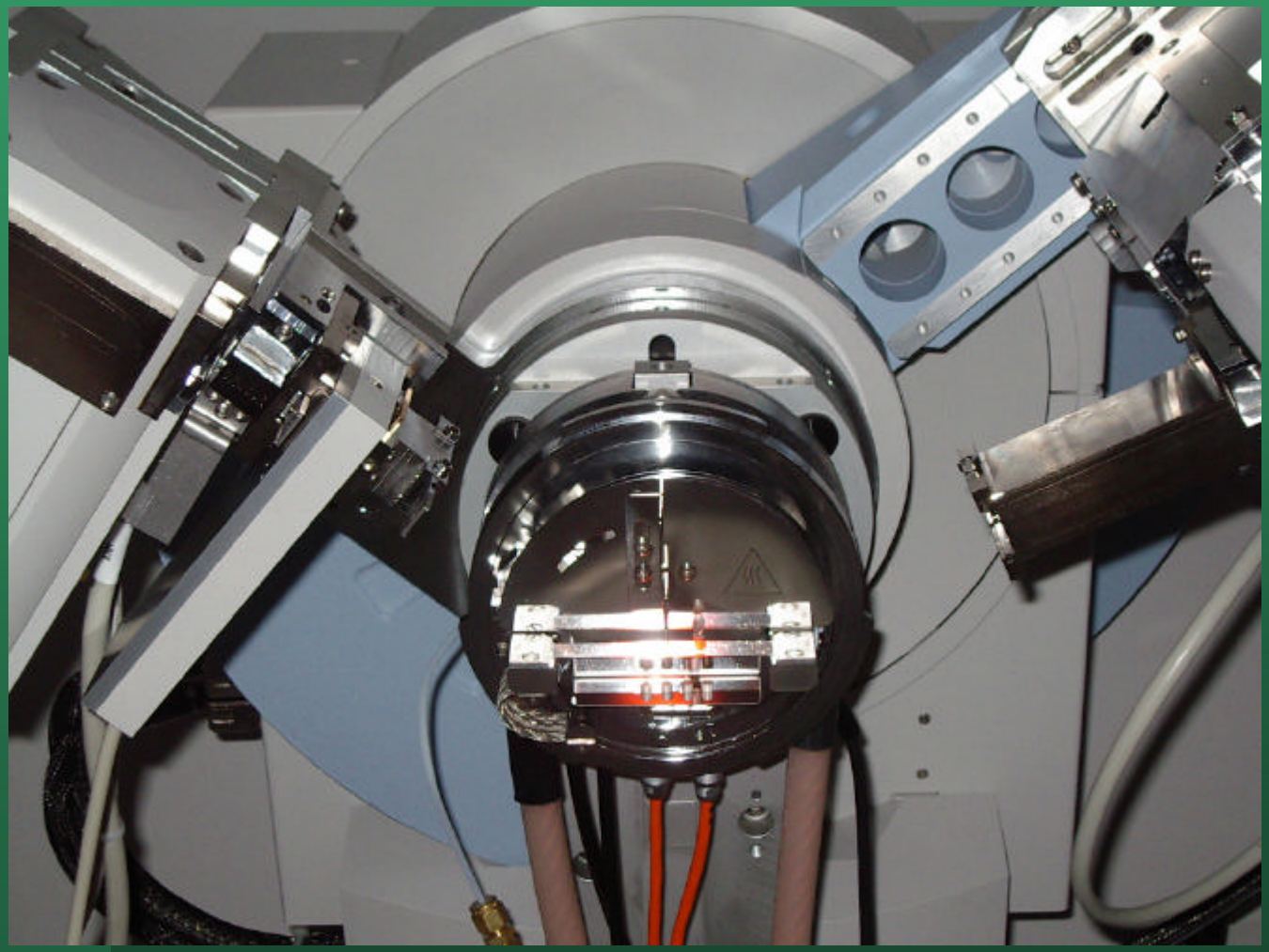

Temperature calibration

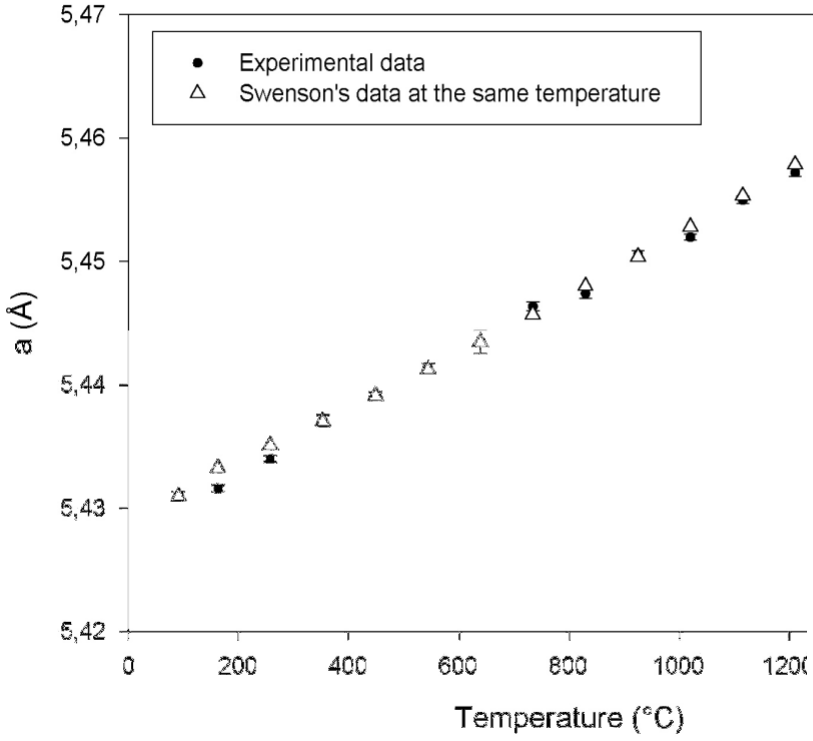

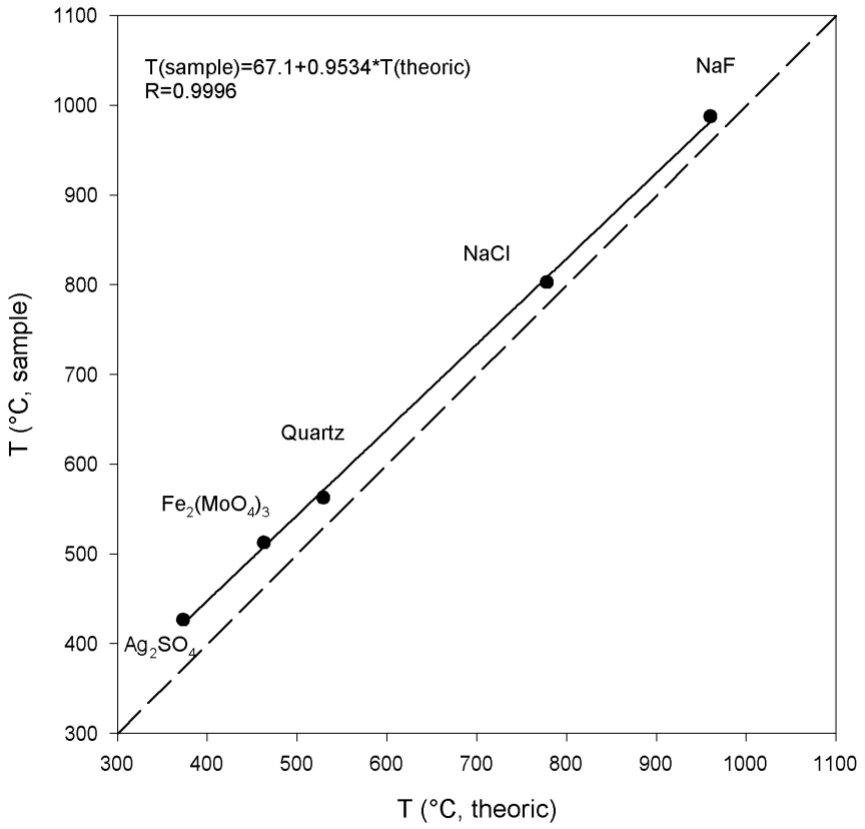

Possible studies

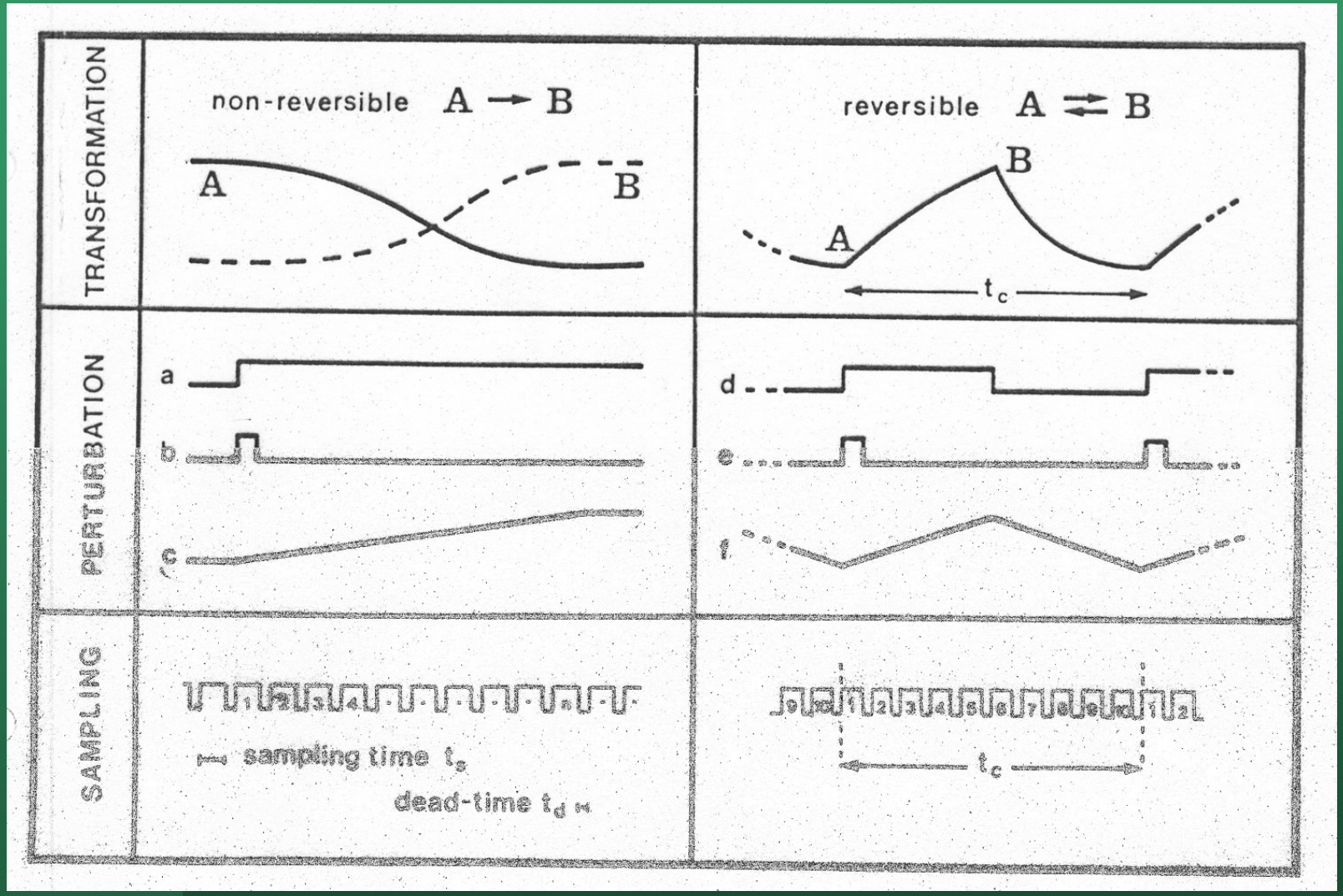

Unusual thermal expansion data

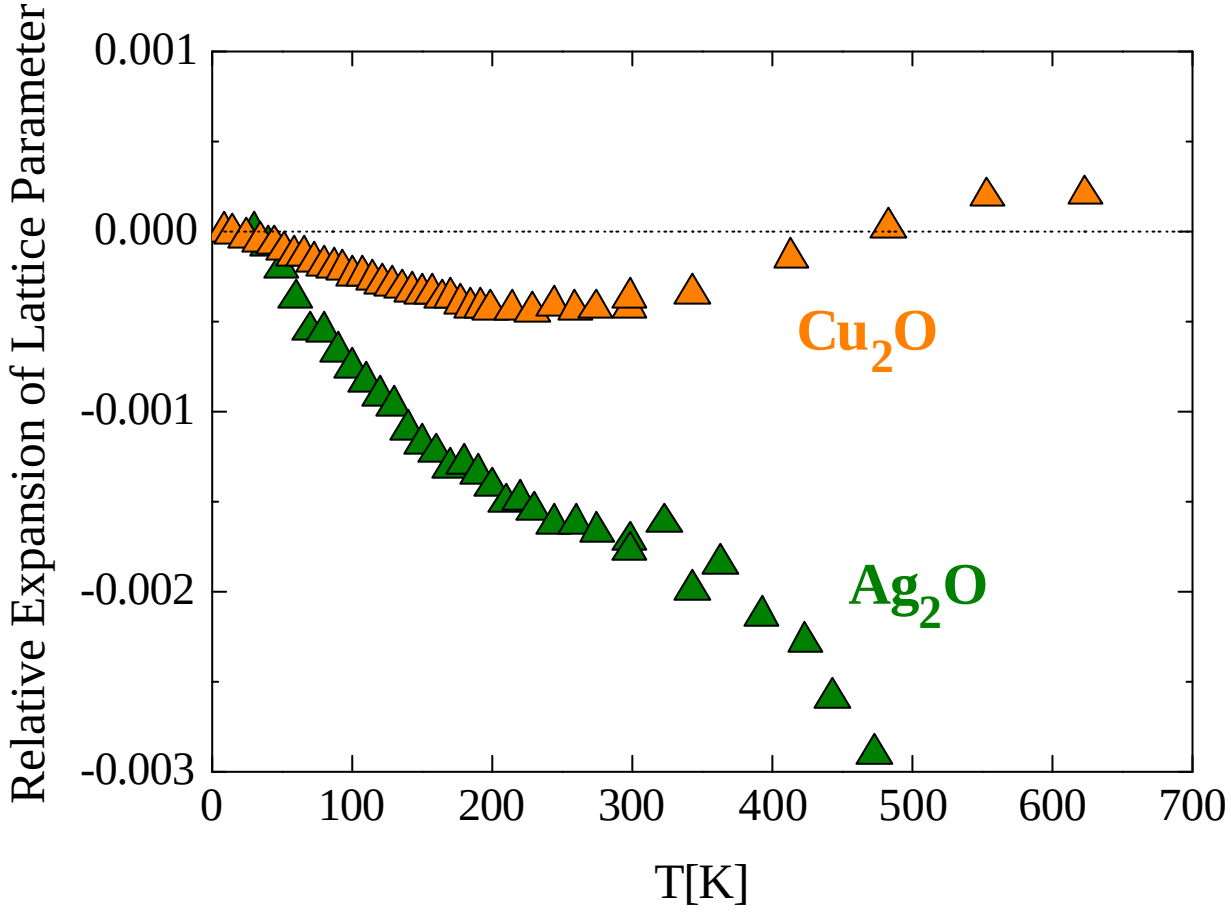

Transformation of quartz

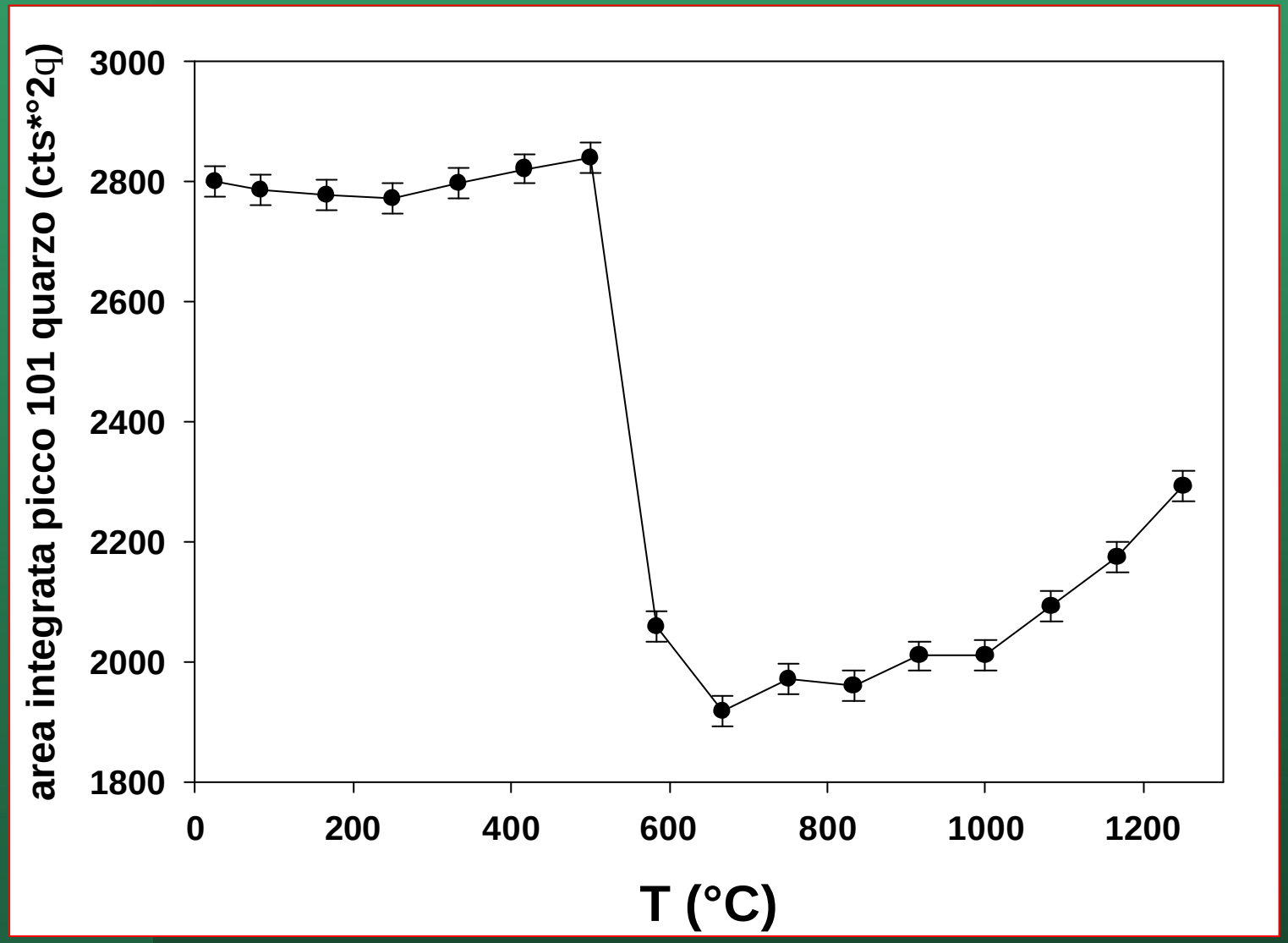

Transformation of quartz

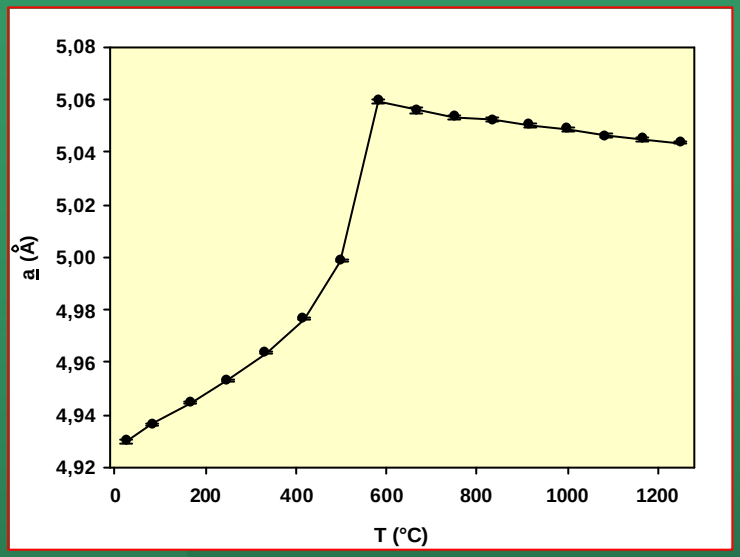

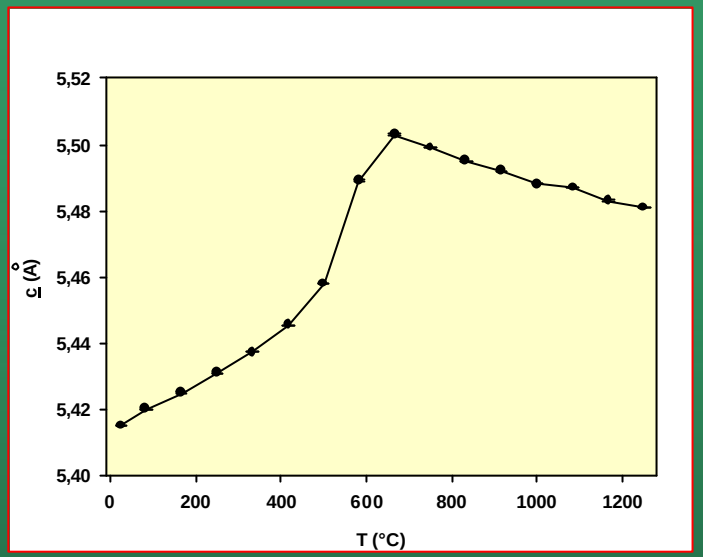

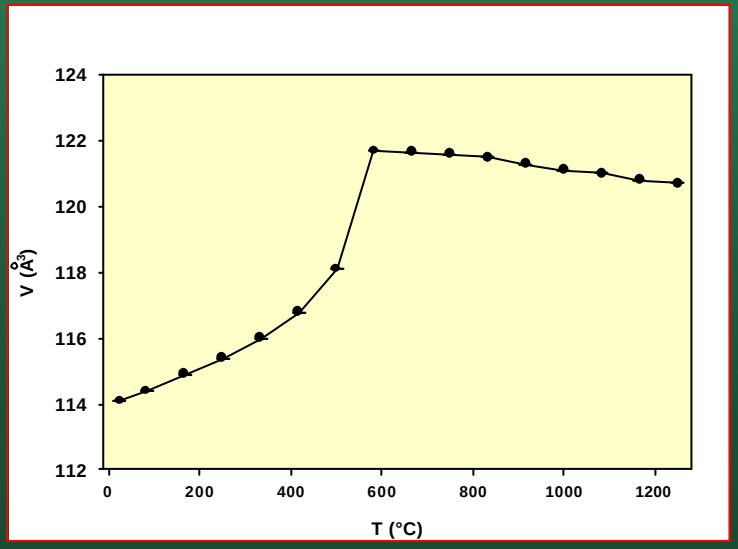

Thermal expansion of α and β quartz

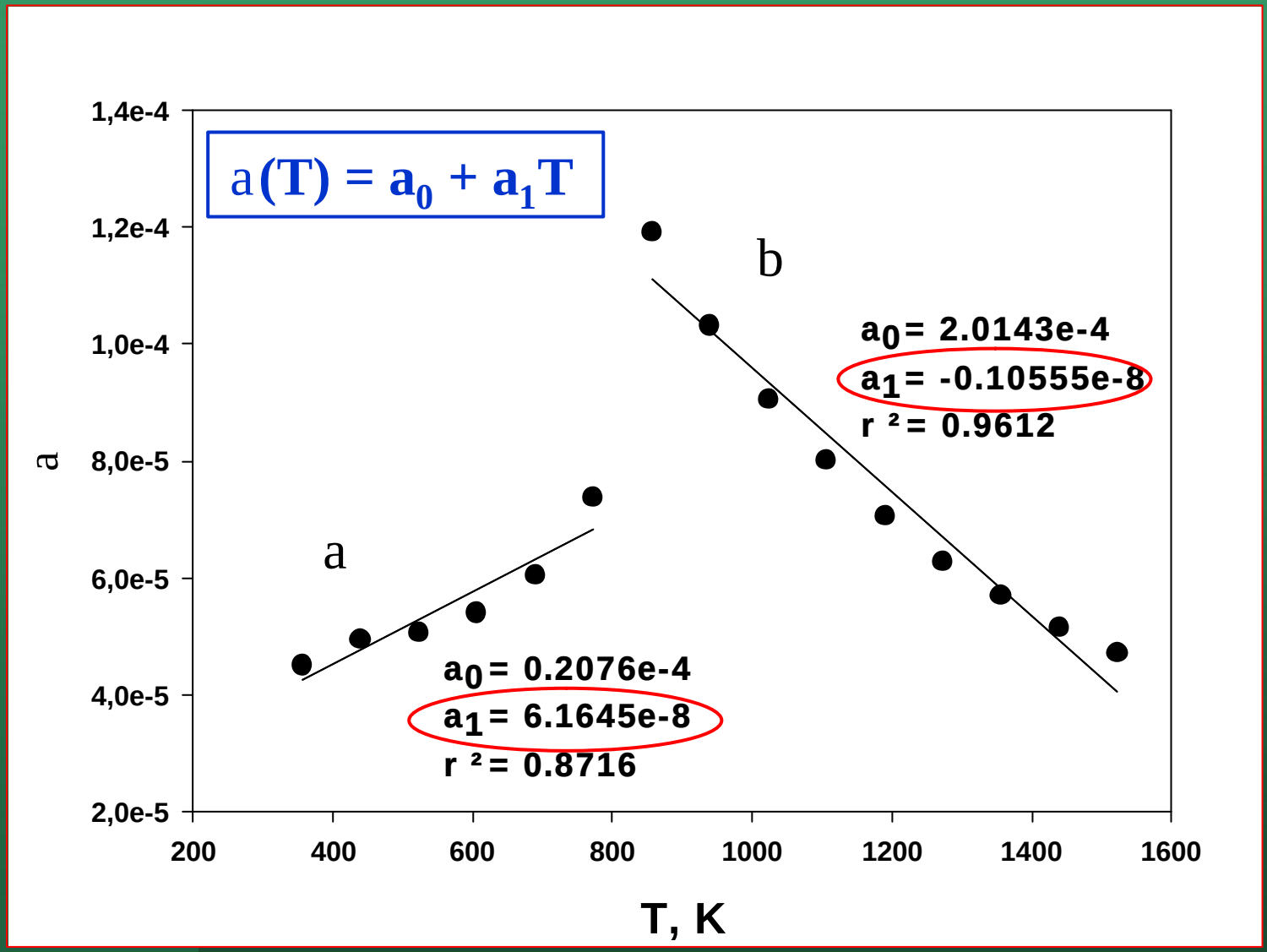

High temperature illite decomposition

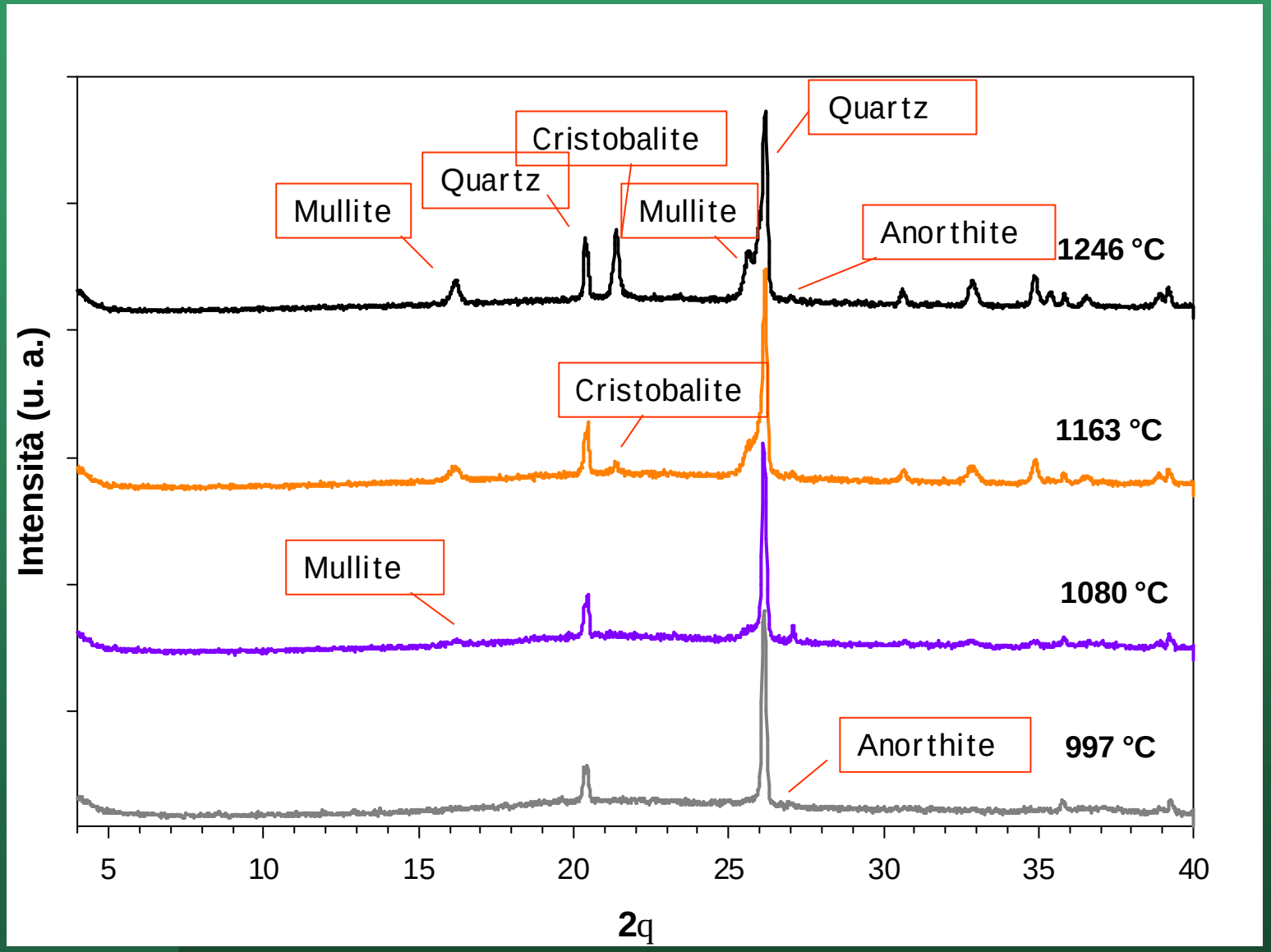

Synchrotron case: specimen heating setup

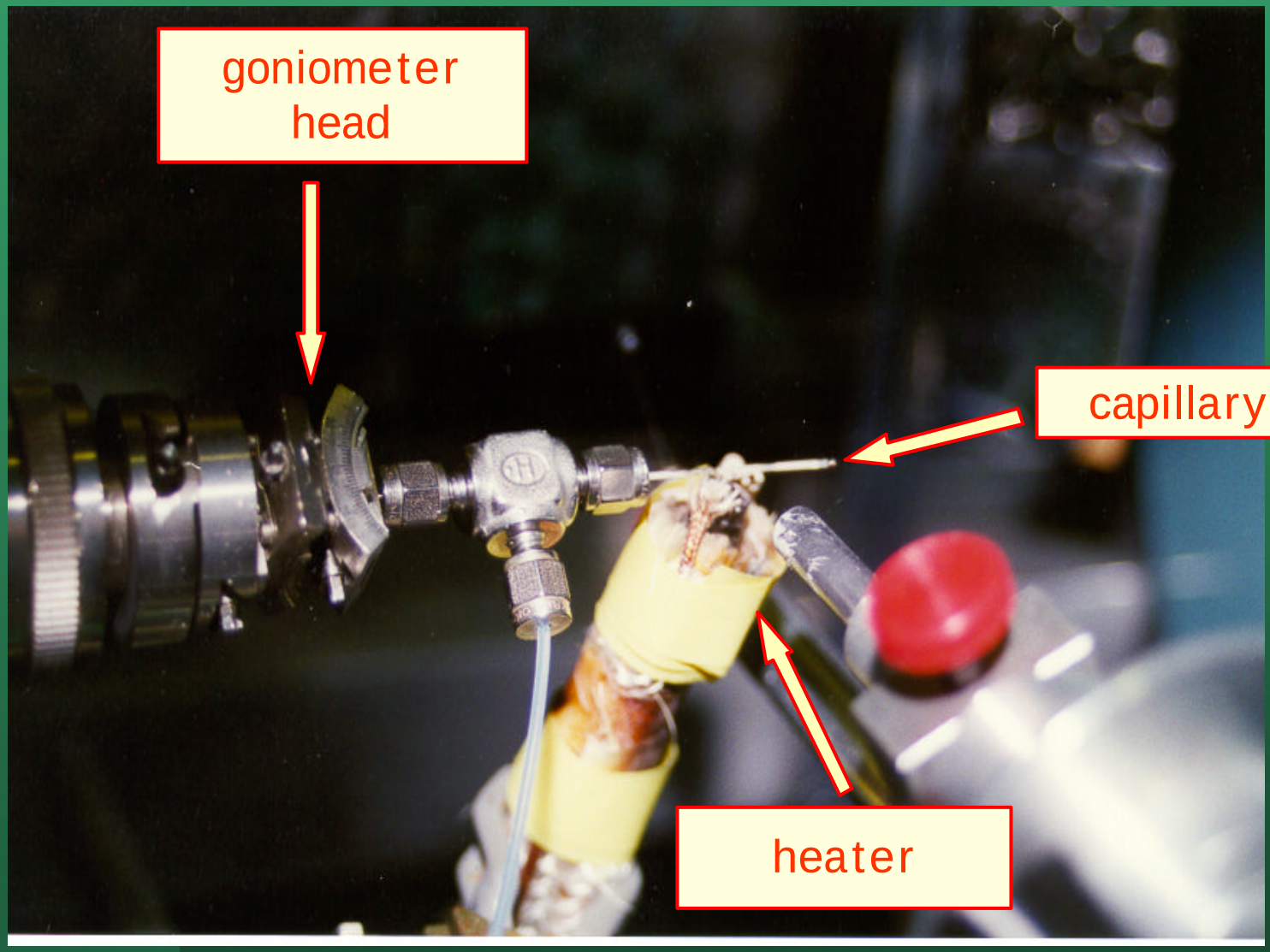

Measurement setup

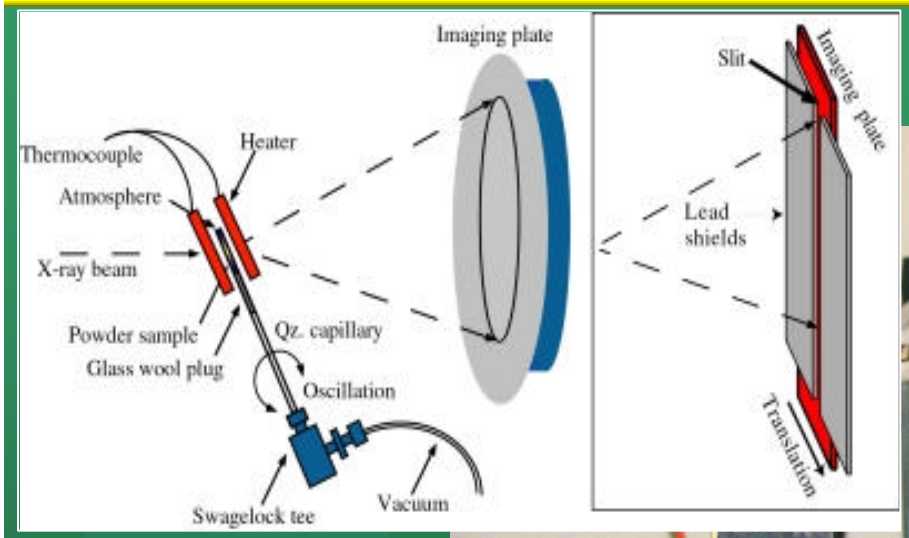

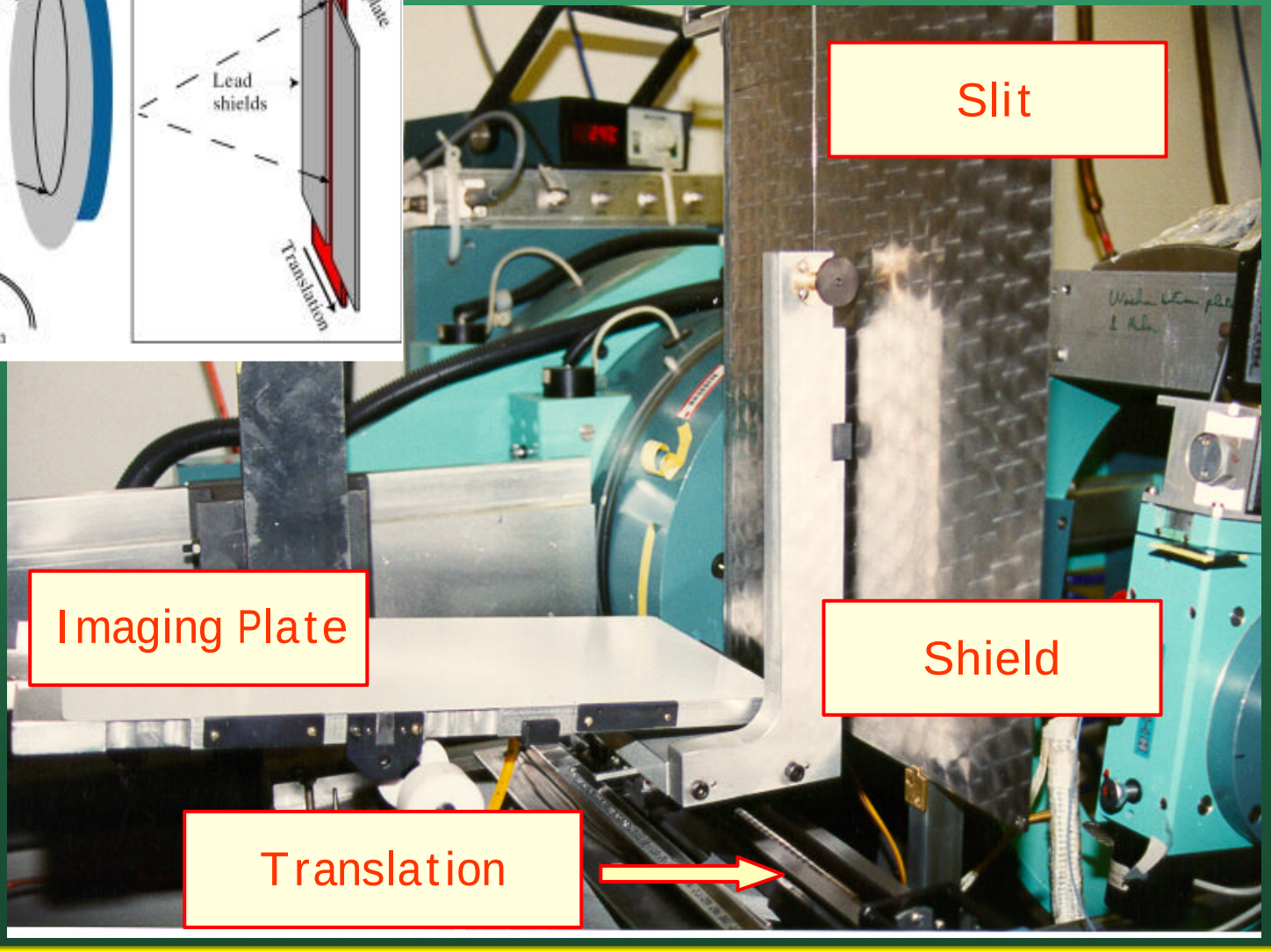

Example: transformation of FeOOH

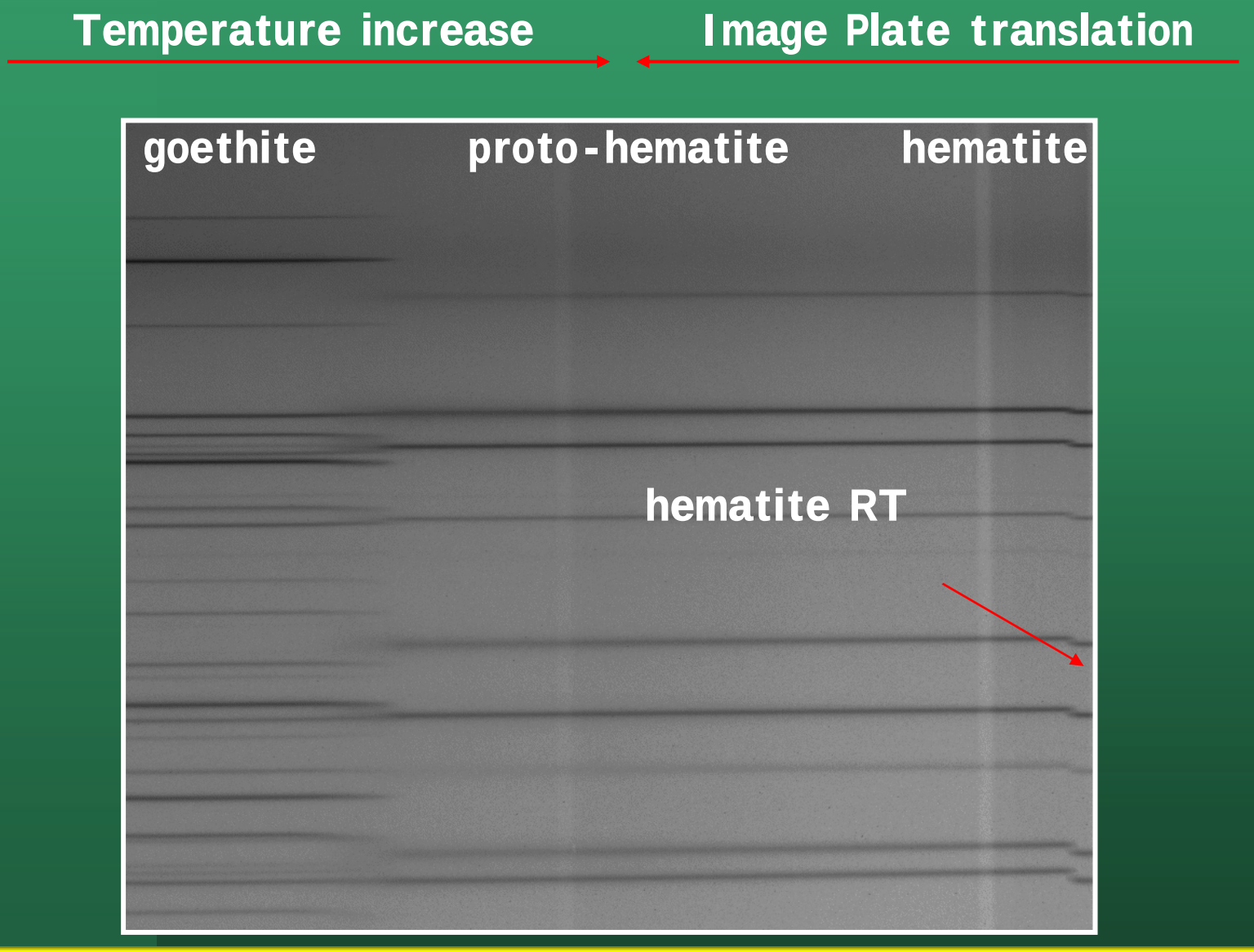

Data after readout

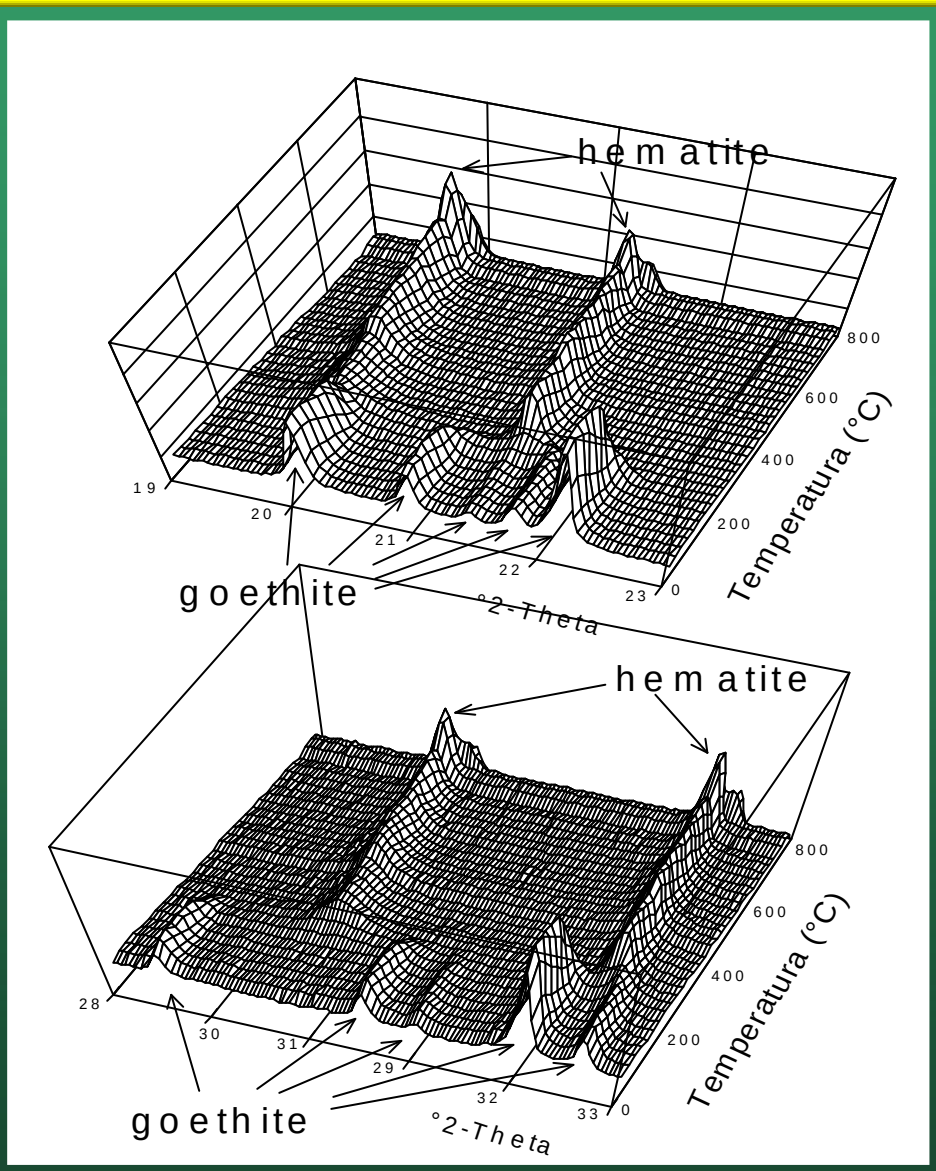

Thin film analysis

Growing a film: lattice mismatch

$c_t > a_L$

$a_t = a_S$

mismatch $m = \frac{(a_L - a_S)}{a_S}$

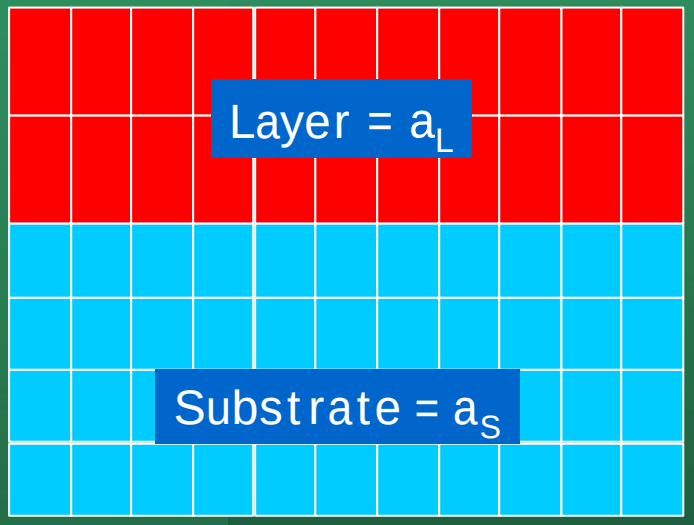

c_t

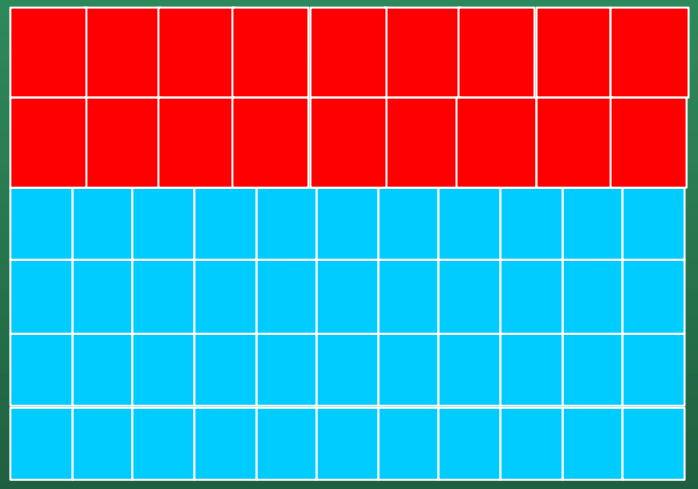

Strained layer

Relaxed layer

Types of thin films

Pseudomorphic epitaxial layers. “No” defects. Strain may be present

Example : AlGaAs/GaAs, SiGe/Si
Applications: Lasers, High-frequency IC’s

Lattice mismatched epitaxial layers. Layers are partly (or fully) relaxed

Example: ZnSe/GaAs, InAsSb/GaSb
Applications: Blue LED’s, IR optopelectronic

Layers with large lattice mismatch and/or dissimilar crystal structures

Example: GaN/Sapphire, YBaCuO/SrTiO3, BST, PZT
Applications: Blue Lasers and LED’s, High Tc Superconductors, Ferro electrics

Layers where the epitaxial relationship is weak. Highly textured

Example: AuCo multilayers on Si
Applications: Thin film media, heads

XRD for thin films and layers

Reflectivity Measurements

- Thickness, Density, Surface Roughness
- Lateral and Depth Correlation
- Curvature

In-plane Scattering

- Nano-layers
- Nano-structures
- In-plane properties

High Resolution Diffraction

- Orientation
- Quality of Epitaxy, Lattice Mismatch
- Phase Composition
- Thickness, Density, Surface Roughness
- Residual macrostress
- Microstructure

Typical Setup for Reflectivity Measurements

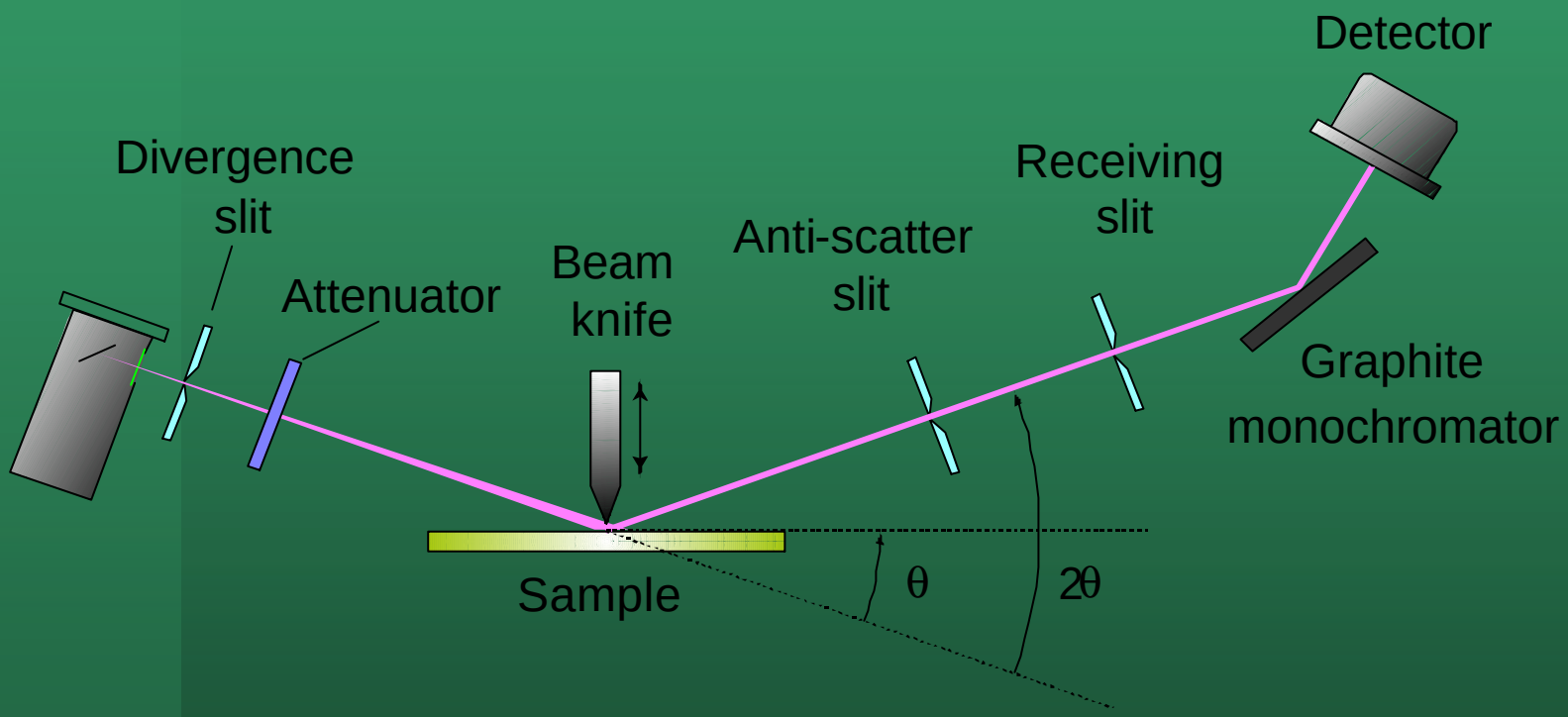

Information from a Reflectivity Curve

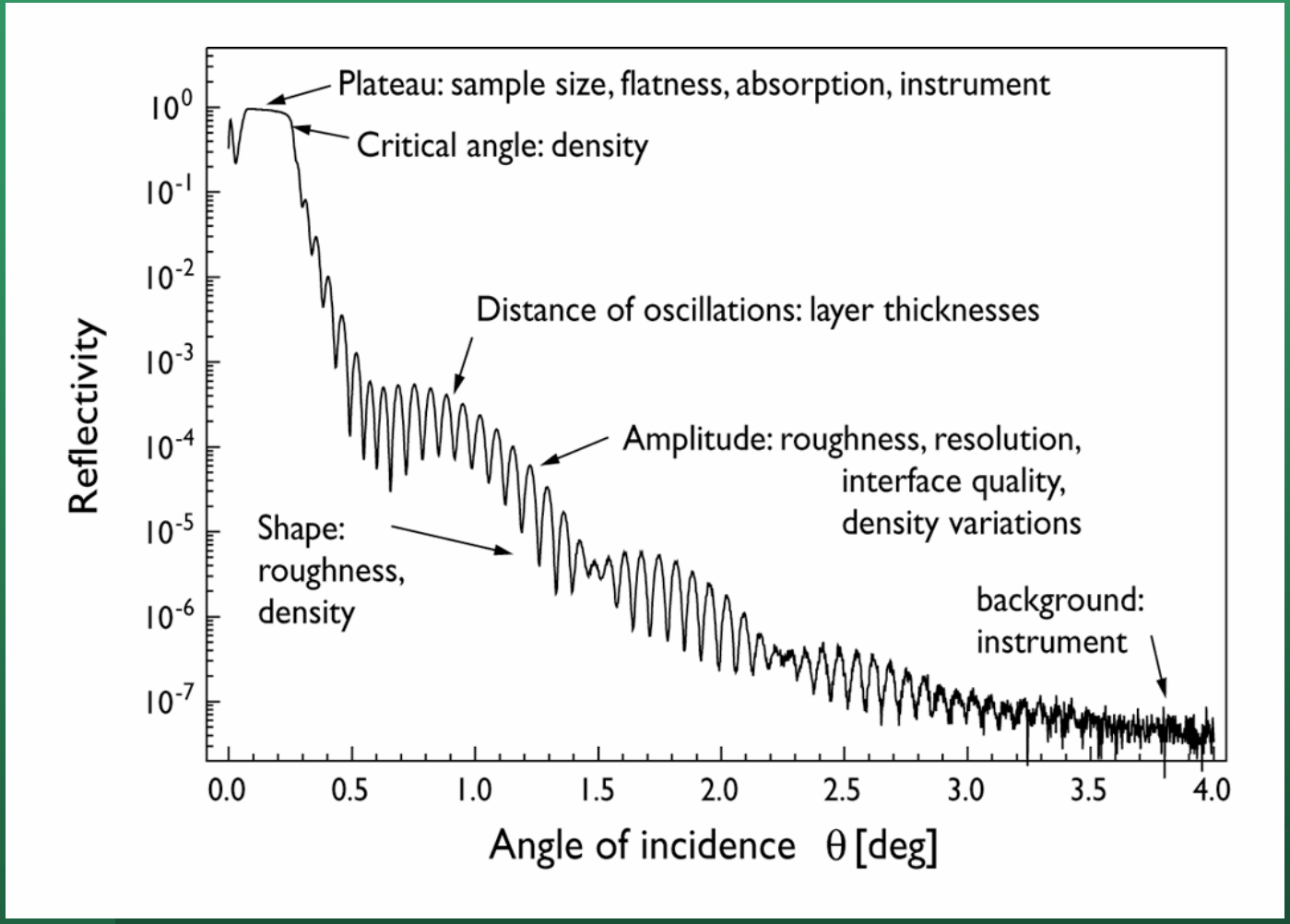

Reflectivity

XRD Study of Self-Assembled Monolayers $C_{18}H_{37}SH$ on Gold

Specular Reflectivity Curve

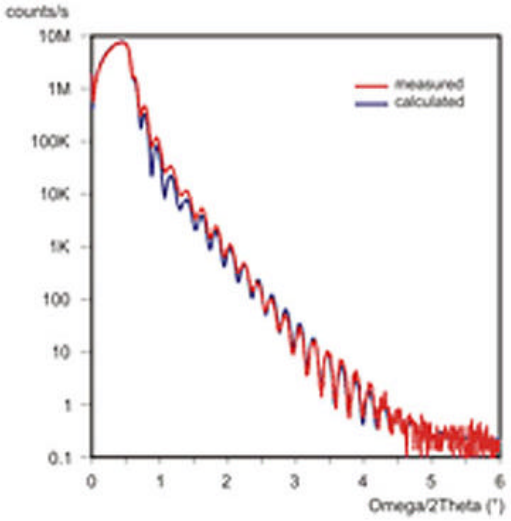

Reflectivity Map, Diffuse Scattering

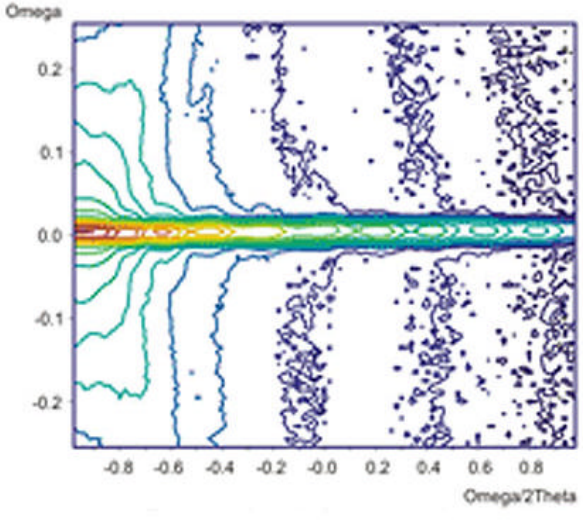

Determined thickness of the layers:

$C_{18}H_{37}SH$	- 1.6nm
Au1	- 0.6nm
Au2	- 19.0nm
Si	> 100000nm

Determined Average Lateral Correlation Length: 2.5nm

High resolution setup

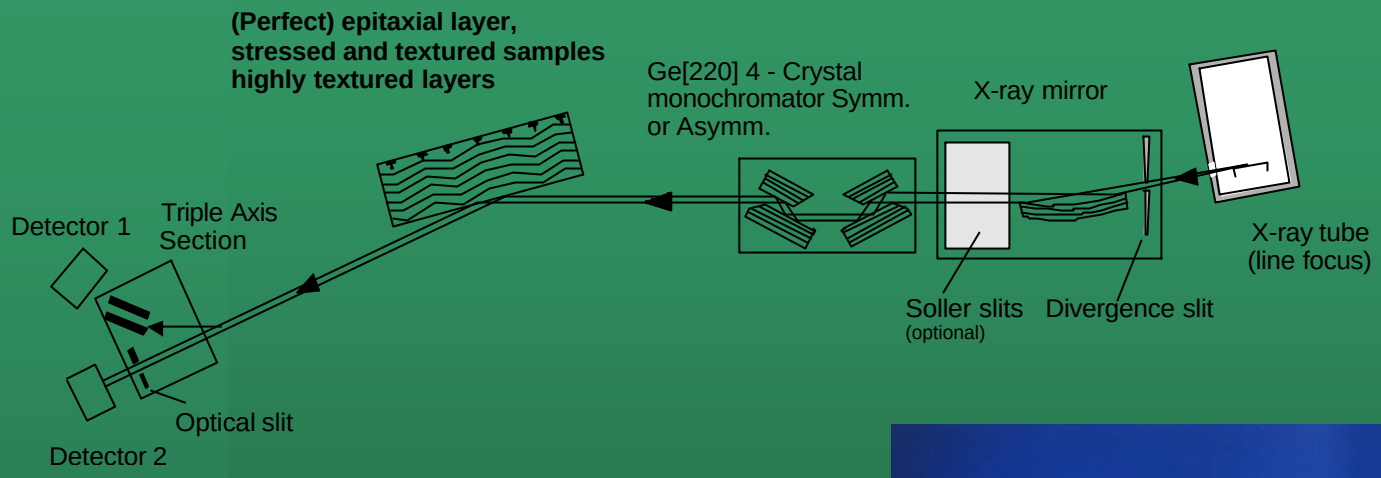

The highly parallel monochromatic beam should be used to study perfect layers

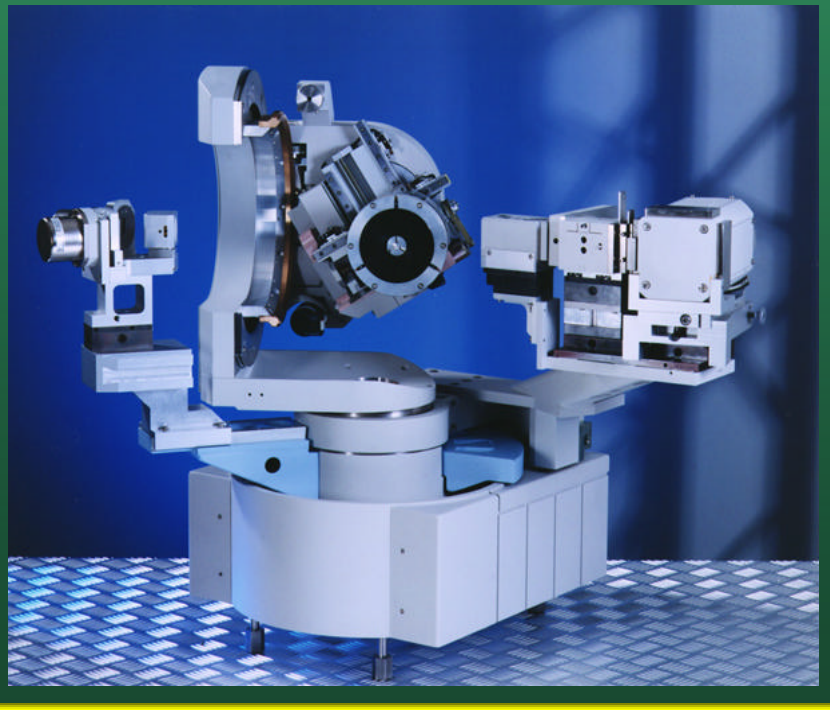

X-Ray rocking curves

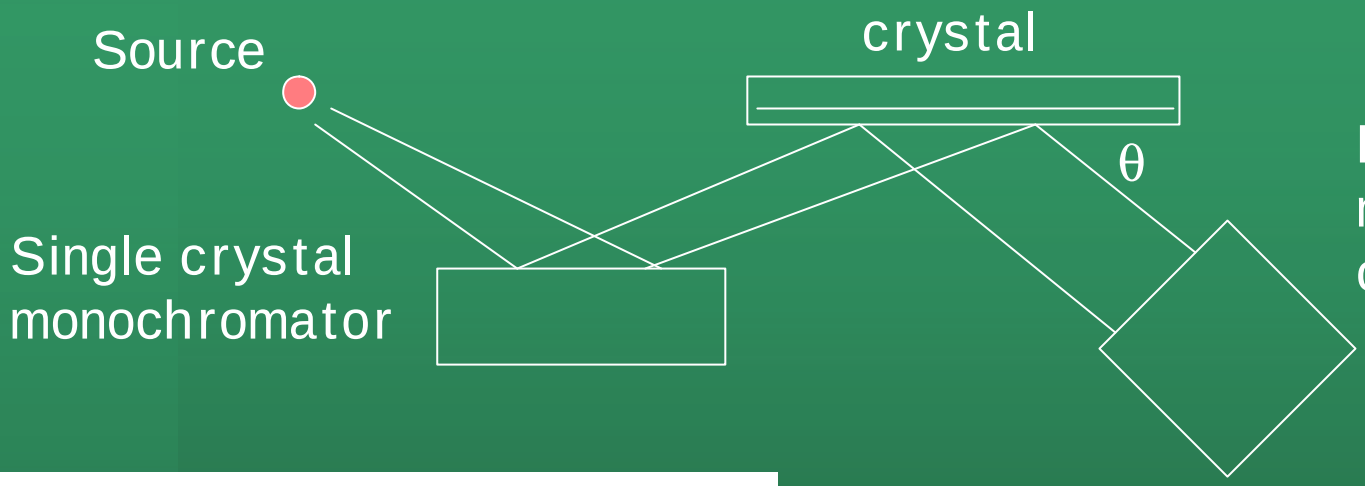

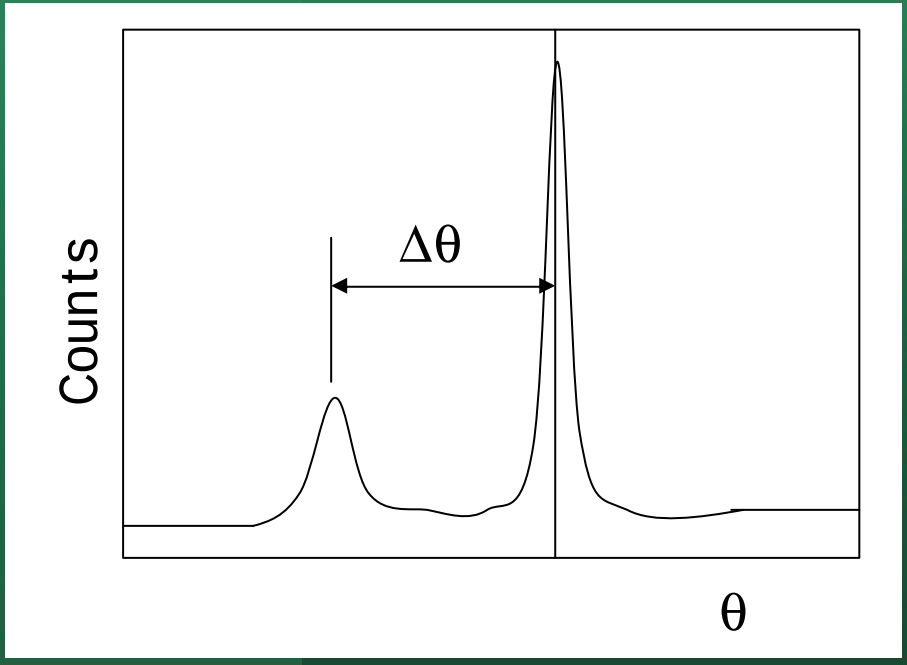

Δθ due to different lattice constant (strains).

Typically used for epitaxial film study. Principle is the same as θ-2θ diffractometer.

X-ray Rocking curves

Analysis of SiGe HBT Structure

The introduction of a SiGe epitaxial layer in the bipolar transistor (HBT) brings significant gains in speed, challenging GaAs in its traditional application fields. New technological step of introducing Ge requires also an accurate method for the characterization of Ge content and gradients.

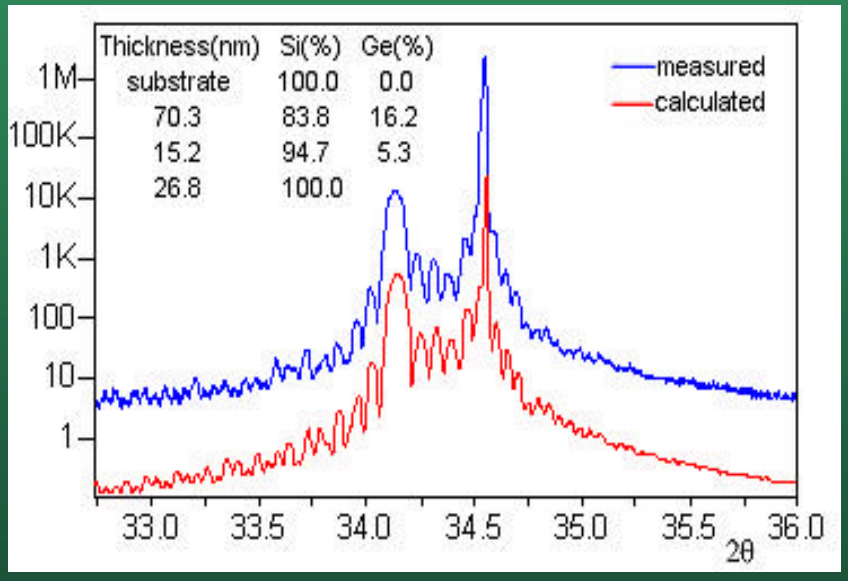

Automatic simulation and refinement of a measured rocking curve helps to identify parameters of individual layers. Method delivers 1 % accuracy for composition and 3 % accuracy for SiGe thickness.

Grazing Incidence XRD (GIXRD)

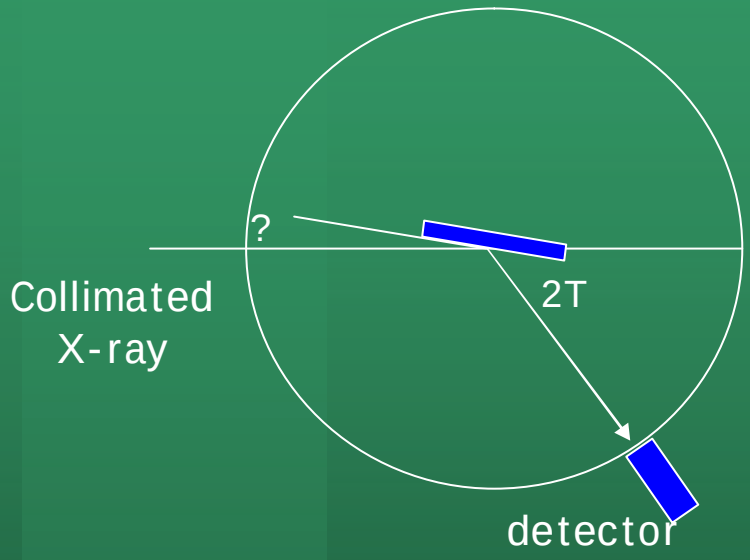

Bragg-Brentano diffractometer

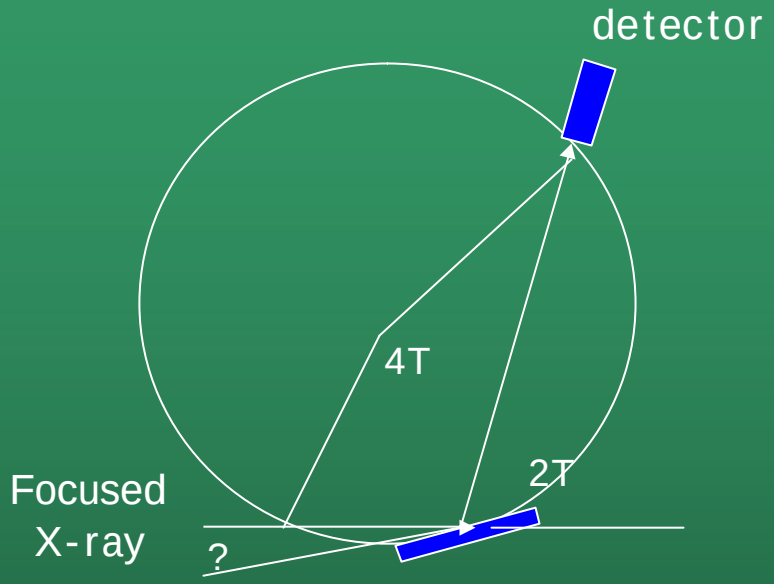

Seemann-Bohlin diffractometer

By varying γ ⇒ rough idea of the phase distribution, microstructure or development of orientation as a function of depth

GIXRD of a magnetic film

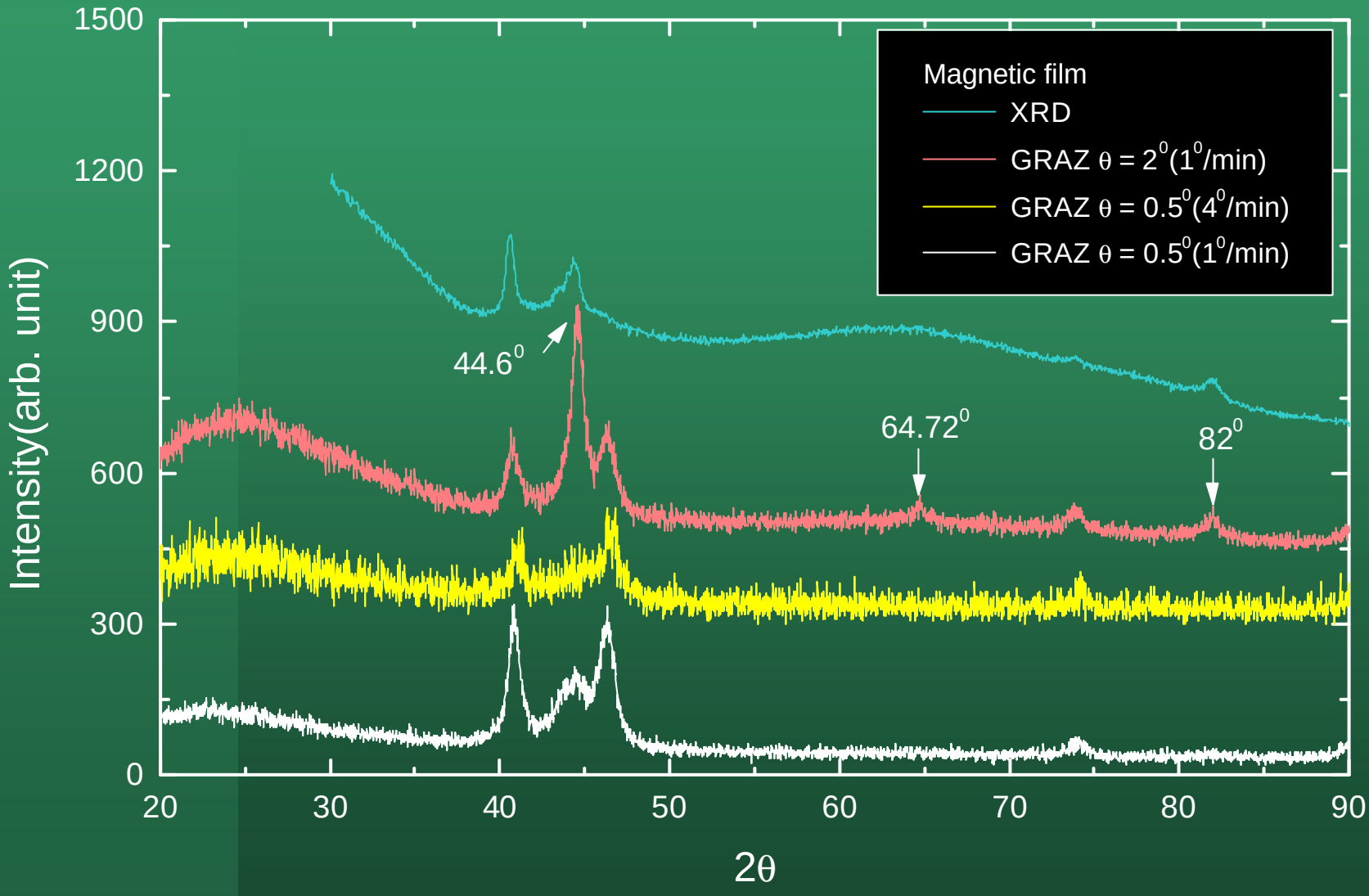

Reciprocal space mapping

Relaxed GaInAs/GaAs (224)